Regulation of Serine Proteases in Blood Clotting and Beyond

by

Fabienne Birkle

A dissertation submitted in partial fulfillment
of the requirements for the degree of
Doctor of Philosophy
(Biological Chemistry)
in the University of Michigan
2022

Doctoral Committee:

Professor James H. Morrissey, Chair
Professor Ryan Bailey
Assistant Professor Michael Cianfrocco
Associate Professor Patrick O'Brien
Professor Janet Smith

Fabienne Birkle

fbirkle@umich.edu

ORCID iD: 0000-0003-0238-8865

Dedication

This dissertation is dedicated to my late grandma, Elizabeth Kögel. She showed me what it means to live with cardiovascular disease. Despite her illness and hardships, she was the most compassionate person and best grandma I could have asked for. Thank you for everything you have done for me.

Acknowledgements

The last five years would not have been possible without the support of many people in my life. No words can ever fully express the gratitude I feel towards all of you.

I would like to thank my PhD advisor, Jim Morrissey, for his support and everything he taught me throughout my time in his lab. When I started my PhD, I was looking for an advisor that would not just value me as a scientist but also as the person I am beyond the bench. I am glad to say that Jim has fulfilled this role. He has always been there when I needed his support, advice, or encouragement. Being able to benefit from his vast scientific knowledge and hearing his personal life experiences has been immensely valuable. Thank you to all current and former members of the Morrissey lab for being my science family. Not many PhD students are fortunate to find both a supportive advisor and colleagues. Moving the lab and our lives to a new state together truly was a bonding experience. Thank you for all the live stories we shared, happy hours we celebrated and failed experiments we commiserated together.

I would like to thank my thesis committee members, Janet Smith, Patrick O'Brien, Michael Cianfrocco and Ryan Bailey, for their valuable advice which helped me to stay on track and don't lose sight of the "big picture". Your positive attitude had me genuinely looking forward to every committee meeting. Thank you to the core facilities at the University of Michigan who supported me during challenging experiments. The staff at the Center for Structural Biology and the Cryo-Electron Microscopy Facility answered my countless questions and were always there to provide a helping hand. Thank you to my collaborators in the Tajkhorshid lab at the University of Illinois Urbana-Champaign, the Rienstra lab at the University of Wisconsin-Madison, the Komives lab at the University of California San Diego and the Cianfrocco lab at the University of Michigan. You all provided scientific expertise that contributed to the success of experiments and manuscripts.

For financial support during my PhD, I would like to thank the National Heart, Lung, and Blood Institute of the National Institutes of Health, Michigan Medicine, the Rackham Graduate School, the Biological Chemistry Department, and the American Heart Association. You provided

the monetary backbone that made it possible to conduct my experiments and attend conferences to share my findings with the scientific community.

I would like to thank the whole Biological Chemistry Department for welcoming me in their midst 4.5 years ago. Thank you to the administration staff for helping me with all the logistics that PhD life entails. Your organizational talent made it so much easier to navigate the bureaucracy at the University of Michigan. You all are so kind and managed to make scheduling seminars, meetings and classes an enjoyable experience for us students. Thank you to the former and current Biological Chemistry students who walked the PhD road along with me. Sharing both our failures and successes with each other was comforting and helped to put things in perspective. Biochem retreats, recruitment events and happy hours were a great way to get out of the lab and have fun together.

Thank you to all the people I met at the University of Michigan outside of science. Being able to step away from the bench at times helped me reevaluate my experiments and come up with new ideas when I least expected it. Thank you to the members of the International Center Student Council, for teaching me to think outside the box and helping me hone my intercultural skills. Thank you to miLEAD, for giving me a new perspective when I needed it. Being a part of miLEAD during the last 1.5 years opened many new doors. The challenges I faced made me grow in new ways and I accomplished goals I never thought I could.

You cannot make it through a PhD without the love and support of your family and friends. Thank you to my close friends here in Michigan and back in Germany. You were always there when I needed you. After the Morrissey lab moved to Ann Arbor, I was fortunate to find a group of amazing friends to go through PhD life with. Sydney, Taylor, Anthony, Meredith and Lara, thank you for making these last 4.5 years such a fun experience. I was always so much looking forward to our movie nights, dinners, tailgates and lake weekends together. Michigan would not have been the same without you. To my best friends in Germany, especially Sina and Anne, thank you for not giving up on me. It is not easy to stay connected across an ocean. But even if we didn't hear from each other for a while, whenever we reconnected, it was as if we had just talked yesterday. If you have known each other for more than a decade, you form a bond that doesn't break easily. You will always be near and dear to my heart, no matter where I am.

To my family back home in Germany, mom, dad, Pascal and Philippe, thank you for supporting my decision to pursue a PhD on another continent. The distance between the US and

Germany has made it hard at times to see each other in person. Not being able to go home at all for 1.5 years during the pandemic was a struggle. However, I always look forward to our weekly Skype dates on Sunday afternoon. Knowing you all are just a virtual call away when I need you makes daily life much easier to master. I am so proud of everything you have accomplished in the time I was gone, from pursuing degrees to graduating and starting new jobs. Being away from my family is one of the hardest things I have ever done, but in a way, it also brought us closer together than ever. Thank you for your never-ending support and love.

To my fiancé Aristides, thank you for being my rock throughout my PhD and beyond. We have been through so much together over the last 7.5 years. Over four years long distance, several moves, three graduations, and the list goes on. There is no one I would rather do life with. Thank you for sharing your passion for science, food and the outdoors with me. Thank you for your kindness, patience, and love. You are one of the most compassionate people I know, and I am grateful every day that we met all those years ago. I cannot wait for our new chapter together.

Table of Contents

List of Tables

List of Figures

Abstract

Blood clotting is a crucial step in the wound healing process. In a series of proteolytic cleavage reactions, inactive blood clotting factors (zymogens) are transformed into active enzymes. The physiologic activator of blood clotting is the tissue factor – factor VIIa (TF-FVIIa) complex. Upon vascular damage, the integral membrane protein TF is exposed and binds the serine protease FVIIa. TF-FVIIa drives blood clotting through proteolytic cleavage of its two major protein substrates, the zymogens factor IX (FIX) and factor X (FX). The activation of FIX and FX is facilitated by TF residues located adjacent to or within the putative substrate binding site on TF (the TF "exosite"). Previous studies have shown that mutating TF exosite and exosite-adjacent residues leads to a strong decrease in activation of FIX and FX. However, it remains unclear how TF-FVIIa exhibits selectivity between these substrates. We hypothesized that an exosite-adjacent TF serine loop mediates substrate selectivity by the TF-FVIIa complex. Through extensive mutagenesis studies in combination with enzymatic assays, we determined that the length of this TF serine loop affected FIX and FX activation very differently. While FX activation was decreased by up to 200-fold when the serine loop length was changed by just one residue, FIX activation was largely unaffected. The serine loop seems to regulate the TF exosite during FX activation but has no effect on the exosite during FIX activation. The results of this study suggest that the TF-FVIIa complex actively selects between its major protein substrates, which is mediated by a TF serine loop.

TF residues are not just involved in TF-FVIIa substrate selectivity but also in substrate recognition. While it is known that mutating TF exosite residues leads to decreased FX activation, it is unclear how the TF exosite interacts with FX. We hypothesized that portions of the FX light chain bind to the TF exosite to facilitate substrate activation. To test this hypothesis, we generated a stable membrane-bound complex comprising TF, FVIIa and a FX mimetic (XK1). XK1 is a hybrid protein that has increased affinity for TF-FVIIa and consists of the FX light chain bound to the Kunitz 1 domain of tissue factor pathway inhibitor. The TF-FVIIa-XK1 complex was generated, validated, and then imaged using negative stain and cryo-electron microscopy (EM).

Our preliminary cryo-EM model, the first model of TF-FVIIa bound to a substrate, indicates potential interactions between the TF exosite and FX light chain. These interactions could mediate substrate recognition by the TF-FVIIa complex.

Serine proteases are not just important for blood clotting but are also involved in many other cellular processes. Serine proteases are typically synthesized as inactive precursors (zymogens) which remain inactive until they reach their target location. However, in some cases serine proteases can be prematurely activated, leading to severe diseases. We hypothesized that millimolar concentrations of ATP and other nucleotides in the Endoplasmic Reticulum (ER) and Golgi could keep prematurely activated zymogens enzymatically inactive while they transition through these compartments. Our kinetic, binding and structural studies revealed that serine proteases are inhibited at low millimolar concentrations of nucleotides. ADP and ATP act as uncompetitive inhibitors and bind to serine proteases cooperatively. Inhibition of serine protease activity by ATP and other nucleotides may serve as a safety mechanism to prevent cellular damage caused by premature activation of proteases.

Chapter 1 Introduction

1.1 Overview of Blood Clotting

Hemostasis is an intricate, tightly regulated process that seals off damage to the vasculature after injury. To guarantee wound healing, the hemostatic system is composed of three major players: blood clotting, platelet activation, and vascular repair.[1] Blood clotting (or coagulation) is the most prominent of the three players. Over 2000 years ago, philosophers in ancient Greece first discovered that blood forms fibers when it leaves the body.[1] However, most blood clotting factors were discovered in the 20th century. Established in the 1960s, the mechanism of blood clotting is described as a series of proteolytic cleavage reactions that are reminiscent of a waterfall or cascade.[2,3] This cascade of reactions transforms inactive clotting factors (zymogens) into active enzymes. Most of these blood clotting enzymes are serine proteases.

The coagulation cascade is divided in two major pathways: the extrinsic pathway (or tissue factor pathway) and the intrinsic pathway (or contact pathway).[4] The pathways are named based on how they are activated. Activation occurs either through tissue factor, an integral membrane protein, or a negatively charged contact surface. After a series of proteolytic cleavages, the two pathways eventually merge into a single pathway known as the common pathway. The final step of the coagulation cascade is the formation of a blood clot, composed of fibrin strands and activated platelets, that seals the injured vasculature.

In contrast to hemostasis, thrombosis is the formation of a blood clot inside the lumen of a blood vessel. These "unwanted" blood clots can lead to obstruction of the arterial or venous circulation. This obstruction can cause heart attacks and strokes, the two leading causes of deaths globally.[5] While only the tissue factor pathway contributes to hemostasis, both the tissue factor and contact pathway play an important role in thrombosis.[4] Thus, it is crucial to understand these pathways on a molecular level. New insights into the initiation of blood clotting could lead toward the development of novel antithrombotic therapies for the treatment of thrombotic diseases.

1.2 The Tissue Factor Pathway

The tissue factor pathway plays a crucial role in hemostasis and many thrombotic diseases.[6] The pathway is initiated by the tissue factor – factor VIIa (TF-FVIIa) complex. Upon vascular injury, TF-expressing cells become exposed to plasma that contains the serine protease FVII (zymogen form) or FVIIa (active enzyme). This leads to the formation of a two-subunit enzyme with TF as the regulatory subunit and FVIIa as the catalytic subunit.[7] The TF-FVIIa complex converts its two main protein substrates, the zymogens factor XI (FIX) and factor X (FX), into active enzymes, propagating the coagulation cascade.

1.2.1 Tissue Factor

TF (also known as coagulation factor III, thromboplastin or CD142) is a 263-amino-acid glycoprotein with a molecular weight of ~46 kDa. TF is expressed on many non-vascular cells, including adventitial and epithelial cells, but there is little to no TF expression on endothelial cells.[8-10] Deletion of the TF gene in mice is embryonically lethal, underlining the essential role of TF in hemostasis.[11-13] As a member of the cytokine class II receptor family, TF is a transmembrane protein that contains three domains (Figure 1.1): an N-terminal extracellular domain (residues 1-219), a transmembrane domain (residues 220-242) and a C-terminal cytoplasmic tail (residues 242-263).[14-17] The extracellular domain, often referred to as soluble TF (sTF), is comprised of two fibronectin type III domains. The X-ray crystal structure of sTF has been determined by several groups.[18-20] The extracellular domain is connected to the transmembrane domain by a six amino acid, flexible linker. The transmembrane domain is comprised of one single alpha helix and its exact composition is unimportant for TF function. Replacing the transmembrane domain with a glycophosphatidylinositol anchor or tethering hexahistidine tagged sTF to the membrane via nickel-chelating lipids retains the procoagulant activity of TF.[21,22] The cytoplasmic domain is dispensable for TF procoagulant activity but contains several post-translation modifications (phosphorylation of Ser^{253} and Ser^{258}, S-palmitoylation of Cys^{245}) that are involved in downstream signalling.[23,24]

The procoagulant activity of TF is not just regulated by high cell-surface expression but also by encryption and decryption of TF. TF is encrypted (inactivated) in healthy cells but upon vascular injury TF gets decrypted (activated). Although the exact mechanism is not fully understood, several hypotheses how TF activity is regulated have been proposed. The first and

most well-known hypothesis states that TF activity is regulated by the phospholipid environment. In resting condition, the phospholipid, phosphatidylserine (PS), is sequestered to the inner membrane leaflet.[25,26] Upon stimulation through vascular injury or increased Ca^{2+} concentrations, selective lipid transporters shuttle PS to the outer membrane leaflet. The negatively charged PS provides a suitable environment for binding of clotting proteins (including FIX and FX) and optimally positions TF-FVIIa for substrate cleavage.[27-29] The second and more controversial hypothesis states that TF activity is regulated by the oxidation and reduction of the Cys^{186}-Cys^{209} bond in the TF extracellular domain. Reduction of this disulfide bond renders TF encrypted/inactive, while oxidation leads to decrypted/active TF.[30,31] This process could be regulated by protein-disulfide isomerase (PDI).[32] However, several studies have disputed the allosteric disulfide bond hypothesis.[33,34]

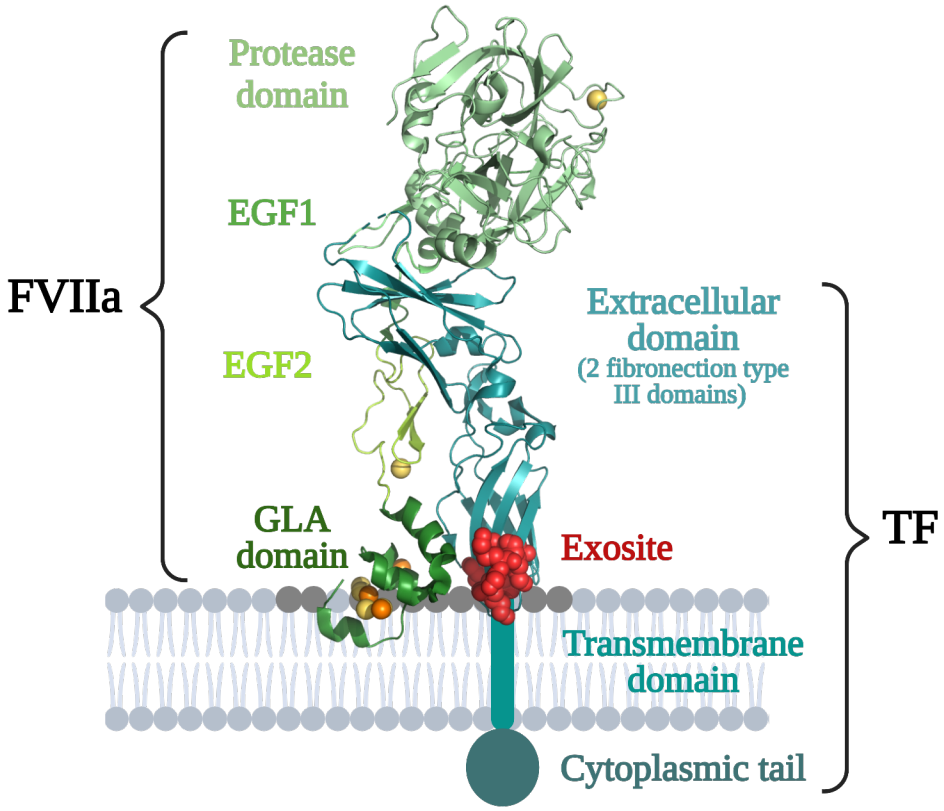

Figure 1.1 The tissue factor - factor VIIa complex. The crystal structure (PDB entry: 3TH2) of sTF (teal) in complex with FVIIa (green), arranged on a cartoon of the phospholipid bilayer (light gray) with phosphatidylserine (dark gray). Cartoon depictions of the TF transmembrane and cytoplasmic domains are added to the C-terminus of TF. FVIIa-bound divalent metal ions are Ca^{2+} (yellow spheres) and Mg^{2+} (orange spheres). The side chains of the TF exosite region are rendered in space-filling (red) and are located near the C-terminus of the sTF. Figure was created with BioRender.com and PyMOL.org.

The third hypothesis states that TF activity is regulated by dimerization, although both monomeric and dimeric TF show procoagulant activity.[35,36] The fourth hypothesis states that TF activity is regulated by localization to lipid rafts. This hypothesis is controversial, as TF located in lipid rafts appears to be both active and inactive.[37,38] The conflicting reports on TF encryption/decryption suggest that the regulation of TF activity is still not fully understood, and several steps might be required to achieve fully decrypted TF.

1.2.2 Factor VII/VIIa

FVII (the zymogen form of FVIIa) is a 406-amino-acid glycoprotein with a molecular weight of ~50 kDa. FVII is synthesized in the liver and then secreted into the blood stream, circulating in the plasma at a concentration of ~10 nM with 1% of the total concentration in the active form (~0.1 nM FVIIa).[39] Deletion of the FVII gene causes fatal perinatal bleeding in mice, highlighting the crucial role of FVII in hemostasis.[40] FVII is comprised of a C-terminal serine protease domain, two epidermal growth factor–like domains (EGF1 and EGF2) and a N-terminal γ-carboxyglutamic acid-rich (GLA) domain (Figure 1.1).[41,42] The domain structure of FVII is homologous to other clotting proteins, including FIX, FX and protein C.

The serine protease domain of FVII is essential for catalytic function, containing the catalytic triad (His^{193}, Asp^{242}, Ser^{344}) and a binding site for one functionally important Ca^{2+} ion.[43-45] A linker region between the protease domain and EGF2 domain contains the Ile^{153}-Arg^{152} bond. Proteolytic cleavage of this bonds leads to activation of FVII to FVIIa, resulting in two polypeptide chains (heavy and light chain) connected by the Cys^{135}-Cys^{262} disulfide bond. Proteolytic cleavage of FVII to FVIIa *in vitro* is triggered by several proteins, including TF-VIIa, FIXa, FXa, FXIIa, thrombin and plasmin.[46-51] However, the protease(s) responsible for cleavage *in vivo* are unclear. Following the cleavage site and EGF2 is the EGF1 domain, which contains another important Ca^{2+} binding site.[44,45] Connected to the EGF1 domain by a short aromatic stack is the GLA domain, which interacts with the phospholipid membrane. The GLA domain comprises ten vitamin K-dependent, post-translationally modified γ-carboxyglutamic acid (Gla) residues which coordinate seven Ca^{2+} ions.[44,52,53] Recent studies suggest that two or three of the Ca^{2+} ions might be replaced by Mg^{2+} ions under physiological conditions, modulating membrane binding and activity of FVIIa.[54-57]

1.2.3 The Tissue Factor – Factor VIIa Complex

The TF-FVIIa complex, the physiological activator of blood clotting, is a two-subunit enzyme composed of the regulatory subunit TF and the catalytic subunit FVIIa. The X-ray crystal structure of the complex shows how the flexible FVIIa wraps around the more rigid sTF (Figure 1.1).[44,58] The main points of interaction are between the EGF1 and serine protease domain of FVIIa and the N-terminal extracellular domain of TF. Interactions between the EGF2 and GLA-domain of FVIIa and the C-terminal extracellular domain of TF are minor. TF interactions are crucial for FVIIa activity. While FVIIa alone is a poor enzyme, in complex with TF, FVIIa's proteolytic activity is increased by up to a million-fold.[6,59,60] In its function as cofactor, TF modulates FVIIa activity in three ways by: (1) inducing a conformational change in the FVIIa active site (allosteric activation), (2) tethering FVIIa to the phospholipid membrane and (3) providing an extended binding site for macromolecular substrates.

Allosteric activation of FVIIa is achieved by TF-induced conformational changes in the FVIIa active site. Upon binding to TF, the catalytic efficiency (k_{cat}/K_m) of FVIIa hydrolysis of small peptidyl substrates (amidolytic activity) is increased by 100-fold, a process largely driven by increases in k_{cat}.[61,62] The conformational changes in FVIIa that lead to higher activity are numerous. Hydrogen-deuterium exchange experiments show that TF stabilizes several loops in the FVIIa protease domain.[63,64] Stabilization of the 170 loop, which is located close to the interaction site with TF, is important for FVIIa amidolytic activity.[65-67] In addition to stabilization, TF binding also repositions the FVIIa active site. While the active site of free FVIIa is located ~80Å above the membrane, the active site of FVIIa bound to TF is lowered by ~6Å which optimally positions it for cleavage of macromolecular substrates, including FIX and FX.[68,69] TF is even able to support GLA-domainless FVIIa in maintaining the same distance to the membrane.[70] These studies support the idea that TF is a fairly rigid protein that is able to optimally position the flexible FVIIa and maintain this position on the phospholipid membrane.

Interactions with the phospholipid membrane, particularly with PS, are crucial for TF-FVIIa activity.[71] TF-FVIIa substrate activation is increased by up to 100-fold in the presence of PS-containing liposomes.[60,72] PS supports TF-FVIIa activity in several ways. PS exposure after vascular injury is known to cause TF activation/decryption. Although the exact process is not fully understood, PS is likely to interact with residues at the C-terminus of the TF extracellular domain. MD simulation studies with both TF and TF-FVIIa have identified potential TF residues that

interact with PS headgroups.[28] Mutation of these membrane-interacting TF residues greatly decreases activation of FIX and FX.[27] In addition to interacting with C-terminal TF residues, PS also provides a surface for binding of FIX and FX. Like FVIIa, FIX and FX contain GLA-domains that preferentially bind negatively charged phospholipids, including PS.[73,74] PS helps bring FIX and FX in close proximity to the TF-FVIIa complex on the membrane, increasing the rate of substrate activation.[75] Interestingly, *in vitro* experiments require PS concentrations of >20% PS in the membrane to achieve full TF-FVIIa activity, while the *in vivo* concentrations of PS in the plasma membrane are only ~10%.[76] This observation led to the hypothesis that other, more abundant phospholipids might be able to substitute for the missing PS *in vivo*. Phosphatidylethanolamine (PE) is the primary phospholipid that synergizes with PS, decreasing the requirement for PS in the membrane.[29,77,78] Essentially any phospholipid headgroup other than choline is able to synergize with PS to enhance TF-FVIIa substrate activation ('ABC hypothesis' = Anything But Choline).[77] However, not just protein-phospholipid interactions are important for substrate activation, but also protein-protein interactions between TF-FVIIa and its substrates.

TF provides a putative substrate-binding site near the C-terminus of its extracellular domain. This solvent-exposed surface is termed the "exosite" and located ~60 Å away from the FVIIa active site, adjacent to membrane-interacting TF residues mentioned above. The exosite was first identified by site-directed mutagenesis studies.[79-81] The largest decrease in TF-FVIIa substrate activation was detected upon mutation of residues Tyr157, Lys159, Ser163, Gly164, Lys165, Lys166, Tyr185.[81,82] Lys165 and Lys166 are the most thoroughly studied and most essential exosite residues.[79,83,84] Mutation of these residues decreases TF-FVIIa activity up to 100-fold.[83,84] However, mutation of exosite residues has no effect on the amidolytic activity of FVIIa[83] which indicates that the exosite is primarily involved in macromolecular substrate activation. The TF exosite has a net positive charge, suggesting that it could interact with negatively charged Gla residues at the N-terminus of FX/FIX or with PS headgroups in the phospholipid membrane. This hypothesis is supported by experiments showing that TF exosite mutants were equivalent to wildtype TF in supporting activation of GLA-domainless FX.[84] Additionally, deletion of the GLA domain of FVIIa decreases FX activation.[72] This suggests that both the TF exosite and FVIIa Gla domain are involved in substrate activation, potentially by binding the GLA domain of FIX and FX. However, FIX and FX have a low affinity for TF-FVIIa[85] and a stable trimolecular complex

has not been generated yet. Novel approaches are needed to obtain structural data of this trimolecular complex.

Full TF-FVII activity is achieved by allosteric activation of FVIIa, exposure of PS and TF exosite interactions. However, additional regulation of TF-FVIIa is crucial to control hemostasis. Two natural anticoagulants that inhibit TF-FVIIa are antithrombin[86] and tissue factor pathway inhibitor (TFPI).[87] Antithrombin inhibits TF-FVIIa in the presence of heparin[88,89] and is the less potent of the two inhibitors.[90] TPFI inhibits TF-FVIIa in the presence of FXa, forming a quaternary complex. TPFI is a Kunitz-type inhibitor composed of three Kunitz domains. The Kunitz 1 domain binds FVIIa, while the Kunitz 2 domain binds FXa.[91] TF exosite residues play an important role in the inhibition of TF-FVIIa-FXa by TFPI.[92] TFPI has also been used as the basis to design artificial inhibitors with the goal to develop novel antithrombotic agents. One of these artificial inhibitors, named XK1, is a hybrid molecule of the light chain of FXa bound to the Kunitz 1 domain of TFPI.[93] XK1 is a potent inhibitor that binds TF-FVIIa with high affinity.[93] Although TF-FVIIa is a promising target for antithrombotic agents, current research focuses on clotting factors that are solely involved in thrombosis to avoid potential bleeding side effects.

1.3 The Contact Pathway and Common Pathway

In contrast to the tissue factor pathway, the contact pathway is dispensable for hemostasis *in vivo* but plays a major role in thrombosis.[4] The main clotting proteins in the contact pathway are the serine proteases factor XI (FXI), factor XII (FXII) and plasma prekallikrein (PK) as well as the non-enzymatic cofactor high-molecular-weight kininogen (HK). Deficiencies of FXII and PK are not associated with excessive bleeding,[94,95] supporting the hypothesis that the contact pathway is dispensable for hemostasis. In contrast, animal studies underline the role of these two proteins in protecting against thrombosis.[96-98]

The contact pathway is initiated by FXII, a ~80 kDa zymogen that circulates in plasma at a concentration of 375 nM.[99] Upon interaction with negatively charged surfaces or polymers, FXII undergoes a conformational change and is converted to its active form FXIIa via autoactivation.[100,101] FXIIa subsequently cleaves PK, a ~85 kDa zymogen that circulates in plasma bound to its cofactor HK. The resulting active form of PK is plasma kallikrein (PKa), which cleaves more FXII to FXIIa through a process known as reciprocal activation.[102,103] Similar to FXII, PK can also undergo autoactivation upon interaction with suitable surfaces and polymers.[104-106]

Once enough FXIIa is generated, it activates the zymogen FXI to its active form FXIa. Unlike other clotting proteins, FXI is a disulfide-linked dimer consisting of two ~80 kDa subunits, circulating in plasma bound to the cofactor HK.[107-109] The FXI subunits are structurally similar to PK, explaining why both proteins bind HK as a cofactor.[108] The FXIa-HK complex subsequently cleaves FIX. The ~57 kDa zymogen FIX serves as an interface between two blood clotting pathways, as it can be activated by both FXIa (contact pathway) and the TF-FVIIa complex (TF pathway).[110,111] FIXa, in complex with its cofactor factor VIIIa (FVIIIa), the activated form of FVIII, cleaves FX to FXa.[112] At the generation of FXa, the contact pathway and tissue factor pathway converge into the common pathway (Figure 1.2).

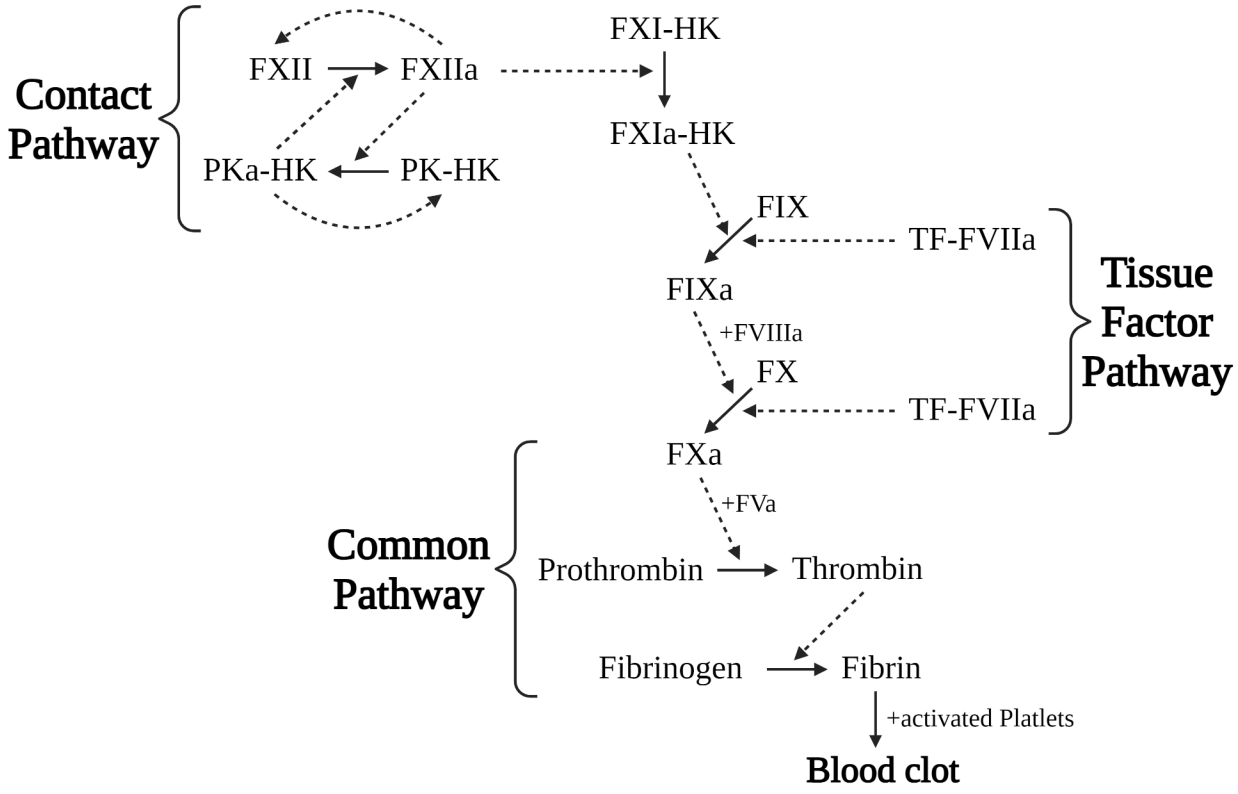

Figure 1.2 The coagulation cascade. Coagulation is initiated by two distinct pathways: the tissue factor (TF) pathway and the contact pathway. The TF pathway is initiated by TF-FVIIa which activates both FIX and FX to FIXa and FXa, respectively. The contact pathway is initiated by reciprocal activation of FXII to FXIIa by PKa-HK, and PK to PKa by FXIIa on negatively charged contact surfaces or polymers. Both FXII and PK-HK can also be activated through autoactivation by FXIIa and PKa-HK, respectively. Subsequently, FXIIa activates FXI-HK to FXIa-HK. FXIa-HK activates FIX to FIXa, which marks the intersection between the TF pathway and the contact pathway. FIXa bound to FVIIIa activates FX to FXa. Upon activation of FXa, the TF pathway and the contact pathway merge into the common pathway. FXa bound to FVa cleaves prothrombin to thrombin. Thrombin cleaves fibrinogen to fibrin (other functions of thrombin are not shown here for simplicity). Together with activated platelets, fibrin forms a stable blood clot. Figure was created with BioRender.com.

The common pathway of blood clotting starts with the zymogen FX, which can be activated to FXa either through the TF-FVIIa complex or the FIXa-FVIIIa complex.[4] FXa together with its cofactor factor Va (FVa), Ca^{2+} and phospholipids form the prothrombinase complex.[113,114] The prothrombinase complex goes on to activate prothrombin to thrombin, a highly abundant clotting protein with plasma concentrations in the micromolar range.[114,115] High thrombin concentrations are maintained through positive feedback loops.[116] Thrombin activates upward clotting enzymes and cofactors, including FV, FVIII and FXI, which accelerates thrombin generation.[116-118] As the final step in the clotting cascade, thrombin activates fibrinogen to fibrin.[119] Fibrin is present in plasma at high concentrations (up to 4 g/L), forming an interconnected mesh of fibrin strands which are stabilized by factor XIII (FXIII).[120-122] This fibrin mesh together with activated platelets forms a stable blood clot.

1.4 Serine Proteases beyond Blood Clotting

Serine proteases play important roles in many cellular processes beyond blood clotting. Within the hemostatic system, serine proteases participate in fibrinolysis. During fibrinolysis, the fibrin clot formed in the final step of coagulation is dissolved. The main enzymes involved in this process are plasmin, tissue plasminogen activator (tPA) and urokinase (uPA).[123] Plasmin is generated by tPA and uPA through cleavage of the zymogen plasminogen. Plasminogen is a ~92 kDa single-chain glycoprotein that is present in plasma at concentrations of 1-2 μM.[124] Cleavage by tPA and uPA yields the active enzyme plasmin which is composed of two polypeptide chains linked by a disulfide bond. Plasmin subsequently cleaves fibrin, dissolving the fibrin clot. All three fibrinolytic enzymes belong to the class of trypsin-like serine proteases.[124]

Beyond hemostasis, serine proteases play a crucial role in food digestion. Two of the most well-known serine proteases are the digestive enzymes trypsin and chymotrypsin. The zymogen form of trypsin, trypsinogen, is produced in the pancreas. Upon entering the small intestine, it is converted to trypsin by enterokinase.[125] Certain mutations in the trypsinogen gene can lead to premature activation of trypsin while the protein is still in the pancreas, causing pancreatitis.[126-128] Like trypsin, chymotrypsin is also produced in the pancreas in its zymogen form chymotrypsinogen. In the small intestine, trypsin activates chymotrypsinogen to chymotrypsin. Although chymotrypsin and trypsin prefer different cleavage sequences (trypsin selects for basic amino acids, chymotrypsin for aromatic amino acids), the enzymes have high sequence identity

and a similar tertiary structure.[129,130] The trypsins also share sequence similarities and cleavage preferences with many blood clotting and fibrinolytic enzymes.[124,130,131] The important role of serine proteases in many cellular processes makes these enzymes an interesting target for structure-function studies. These studies will help us to gain new insights into the regulation of serine proteases in blood clotting, fibrinolysis, digestion and many other processes.

Chapter 2 A Serine Loop in Tissue Factor Mediates Substrate Selectivity by the Tissue Factor - Factor VIIa Complex[a]

2.1 Introduction

The complex of TF and FVIIa triggers blood clotting in hemostasis and many thrombotic diseases.[132,133] TF is highly expressed in atherosclerotic plaques[134] and plays a major role in thrombosis associated with myocardial infarction[135] and ischemic stroke.[136] TF is an integral membrane glycoprotein that is present on the surface of many extravascular cells.[137] Upon vascular damage, TF is exposed to plasma and binds the serine protease FVIIa (Figure 2.1 A), yielding a two-subunit enzyme (TF-FVIIa) in which TF is the regulatory subunit and FVIIa is the catalytic subunit. In blood clotting, TF-FVIIa initiates clotting by proteolytically activating two substrates, the zymogens FIX and FX, which then propagate the clotting cascade (Figure 2.1 A). Although FX is the preferred substrate for TF-FVIIa under most conditions, it is unclear how TF-FVIIa selects between FIX and FX.[138]

Activation of both FIX and FX by TF-FVIIa is thought to be promoted by a solvent-exposed surface ("exosite") near the C-terminus of TF.[138-140] Defined by mutagenesis studies, the exosite appears to function as a putative substrate-binding site, located ~60 Å away from the active site of FVIIa (Figure 2.1 B). The exosite comprises TF residues Y157, K159, S163, G164, K165, K166 and Y185.[138] Mutation of TF residues in the exosite, especially K165 and K166, decreases FX and FIX activation by up to 100-fold, while FVIIa binding and allosteric activation are not impaired.[138,139,141] Although there are quantitative differences in the impact of specific exosite mutations on FIX versus FX activation, the magnitude of these differences is relatively small.[138]

The TF exosite partially overlaps a stretch of four consecutive serine residues, S160-S161-S162-S163 (Figure 2.1 B), that form a solvent-exposed loop which is unresolved in most soluble

[a] This chapter was adapted from a research article published in the Journal of Thrombosis and Haemostasis in accordance with the publisher's copyright privileges for publication in a dissertation. Full citation: Birkle, F, Morrissey, JH. A serine loop in tissue factor mediates substrate selectivity by the tissue factor–factor VIIa complex. *J Thromb Haemost* 2021; 19: 75– 84. https://doi.org/10.1111/jth.15087

TF crystal structures.[142,143] However, this loop connects to a region on the TF ectodomain that we previously proposed to interact with PS headgroups.[27,57] In the present study, we hypothesized that this flexible S160-S163 loop might function as a linker between the TF exosite and the nearby region that interacts with PS residues, and thus might mediate allosteric activation of the TF exosite when this protein engages PS. Accordingly, we hypothesized that changing the length of this loop could disrupt this allosteric linkage.

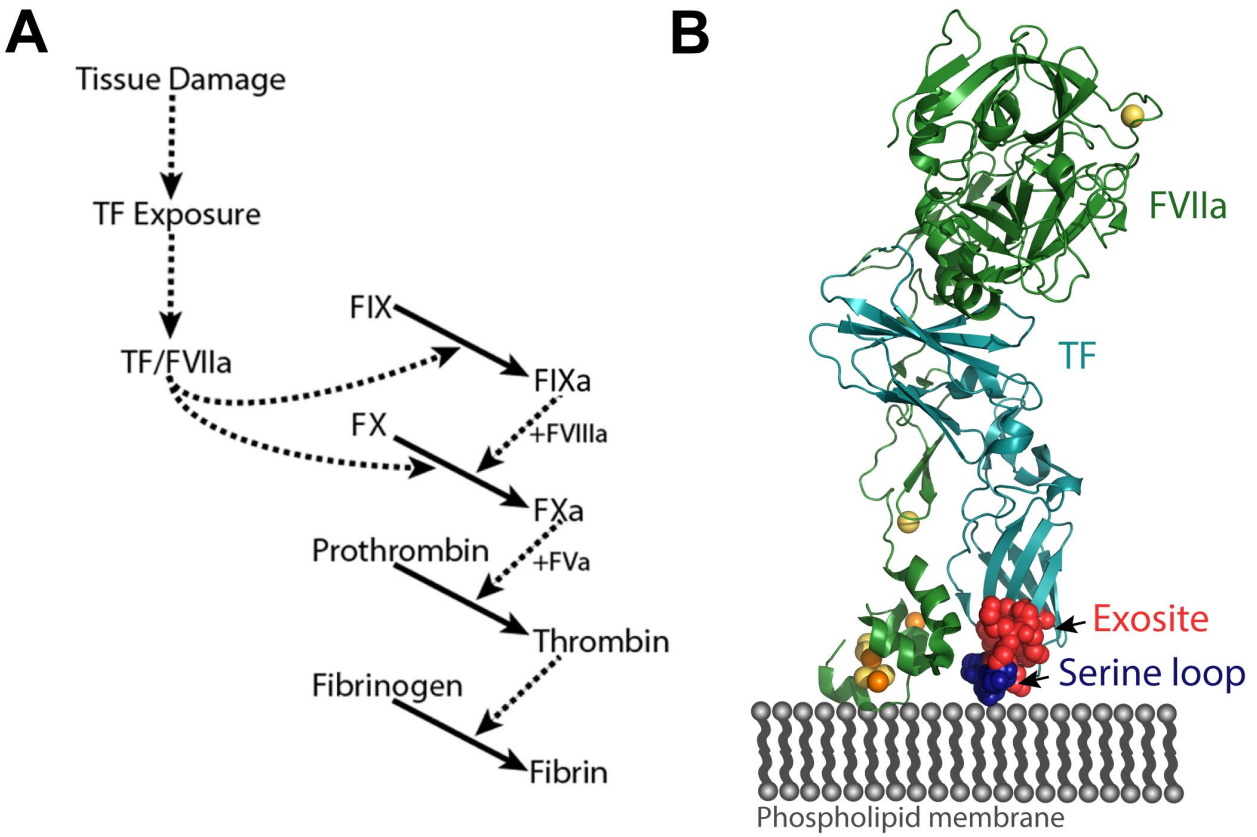

Figure 2.1 TF pathway of blood clotting and the structure of TF-FVIIa. (A) Upon vascular damage, TF is exposed to blood after which the TF-FVIIa complex activates its major substrates, FIX and FX by limited proteolysis. Downstream proteolytic reactions lead to thrombin generation and fibrin clot formation. (B) The crystal structure (PDB entry: 3TH2) of the isolated TF ectodomain (teal) in complex with FVIIa (green), arranged on a cartoon of the phospholipid bilayer (grey). Bound divalent metal ions are Ca^{2+} (yellow spheres) and Mg^{2+} (orange spheres). The side chains of the TF exosite region are rendered in space-filling (red) and are located near the C-terminus of the TF ectodomain. The TF serine loop S160-S163, which is also rendered in space filling (dark blue), is adjacent to both the exosite and the proposed location of the phospholipid membrane. Figure was created with Adobe Illustrator and PyMOL.org

To test this hypothesis, we generated an extensive set of TF exosite and serine loop mutants, including multiple deletions and insertions within the S160-S163 loop. We tested the activity of these mutants in substrate activation assays and thrombin generation assays. We now

report the surprising result that, while increasing or decreasing the length of the S160-S163 loop had little to no effect on the rate of FIX activation, inserting or deleting even a single serine residue within this loop decreased FX activation by up to 200-fold. These findings suggest that the precise length of the S160-S163 loop strongly contributes to substrate selectivity by TF-FVIIa.

2.2 Materials and Methods

2.2.1 Materials

Materials were from the following sources: 1-palmitoyl-2-oleoyl-sn-glycero-3-phosphocholine (POPC) and 1-palmitoyl-2-oleoyl-sn-glycero-3-phospho-L-serine (POPS), Avanti Polar Lipids (Alabaster, AL); Bio-Beads SM-2 absorbent, Bio-Rad Laboratories (Hercules, CA); recombinant human FVIIa, American Diagnostica (now Sekisui Diagnostics, Lexington, MA); FIX-immunodepleted plasma and purified human FIX, FIXa and FX, Haematologic Technologies (Essex Junction, VT); Pefachrome FIXa, DSM Nutritional Products Ltd., Branch Pentapharm (Parsippany, NJ); methoxycarbonyl-D-Nle-Gly-Arg-pNA acetate salt (FXa substrate), Bachem (Bubendorf, Switzerland); pooled normal plasma (PNP) and FVIII-deficient plasma (< 1% activity), George King Bio-Medical (Overland Park, KS); Thrombin Calibrator and FluCa-Kit (including Fluo-Buffer and Fluo-Substrate), Diagnostica Stago (Parsippany, NJ); and medium-binding microplates, Corning (Tewksbury, MA).

2.2.2 Production and relipidation of recombinant TF

Recombinant human membrane-anchored TF (residues 3-244) was expressed in *Escherichia coli* and purified as described.[78] Expression constructs for TF mutants with serine loop insertions and deletions had an N-terminal HPC4-epitope tag[144] and were generated by GenScript Biotech (Piscataway, NJ). They were purified by affinity chromatography using an HPC4-antibody column. TF mutants with serine loop substitutions had a N-terminal 6×His-tag and were generated using the Q5 site-directed mutagenesis kit from New England Biolabs (Ipswich, MA). These mutants were purified using nickel-NTA affinity chromatography. TF-liposomes were prepared by incorporating TF into phospholipid vesicles of varying composition (POPS and POPC) as described,[145] using 15 mM deoxycholate as the detergent.

2.2.3 Activation of FX and FIX

For most assays, initial rates of FX activation by TF-FVIIa were quantified using a continuous (one-stage) FX activation assay[22,146] in 96-well plates with the following modifications. TF-liposomes (0.6 nM TF, with 10 μM total phospholipid) and FVIIa (3 to 150 pM) were incubated in HBSA buffer (20 mM HEPES pH 7.4, 100 mM NaCl, 0.1% bovine serum albumin, 0.02% NaN_3) with 5 mM $CaCl_2$. Reactions were initiated by addition of 0.5 mM FXa substrate and 30 nM FX. The rate of change in A_{405} was measured at ambient temperature using a Spectramax 96-well spectrophotometer (Molecular Devices, San Jose, CA). Initial rates of FX activation in the presence of TF mutants were normalized to those measured in the presence of wild-type (WT) TF with the same phospholipid composition. K_m and k_{cat} values for FX activation were measured in discontinuous (two-stage) assays in 96-well plates. TF-liposomes and FVIIa (same concentrations as for the one-stage assay) were incubated in HBSA with 5 mM $CaCl_2$ at 37° C for 5 min, after which we initiated reactions by adding 25 to 400 nM FX. Timed, 10 μL aliquots were taken over 20 min and quenched on ice in a microwells containing 80 μL stop buffer (made by mixing, in each well, 50 μL of 2× concentrated HBSA plus 20 mM EDTA, and 30 μL water). For the second stage, plates were warmed to ambient temperature and 10 μL of 5 mM FXa substrate (0.5 mM final) was added per well, after which the rate of change in A_{405} was measured. Rates of chromogenic substrate hydrolysis were then converted to FXa concentrations by reference to a standard curve. To extract K_m and k_{cat} values, initial rates of FX activation were plotted versus FX concentration, to which the Michaelis-Menten equation was fitted by nonlinear regression.

Initial rates of FIX activation by TF-FVIIa were quantified using a discontinuous (two-stage) FIX activation assay in 96-well plates. TF-liposomes (10 nM TF, with 175 μM total phospholipid) and FVIIa (1 nM) were incubated in HBSA with 5 mM $CaCl_2$ at 37° C for 5 min. Reactions were initiated by addition of 2 μM FIX. Timed, 10 μL aliquots were taken over the course of 5 min and quenched on ice in a microwell containing 80 μL stop buffer (made by mixing, in each well, 50 μL of 2× concentrated HBSA plus 20 mM EDTA, and 30 μL of 75% (v/v) ethylene glycol). For the second stage, the plates were warmed to ambient temperature and 10 μL 5 mM Pefachrome FIXa (0.5 mM final) was added per well, after which the rate of change in A_{405} was measured. Rates of chromogenic substrate hydrolysis were then converted to FIXa concentrations by reference to a standard curve. Initial rates of FIX activation in the presence of TF mutants were normalized to those measured in the presence of WT TF with the same phospholipid composition.

Measurement of rates of FIX activation for determining k_{cat} and K_m values used the same two-stage assay configuration, with 0.1 to 2 μM FIX and with 10 μL aliquots taken over the course of 10 min. Initial rates of FIX activation were then plotted versus FIX concentration, to which the Michaelis-Menten equation was fitted by nonlinear regression.

2.2.4 Thrombin generation

Thrombin generation in clotting plasma was measured using the calibrated automated thrombogram (CAT) assay (using Thrombinoscope reagents and software; Diagnostica Stago).[147,148] TF-liposomes (made with either WT TF or the 3S2T mutant) were diluted in HBSA to yield TF concentrations that generated a similar lag time. For 20% POPS/80% POPC liposomes, this was 60 pM WT TF or 15 nM 3S2T TF as well as 6 pM WT TF or 1.5 nM 3S2T TF. For 10% POPS/90% POPC liposomes, this was 30 pM WT TF or 30 nM 3S2T TF. Final phospholipid concentrations in all cases were 60 μM (made by supplementing with TF-free liposomes of the same phospholipid composition). CAT assays were performed in 96-well plates by mixing 20 μL TF and 80 μL plasma (PNP, FVIII-deficient or FIX-immunodepleted plasma) at 37° C for 10 min. The reaction was then started by adding pre-warmed 20 μL FluCa buffer. The change in fluorescence was measured using a Fluoroskan Microplate Fluorometer (ThermoFisher Scientific, Waltham, MA), and converted to thrombin concentrations using Thrombinoscope software according to the manufacturer's recommendations. Measured parameters (lag time, peak thrombin, and time to peak (ttPeak) for deficient plasmas were normalized to PNP for WT and mutant TF to generate a fold-change.

2.2.5 Production of XK1

XK1, a slow, tight-binding inhibitor of the TF-FVIIa complex, is an engineered hybrid protein consisting of the human FX light chain linked to the Kunitz 1 (K1) domain of human tissue factor pathway inhibitor.[149] The XK1 coding sequence was prepared in the pcDNA3.1(+) expression vector by GenScript Biotech (Piscataway, NJ) and transfected into HEK293/VKOR cells (HEK293 cells that overexpress vitamin K 2,3-epoxide reductase C1, the expression vector for which was a kind gift of Darrell Stafford). These cells were cultured in cell factories (Corning HYPERFlask M Cell Culture Vessel) in a 1:1 mixture of DMEM and F12 media supplemented with L-Glutamine, 15 mM HEPES (Corning), 10 μg/mL vitamin K1 (Phytonadione, Henry Schein Medical, Melville, NY), 2 μg/mL puromycin and 400 μg/mL G-418. XK1 levels in culture

supernatants were measured using the FX ELISA from Enzyme Research Laboratories (South Bend, IN). XK1 was affinity-purified from cell supernatants using immobilized 4G3, a Ca^{2+}-dependent mouse monoclonal antibody targeting the human FX light chain.[150] Fully carboxylated XK1 was subsequently separated from any undercarboxylated protein via anion-exchange chromatography as previously described for recombinant factor VII.[151]

2.2.6 Inhibition of TF-FVIIa by XK1

The ability of XK1 to inhibit the TF-FVIIa complex was assessed by quantifying its effects on the rate of FX activation, using a modification of the continuous FX activation assay described above. TF-liposomes (0.6 nM TF, with 10 μM total phospholipid) and FVIIa (3 - 150 pM) were incubated in HBSA with 5 mM $CaCl_2$. Varying concentrations (0 – 100 nM) of XK1 were added, and after 5 min, reactions were initiated by addition of 0.5 mM FXa substrate and 30 nM FX. The rate of change in A_{405} was measured at ambient temperature. FX activation rates for WT or mutant TF in the presence of different XK1 concentrations were normalized to activation rates in the absence of XK1.

2.3 Results

2.3.1 The precise length of the TF serine loop is essential for activation of FX but not FIX

We performed mutagenesis studies to investigate the role of the TF serine loop S160-S163 in substrate activation. Multiple sequence alignment showed that the TF serine loop region is highly conserved, especially among mammals (Figure 2.2 A). Thus, S161, S162 and S163 are almost always serine or the similar amino acid, threonine, while S160 is less well conserved. Notably, the length of the solvent exposed loop is always exactly four amino acid residues. Based on the alignment, we generated a total of fifteen TF serine loop mutants (Table 2.1).

The first set of mutants tested how replacing each of the four serine residues individually with threonine affected substrate activation rates. The S161T substitution was without effect on FX activation, while the S160T, S162T and S163T substitutions decreased the rate of FX activation by up to 3-fold (Figure 2.2 B). On the other hand, replacing any of these four serine residues with threonine had little effect on the rate of FIX activation (Figure 2.2 C).

We next tested how changing the length of this loop affected substrate activation rates. We therefore generated mutants with deletions of one or two serine residues (termed 2S or 3S),

insertion of one, two or three serines (termed 5S, 6S or 7S), insertion of one threonine residue after serine 163 (termed 4ST) or replacement of serine 163 with threonine together with insertion of an additional threonine (termed 3S2T). To create longer runs of serine residues without insertions, we also replaced the adjacent residues K159 and G164 with serine (K159S and G164S, respectively). We also attempted to delete 3 serines or all 4 serines, but the resulting constructs did not express detectable protein and are therefore not listed in Table 1. The remaining TF mutants were successfully expressed, purified, and tested for their ability to support FIX and FX activation by TF-FVIIa.

We found that any insertions or deletions within this serine loop profoundly diminished the rate of FX activation, with reductions ranging from 62.5-fold to 200-fold (Figure 2.2 D). In contrast, changing the length of the serine loop had much more modest effects on the rate of FIX activation (Figure 2.2 E). Lengthening the serine loop was relatively benign toward FIX activation, as the 5S mutant supported essentially wild-type levels of FIX activation while the 6S and 7S mutants supported FIX activation at levels that were reduced less than 2-fold relative to wild type. Shortening the serine loop resulted in somewhat diminished FIX activation rates (2.3-fold and 4.6-fold for the 2S and 3S mutants, respectively), although these reductions were far less than when FX was the substrate (Figure 2.2 D and 2.2 E). Increasing the length of the serine loop by one residue via inserting a threonine residue, with or without replacing Ser163 with threonine (the 4ST or 3S2T mutants, respectively), resulted in only a 1.3-fold reduction in the rate of FIX activation but caused the most profound reductions in the rate of FX activation (158-fold and 200-fold, respectively). Finally, changing the run of serine residues from four to five in a row via substituting the adjacent lysine or glycine residues with serine (K159S or G164S) caused less than a 2-fold reduction in the rate of FIX activation but a 55-fold or 6-fold reduction in the rate of FX activation, respectively.

When we directly compared the relative reductions in the rate of FIX activation versus factor X activation (last column in Table 2.1), we found the largest differential in rates when just one serine residue was inserted in the loop and one serine was substituted to threonine (3S2T). This TF mutant exhibited almost a 150-fold greater reduction in the rate FX activation relative to its impact on FIX activation. Together, these results show that the precise length of the serine loop is crucial for TF-FVIIa-mediated FX activation, but far less important for FIX activation.

Next, we investigated the role of the TF serine loop in greater detail by determining K_m and k_{cat} values for FX and FIX activation supported by WT TF versus the 3S2T mutant (Figure 2.2 F and 2.2 G). For FX activation, the K_m was increased 3.4-fold for the 3S2T mutant relative to WT, while the k_{cat} was decreased over 50-fold (Table 2.2). In contrast, the K_m and k_{cat} values for FIX activation varied by only 1.4- and 1.2-fold when comparing the 3S2T mutant to WT TF (Table 2.2). Thus, the 3S2T mutation decreased the k_{cat}/K_m for FX by 181-fold while decreasing the k_{cat}/K_m for FIX by only 1.76-fold. These results demonstrate that FX activation supported by 3S2T is significantly reduced due to changes in substrate binding and turnover.

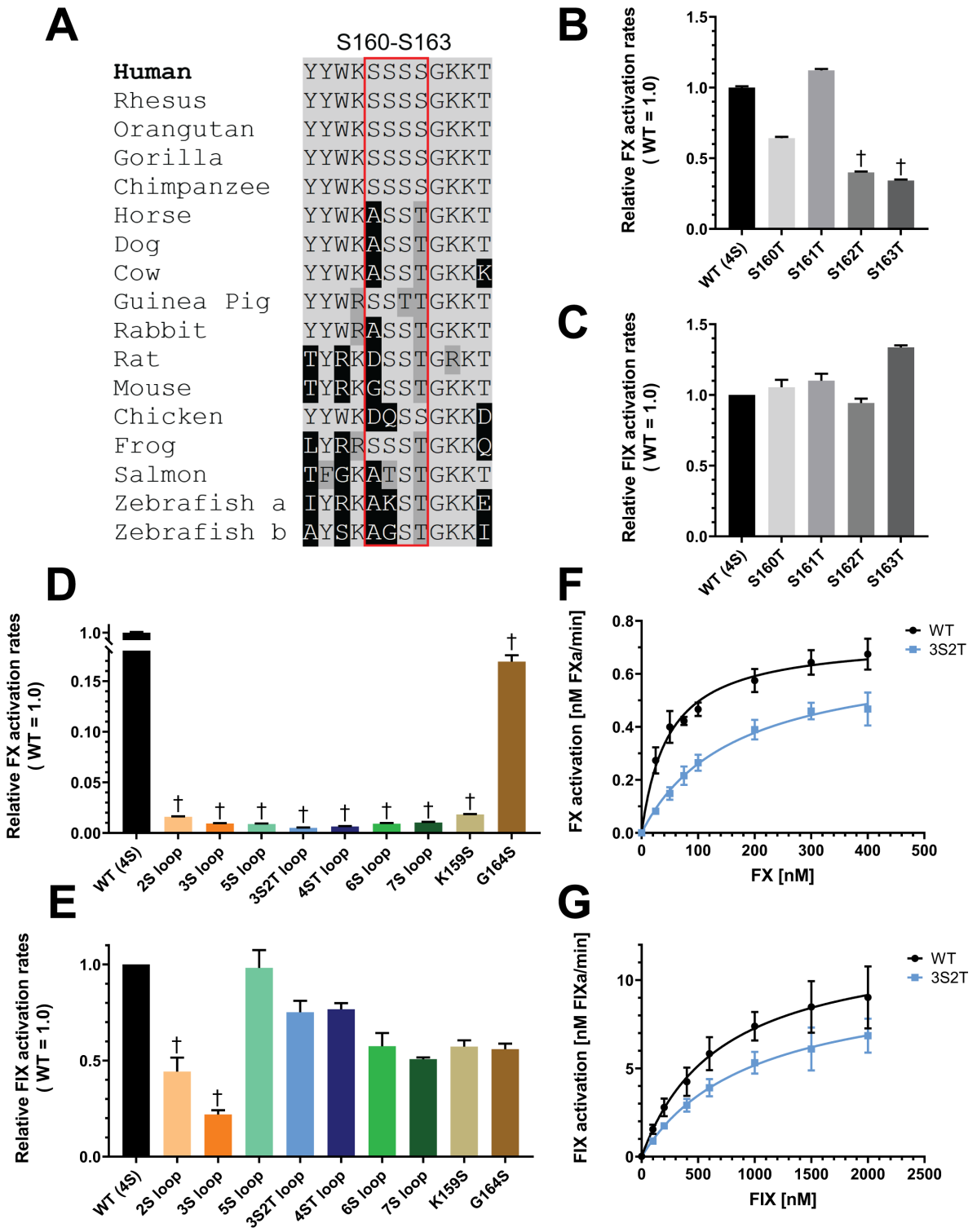

Figure 2.2 Changes in the length of the TF serine loop differentially effect rates of FIX vs. FX activation. (A) Multiple sequence alignment of TF serine loop region was performed using the online tool T-Coffee (https://www.ebi.ac.uk/Tools/msa/). The alignment shows TF residues 156-168 (numbering according to human TF). Serine loop residues S160-S163T are marked by red box. (B-E) Initial rates of FIX and FX activation by TF-FVIIa

(using WT or mutant TF in 20% POPS/80% POPC liposomes) were measured, and the rates obtained with TF mutants were normalized to those with WT TF. Relative rates that were more than twofold lower than WT are indicated with a dagger. (B) Relative rates of FX activation with TF mutants S160T, S161T, S162T and S163T. (C) Relative rates of FIX activation with TF mutants S160T, S161T, S162T and S163T. (D) Relative rates of FX activation with TF mutants of different serine loop length or composition. (E) Relative rates of FIX activation with TF mutants of different serine loop length or composition. (F, G) Kinetics of the activation of FX (F) or FIX (G) supported by WT TF or the 3S2T mutant. Initial rates of substrate activation were plotted versus substrate concentration, to which the Michaelis-Menten equation was fitted. All data are mean ± SE ($n \geq 3$).

Table 2.1 TF serine loop mutations.

TF mutant	Amino acid sequence*	Change in loop length	FIX/FX ratio**
WT (4S)	KSSSSG	0	1
S160T	K**T**SSSG	0	1.6
S161T	KS**T**SSG	0	1
S162T	KSS**T**SG	0	2.4
S163T	KSSS**T**G	0	3.9
2S	KSS - - G	−2	28
3S	KSSS - G	−1	24
5S	KSSSS**S**G	+1	111
3S2T	KSSS**TT**G	+1	147
4ST	KSSSS**T**G	+1	121
6S	KSSSS**SS**G	+2	63
7S	KSSSS**SSS**G	+3	49
K159S	**S**SSSSG	0	31
G164S	KSSSS**S**	0	3

*Amino acid sequences of human TF from positions 159-164 are given. Substitutions are in bold, insertions are in bold underline, and deletions are indicated with dashes.
**FIX/FX ratios were calculated for each TF mutant by dividing the relative rate of FIX activation by the relative rate of FX activation, from the values plotted in Figure 2.2 B-E.

Table 2.2 Kinetics of FX and FIX activation by TF-FVIIa.

TF variant	Substrate	K_m [nM]*	Fold increase in K_m [3S2T/WT]	k_{cat} [sec^{-1}]*	Fold decrease in k_{cat} [WT/3S2T]	k_{cat}/K_m [$M^{-1}sec^{-1}$]
WT	FX	48 ± 10	3.4	4.07 ± 0.23	51.3	8.5×10^7
3S2T	FX	163 ± 40		0.076 ± 0.008		4.7×10^5
WT	FIX	700 ± 233	1.4	0.21 ± 0.03	1.2	3.0×10^5
3S2T	FIX	974 ± 297		0.17 ± 0.03		1.7×10^5

*K_m and k_{cat} values are derived from plots in Figure 2.2 F and 2.2 G.

2.3.2 TF serine loop provides selectivity for FX over FIX

We further tested if the TF serine loop provides substrate selectivity in human plasma using calibrated automated thrombogram (CAT) assays.[147] In this study, we compared thrombin generation triggered by WT TF versus the 3S2T mutant (incorporated into liposomes with either 20% POPS/80% POPC or 10% POPS/90% POPC), using PNP, FIX-immunodepleted and FVIII-deficient human plasmas. Figure 2.3 reports three parameters from the thrombin generation curves: lag time, time to peak (ttPeak), and peak thrombin. For each combination of TF and lipids, the parameters were normalized to those obtained with PNP. The absolute values of these parameters are available in Figure S 2.1.

Thrombin generation by the 3S2T mutant was significantly altered in FIX- and FVIII-deficient human plasmas relative to WT TF. Thus, the lag time was prolonged up to 1.5-fold in FIX- and FVIII-deficient plasmas relative to PNP for 3S2T in both lipid compositions, while the only significant prolongation in lag time with WT TF (relative to PNP) was seen with FIX-deficient plasma using TF in 10% POPS/90% POPC liposomes (Figure 2.3 A and 2.3 B). A larger difference was encountered with the ttPeak parameter, which was prolonged up to 2-fold in FIX- and FVIII-deficient plasmas relative to PNP with the 3S2T mutant in both lipid compositions (Figure 2.3 C and 2.3 D). In contrast, WT TF showed a significant prolongation only with FVIII-deficient plasma, and the magnitude of the prolongation was smaller than that observed with the 3S2T mutant. Similarly, the peak thrombin level was decreased 2- to 3-fold in FIX- and FVIII-deficient plasmas relative to PNP triggered with the 3S2T mutant in both lipid compositions (Figure 2.3 E and 2.3 F). When triggered by WT TF, however, the peak thrombin level was only significantly reduced in FVIII-deficient plasma using TF in 20% POPS/80% POPC liposomes, or in FIX-deficient plasma using TF in 10% POPS/90% POPC liposomes.

To investigate if thrombin generation was more FIX-dependent at lower TF concentrations, we reduced the TF concentrations another tenfold (to 1 pM WT and 0.25 nM 3S2T). Figure S 2.2 shows that both TF concentrations followed the same trends for lag time, ttPeak and peak thrombin in WT and 3S2T. The difference in ttPeak between WT and 3S2T was somewhat more amplified with lower TF concentrations, however.

These results demonstrate that triggering of the plasma clotting cascade by the 3S2T mutant exhibits a significantly increased dependence on FIX and FVIII for thrombin generation relative to when the clotting is triggered by WT TF.

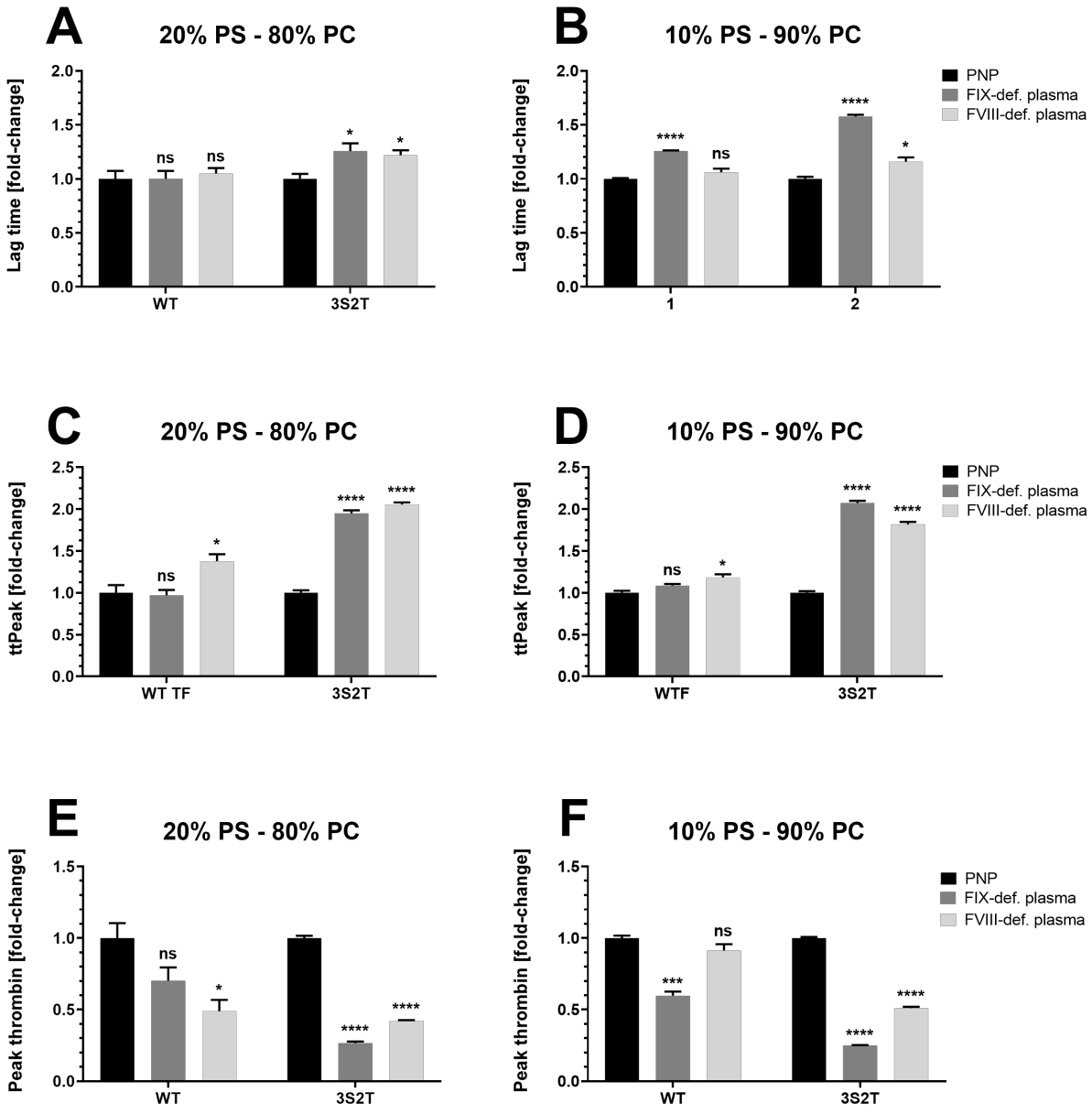

Figure 2.3 Substrate selectivity of TF serine loop mutants detected via thrombin generation assay. WT or mutant TF were incorporated in liposomes containing 20% POPS/80% POPC or 10% POPS/90% POPC. TF-liposomes were incubated with PNP, FIX-deficient plasma or FVIII-deficient plasma and thrombin generation was measured over 60 min in CAT assays. Lag time, ttPeak and peak thrombin obtained with deficient plasmas were normalized to the values obtained with PNP for each type of TF. Changes in lag time, ttPeak and peak thrombin for deficient plasmas that were significantly different from PNP are indicated with asterisk (t-test, $p < 0.05$; ns = not significant). (A) Fold-change in lag time for WT versus 3S2T TF in 20% POPS/80% POPC. (B) Fold-change in lag time for WT versus 3S2T TF in 10% POPS/90% POPC. (C) Fold-change in ttPeak for WT versus 3S2T TF in 20% POPS/80% POPC. (D) Fold-change in ttPeak for WT versus 3S2T TF in 10% POPS/90% POPC. (E) Fold-change in peak thrombin for WT versus 3S2T TF in 20% POPS/80% POPC. (F) Fold-change in peak thrombin for WT versus 3S2T TF in 10% POPS/90% POPC. All data are mean ± SE ($n \geq 3$).

2.3.3 Serine loop provides substrate selectivity through differential regulation of the TF exosite

The serine loop of TF is immediately adjacent to, and partially overlaps, the putative exosite region defined by prior mutagenesis studies. It also overlaps a region that we previously identified as a putative PS-binding region on the TF ectodomain.[27,57] We therefore hypothesized that the serine loop could act as a "connector" that regulates the activity of the adjacent substrate-binding exosite. To test this hypothesis, we generated TF constructs with mutations in both the serine loop (3S2T) and the exosite (either K165A, K166A, or the K165A- K166A double mutant). These TF mutants were incorporated into 20% POPS/80% POPC liposomes and tested in FIX and FX activation assays, normalized to the rates with WT TF (Figure 2.4 A and 2.4 B). By themselves, the exosite mutations resulted in 11- to 104-fold reductions in the rate of FX activation but more modest (1.2- to 4.5-fold) reductions in FIX activation. The 3S2T mutant exhibited a 103-fold reduction in FX activation by itself, with some further reduction observed in the rate of FX activation in conjunction with the exosite mutants. On the other hand, the 3S2T mutation resulted in only a 1.2-fold reduction in FIX activation by itself, with further reductions when combined with the exosite mutations.

In order to clarify the combined effect of these mutations, we replotted the data from Figure 2.4 A and 2.4 B in Figure 2.4 C and 2.4 D, respectively. In this case, the FX or FIX activation data using the combined 3S2T and exosite mutations were normalized to the rates obtained with the 3S2T mutant. With FX as substrate (Figure 2.4 C), exosite mutations that resulted in 11-, 18-, or 104-fold reductions in the activation rate instead resulted in a much more modest relative reduction of 1.8-, 2.1- or 2.8-fold when combined with the 3S2T mutation (as normalized to the rate with the 3S2T mutation alone). On the other hand, when FIX was substrate, the exosite mutations resulted in very similar fold reductions in activation rates with or without the 3S2T mutation (Figure 2.4 D). In summary, when FX was the substrate, the exosite mutations were epistatic to the serine loop mutations, whereas when FIX was the substrate, the effects of the exosite and serine loop mutations appeared to be independent. Overall, these results are consistent with the idea that the serine loop regulates the TF exosite during FX activation but not FIX activation.

The substantial reductions in FX activation brought about by the exosite mutations might mask the effects of the loop mutations. To address this question, we performed FX activation assays in the presence of a TF-FVIIa inhibitor, XK1 (Figure 2.4 E). XK1 is a hybrid protein consisting of the FX light chain linked to the first Kunitz 1 domain of tissue factor pathway

inhibitor.[149] It is a slow, tight-binding inhibitor that was designed to be recognized by TF-FVIIa as a pseudosubstrate.

In the presence of TF exosite mutants K165A, K166A and K165A-K166A, 7- to 16-fold higher XK1 concentrations are required to inhibit FX activation relative to WT TF (WT IC_{50} = 44±2 pM, K165A IC_{50} = 305±18 pM, K166A IC_{50} = 394±88 pM, and K165A-K166A IC_{50} = 693±34 pM). In contrast, in the presence of TF serine loop mutant 3S2T, 24-fold higher XK1 concentrations were needed to inhibit TF-FVIIa relative to WT TF (3S2T IC_{50} = 1063±64 pM). Somewhat surprisingly, for TF with mutations in both the serine loop and exosite (3S2T-K165A, 3S2T-K166A and 3S2T-K165A-K166A) the IC_{50} values for XK1 were somewhat lower than those observed with the 3S2T mutant alone (3S2T-K165A IC_{50} = 717±35 pM, 3S2T-K166A IC_{50} = 710±34 pM, and 3S2T-K165A-K166A IC_{50} = 757±46 pM). These results are consistent with the idea that the exosite mutations are epistatic to the TF serine loop mutations regarding the recognition of FX as a TF-FVIIa substrate.

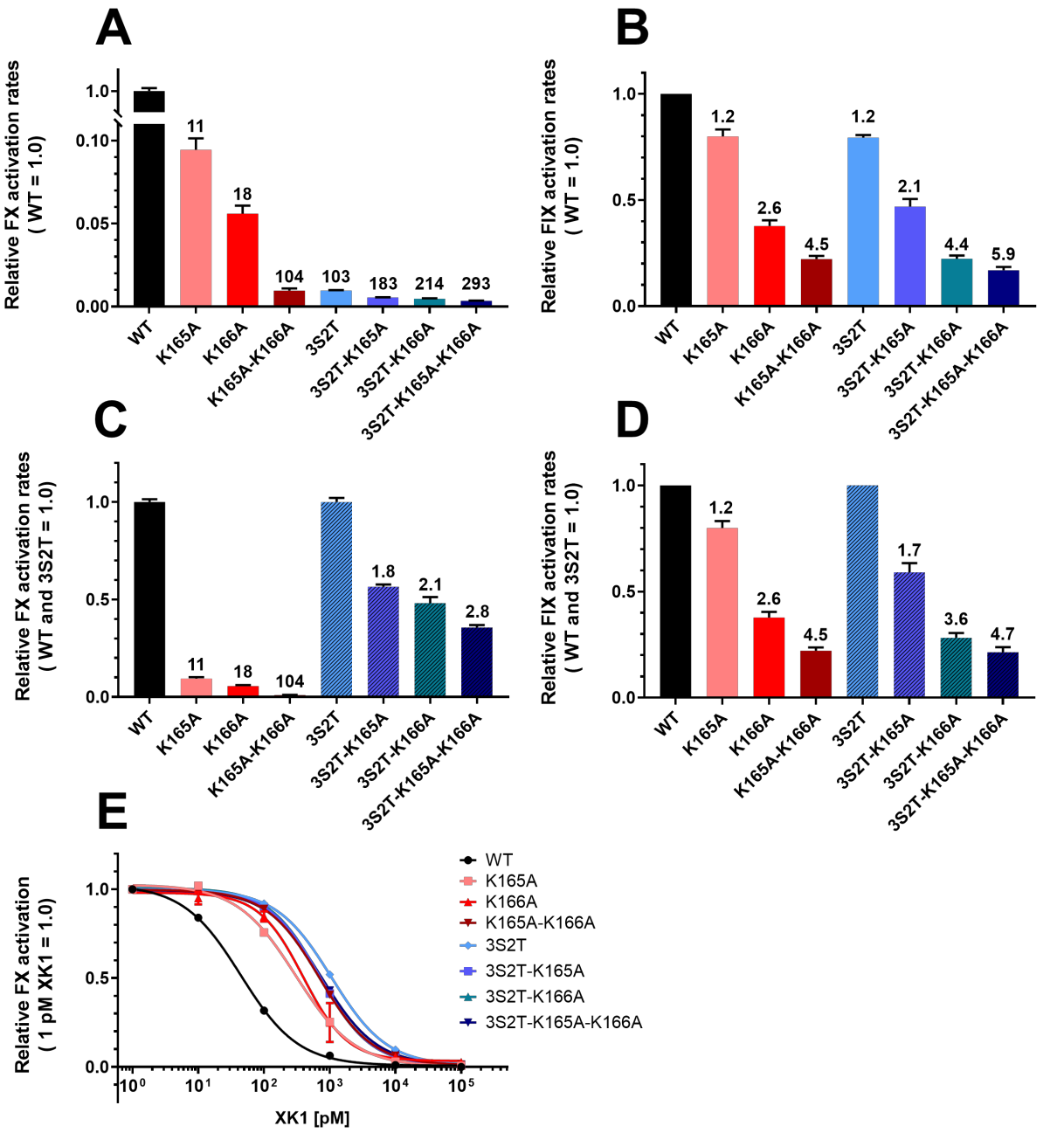

Figure 2.4 TF serine loop regulates the TF exosite for activation of FX but not FIX. Initial rates of FIX and FX activation by TF-FVIIa were measured using WT or mutant TF in 20% POPS/80% POPC liposomes. (A) Relative rates of FX activation and (B) FIX activation with TF mutations in the exosite (K165A, K166A and K165A-K166A), serine loop (3S2T), or both the exosite and serine loop (3S2T-K165A, 3S2T-K166A and 3S2T-K165A-K166A). Activation rates in panels A and B with mutant TF were normalized to those obtained with WT TF. Numbers above the bars are fold-reduction in rate, relative to WT. (C, D) Replotting of the data from panels A and B to more clearly visualize the combination of exosite and serine loop mutations. In each panel, rates obtained with exosite mutants (K165A, K166A and K165A-K166A) are normalized to WT TF, while the rates obtained with combination exosite and serine loop mutants (3S2T-K165A, 3S2T-K166A and 3S2T-K165A-K166A) are normalized to the 3S2T mutant. Normalization to 3S2T in panels C and D is indicated by striped bars. Accordingly, numbers above the bars in panels C and D are the fold-reduction in rate, relative to WT for the exosite mutants (K165A, K166A and K165A-K166A),

or relative to 3S2T for combination mutants (3S2T-K165A, 3S2T-K166A and 3S2T-K165A-K166A). (E) Ability of XK1 to inhibit TF-FVIIa. Relative rates of FX activation by TF-FVIIa were measured in the presence of increasing XK1 concentrations, using TF with mutations in exosite (K165A, K166A and K165A-K166A), serine loop (3S2T), or both (3S2T-K165A, 3S2T-K166A and 3S2T-K165A-K166A). All data are mean ± SE ($n \geq 3$).

2.4 Discussion

This study probed how TF-FVIIa selects between its major protein substrates, FIX and FX. We now report that substrate selectivity is strongly influenced by the TF serine loop, S160-S163, with the precise length of this loop being crucial for FX activation but relatively unimportant for FIX activation. FIX activation was especially tolerant of insertions within this loop. To our knowledge, no prior study has reported TF mutations that differentially decrease substrate activation (FIX versus FX) to the extent observed here with serine loop mutations. Numerous studies have previously identified the importance of TF exosite residues in substrate activation,[138-141,152] with some exosite mutations having a bigger effect on activation of FX than FIX.[138,153] However, none of those studies reported such a strong influence on one substrate over another as we observed with the serine loop mutations in this study.

Previous mutational studies defined the putative substate-binding exosite of TF as including residues Y157, K159, S163, G164, K165, K166,[138-140] a sequence which partially overlaps the serine loop. We also note that nearby residues, like the more N-terminal parts of the serine loop and immediately adjacent residues are postulated to interact with PS in the phospholipid membrane.[27,57] Whether our findings indicate that the serine loop is actually part of the TF exosite or if it modulates the adjacent exosite is not entirely clear and will require further study. Curiously, we found that exosite mutations were epistatic to the serine loop mutations when FX was the substrate, but not when FIX was the substate. Elucidating the physical basis for this epistasis will take further study, but this finding is consistent with the notion that the serine loop mediates the regulation of the adjacent TF exosite when FX is the substrate, but not FIX. The activity of TF-FVIIa is tightly regulated by the presence PS in the membrane.[154,155] Recently, our lab showed that exosite-adjacent TF residues, which are predicted to interact with the phospholipid membrane,[156] are also involved in regulating substrate activation.[27,57] Thus, the serine loop may play a role in positioning of the exosite for optimal interaction with FX, via transducing information from interaction of the TF ectodomain with anionic phospholipid headgroups.

The TF-FVIIa complex is known to have additional protein substates, including FVII[157] and proteinase-activated receptors (PARs)—in particular, PAR2.[158,159] In further studies, it would

be interesting to examine the role of the TF serine loop in recognizing these alternative macromolecular substrates. Overall, our study provides insights into the mechanisms of substrate selectivity by TF-FVIIa, showing an unexpected role for the serine loop of TF.

2.5 Supplementary Information

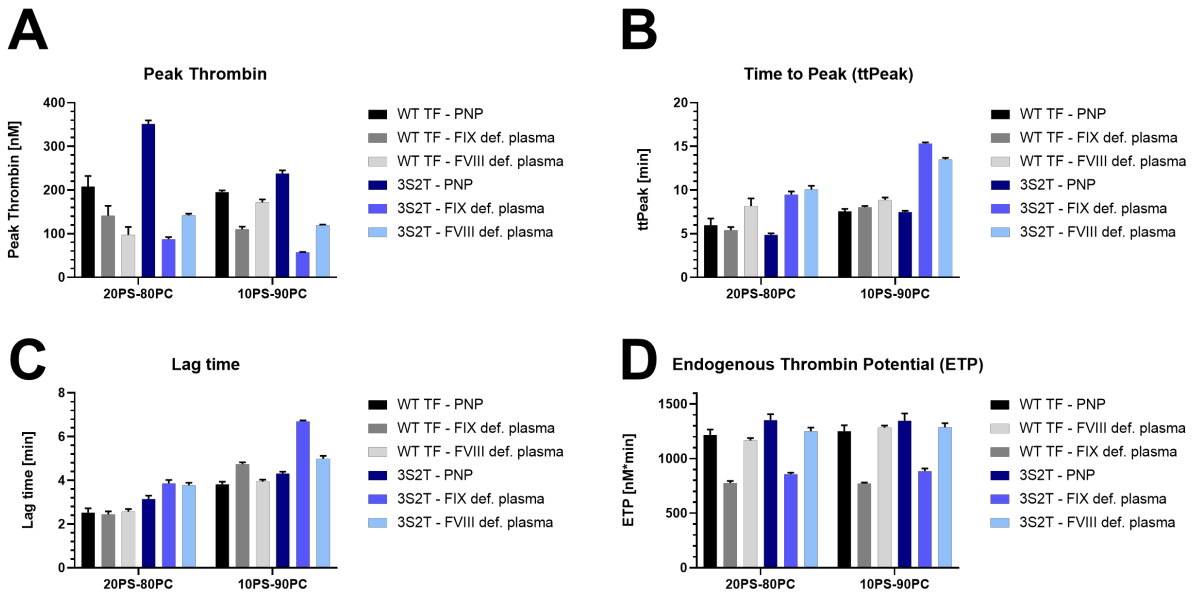

Figure S 2.1 Absolute values for peak thrombin, ttPeak, lag time and endogenous thrombin potential (ETP) in thrombin generation assays. WT or mutant TF 3S2T were incorporated in liposomes containing 20% POPS/80% POPC or 10% POPS/90% POPC. TF-liposomes were incubated with PNP, FIX-deficient plasma or FVIII-deficient plasma. Thrombin generation was measured over 60 min in CAT assays. Peak thrombin, ttPeak, lag time and ETP were determined from thrombin generation curves. (A) Peak thrombin for WT TF and 3S2T. (B) ttPeak for WT TF and 3S2T. (C) Lag time for WT TF and 3S2T. (D) ETP for WT TF and 3S2T. All data are mean ± SE ($n \geq 3$).

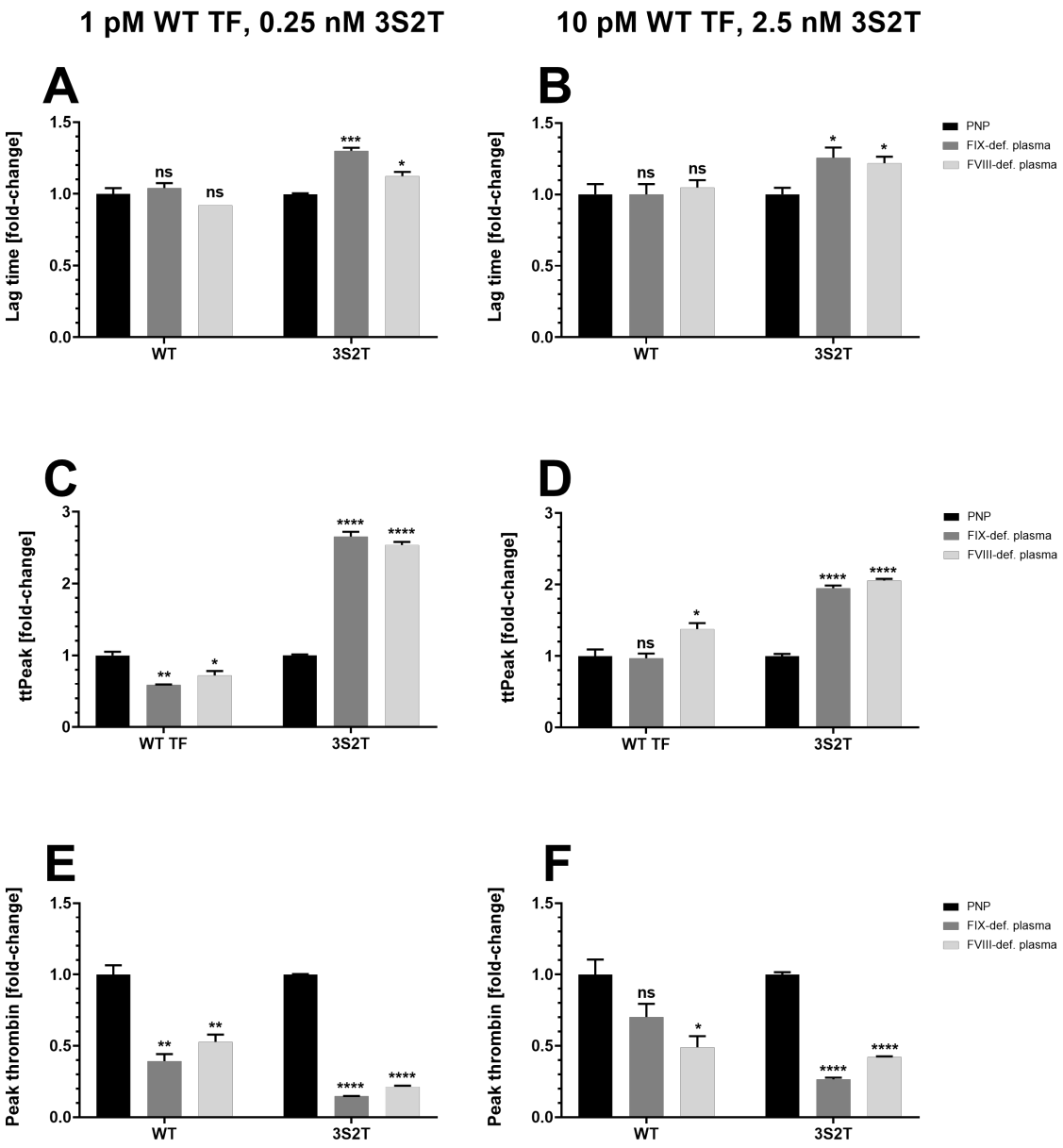

Figure S 2.2 Comparison of the effect of two different TF concentrations (WT and 3S2T mutant) in the thrombin generation assay. WT or mutant TF were incorporated in liposomes containing 20% POPS/80% POPC. TF-liposomes were incubated with PNP, FIX-deficient plasma or FVIII-deficient plasma and thrombin generation was measured over 60 min in CAT assays. Lag time, ttPeak and peak thrombin obtained with deficient plasmas were normalized to the values obtained with PNP for each type of TF. Changes in lag time, ttPeak and peak thrombin for deficient plasmas that were significantly different from PNP are indicated with asterisk (t-test, $p < 0.05$; ns = not significant). (A, C, E) Thrombin generation assays performed with 1 pM WT and 0.25 nM 3S2T TF. Fold-change is shown for lag time (A), ttPeak (C) and peak thrombin (E) for WT versus 3S2T. (B, D, F) Thrombin generation assays performed with tenfold higher TF concentrations: 10 pM WT and 2.5 nM 3S2T TF. (Note: panels B, D and F are the same data as in Figure 2.3 A, 2.3 C and 2.3 E, reproduced here to allow a side-by-side comparison of the tenfold difference in TF concentrations). Fold-change is shown for lag time (B), ttPeak (D) and peak thrombin (F) for WT versus 3S2T. All data are mean ± SE ($n \geq 3$).

Chapter 3 Structural Basis of Substrate Recognition by the Tissue Factor – Factor VIIa Complex[b]

3.1 Introduction

The TF-FVIIa complex initiates blood clotting in hemostasis and many thrombotic diseases.[6,7,160] TF-FVIIa is a two-subunit enzyme with TF serving as the regulatory subunit and FVIIa serving as the catalytic subunit. TF is an integral membrane protein present on the surface of many extravascular cells.[8] Upon vascular damage, TF is exposed to blood and binds the serine protease, FVIIa. TF-FVIIa subsequently activates its two canonical protein substrates, FIX and FX, via limited proteolysis which propagates the blood clotting cascade.

The crystal structure of soluble TF-FVIIa was solved over twenty years ago.[44] However, a structure of the membrane-bound TF-VIIa complex, with or without substrates, has not been determined yet, impeding progress toward understanding protein-protein and protein-lipid interactions of the complex. Previous studies indicated that mutations of a patch of TF residues located close to the membrane (the putative substrate-binding or exosite of TF)[27,57,79,81,84] as well as deletion of the N-terminal GLA domain of FVIIa,[72] greatly decrease activation of FIX and FX. In contrast, these same TF exosite mutants had no effect on activation of GLA-domainless FX.[84]

We hypothesize that the TF exosite and the FVIIa GLA domain contribute to substrate recognition by binding to the GLA domain of FIX and FX, respectively. To test this hypothesis, we generated stable, membrane-bound complexes of TF, FVIIa and the FX mimetic, XK1. XK1 is a hybrid protein consisting of the FX light chain (i.e., the GLA and two EGF-like domains) linked to the Kunitz 1 (K1) domain of TFPI.[93] XK1 is a slow, tight-binding inhibitor that binds TF-FVIIa. The K1 domain inhibits FVIIa, while the light chain of FX is thought to bind the TF exosite. TF, FVIIa and XK1 were purified and the complex was assembled into Nanodiscs (ND).[75] ND are nanoscale phospholipid bilayers stabilized by two copies of an amphipathic protein

[b] Negative stain EM and cryo-EM experiments in this chapter were performed in collaboration with the Mike Cianfrocco and Sarah Kearns (University of Michigan).

(membrane scaffold protein, or MSP), which wraps around the bilayer in a belt-like fashion. The activity of the complex was validated using enzymatic assays. While FX has a low affinity for TF-FVIIa,[85] XK1 binds and inhibits TF-FVIIa with an IC_{50} value of 43 pM. Additionally, enzymatic assays revealed that XK1 interacts with TF similarly to wildtype FX. In collaboration with the Cianfrocco lab at the University of Michigan, the TF-FVIIa-XK1 complex was imaged using negative stain electron microscopy (negative stain EM) and cryo-electron microscopy (cryo-EM). Preliminary studies provide a 3D cryo-EM density map that resembles the structure of the three proteins. Although density of the ND is still missing, the map indicates potential interactions between the TF exosite region and the N-terminal portion of the FX light chain, suggesting that the TF exosite could be an extended substrate recognition site. High-resolution structures of TF-FVIIa bound to XK1 could provide new insights into how TF-FVIIa recognizes its protein substrates.

3.2 Materials and Methods

3.2.1 Materials

Materials were from the following sources: 1-palmitoyl-2-oleoyl-*sn*-glycero-3-phosphocholine (POPC) and 1-palmitoyl-2-oleoyl-*sn*-glycero-3-phospho-L-serine (POPS), Avanti Polar Lipids (Alabaster, AL); Bio-Beads SM-2 absorbent, Bio-Rad Laboratories (Hercules, CA); recombinant human FVIIa, American Diagnostica (now Sekisui Diagnostics, Lexington, MA); purified human FX, Haematologic Technologies (Essex Junction, VT); methoxycarbonyl-D-Nle-Gly-Arg-pNA acetate salt (FXa substrate), Bachem (Bubendorf, Switzerland); N-methylsulfonyl-D-Phe-Gly-Arg-pNA (FVIIa substrate), Sigma (St. Louis, MI); medium-binding 96-well microplates, Corning (Tewksbury, MA); Carbon grids (CF400-CU-UL, ultra-thin, 400 mesh) and UltrAuFoil® Grids (Q350AR13A, hole shape: R 1.2/1.3, hole size: 1.2µ, 300 mesh, gold), Electron Microscopy Sciences (Hatfield, PA).

3.2.2 Production and relipidation of recombinant TF

Recombinant human membrane-anchored TF (mTF, residues 3-244) with an N-terminal HPC4-epitope tag was expressed in *Escherichia coli* and purified as described.[78,161] TF-liposomes were prepared by incorporating mTF into phospholipid vesicles containing 80-95%

phosphatidylcholine (POPC) and 5-20% phosphatidylserine (POPS), as described [145], using 15 mM deoxycholate as the detergent.

3.2.3 Production of XK1

XK1, a slow, tight-binding inhibitor of the TF-FVIIa complex, is an engineered hybrid protein consisting of the human FX light chain linked to the K1 domain of human TFPI.[93] XK1 was expressed in HEK293 cells and purified as described in our previously published study.[162]

3.2.4 Production and validation of TF-FVIIa-XK1 Nanodiscs

TF was incorporated into Nanodiscs (ND) as described.[75] The ND contained 50% POPC and 50% POPS, yielding 5.2 mM total phospholipids which were dissolved in 10.4 mM sodium deoxycholate in TBS (50 mM Tris-HCl, pH 7.4, 150 mM NaCl). MSP was expressed and purified as described.[163] HPC4-tagged TF was expressed and purified as described above ("Production of recombinant TF"). MSP and TF were combined to yield a phospholipid:MSP molar ratio of 70:1 and an MSP:TF molar ratio of 20:1. This large excess of MSP to TF minimizes the occurrence of >1 TF molecules per ND. ND with a single TF molecule embedded in each ND (TF-ND) were isolated using affinity chromatography that took advantage of an HPC4 epitope tag on the N-terminus of the TF construct. Purification was performed as described for TF[78,164] but omitting the 1 mM NaCl wash step. Size exclusion chromatography was used as the final purification step to confirm size and uniformity of the TF-ND. Concentrations of functional (available) TF in ND were determined by titrating TF-ND against 5 nM FVIIa. The stoichiometries of TF and MSP in preparations of TF-ND were then assessed via gel electrophoresis followed by Coomassie staining and densitometry. Known concentrations of all protein components were used as a control.

The final trimolecular complex was generated by combining TF-ND, FVIIa and XK1 in a molar ratio of 1:1:1. Stoichiometries of TF, MSP, FVIIa and XK1 were assessed via gel electrophoresis followed by Coomassie staining and densitometry. Full inhibition of TF-FVIIa by XK1 was verified enzymatically by chromogenic substrate hydrolysis. The TF-FVIIa-XK1 ND complex (5 nM) was diluted in HBSA buffer (20 mM HEPES pH 7.4, 100 mM NaCl, 0.1% bovine serum albumin, 0.02% NaN_3) with 5 mM $CaCl_2$. The reaction was initiated by addition of 0.5 mM FVIIa substrate. The rate of change in A_{405} was measured at

ambient temperature using a Spectramax microplate reader (Molecular Devices, San Jose, CA). The complex was fully inhibited if no signal was detected (A_{405} = 0). TF-FVII complex without XK1 was used as a control.

3.2.5 FX activation by TF-FVIIa

Initial rates of FX activation by mTF–FVIIa were quantified using a continuous (one-stage) FX activation assay[22,75] in 96-well plates with the following modifications.[162] TF-liposomes (0.6 nM TF, with 10 μM total phospholipid) and FVIIa (3 pM) were incubated in HBSA buffer with 5 mM $CaCl_2$. Reactions were initiated by addition of 0.5 mM FXa substrate and 30 nM FX. The rate of change in A_{405} was measured at ambient temperature using a Spectramax 96-well spectrophotometer (Molecular Devices). Initial rates of FX activation in the presence of TF mutants (K165A, K166A) were normalized to those measured in the presence of wild-type (WT) TF with the same phospholipid composition.

3.2.6 Inhibition of TF-FVIIa by XK1

The ability of XK1 to inhibit the TF–FVIIa complex was assessed by quantifying its effects on the rate of FX activation,[162] using a modification of the continuous FX activation assay described above ("FX activation by TF-FVIIa"). TF-liposomes (0.6 nM mTF, with 10 μM total phospholipid) and FVIIa (3-20 pM) were incubated in HBSA buffer with 5 mM $CaCl_2$. Varying concentrations of XK1 (0-100 nM) were added, and after 5 minutes, reactions were initiated by addition of 0.5 mM FXa substrate and 30 nM FX. The rate of change in A_{405} was measured at ambient temperature using a Spectramax 96-well spectrophotometer (Molecular Devices). FX activation rates for WT or mutant TF in the presence of different XK1 concentrations were normalized to activation rates in the absence of XK1.

3.2.7 Imaging of the TF-FVIIa-XK1 complex by negative stain EM and cryo-EM

For negative stain EM experiments, TF-FVIIa-XK1 ND were diluted to 10 μg/mL in buffer containing 100 mM NaCl, 20 mM Hepes pH 7.4 and 5 mM $CaCl_2$. The sample was applied to a glow discharged carbon grid (CF400-CU-UL, ultra-thin, 400 mesh) and stained with 0.75% uranyl formate solution. Micrographs were collected on a T12 Tecnai electron microscope operated at 120 kV with a CCD camera at nominal magnification of 67,000x, calibrated pixel size of 1.68 Å and exposure time of 1 s. A total of 131 images were collected at a nominal defocus of 1.5 μm

using Leginon.[165] Data analysis, including particle picking and 2D classification, was performed using cryoSPARC.[166]

For cryo-EM experiments, TF-FVIIa-XK1 ND were diluted to 0.3 mg/mL in buffer containing 100 mM NaCl, 20 mM Hepes pH 7.4 and 5 mM $CaCl_2$. The sample was applied to a glow discharged UltrAuFoil® grid (R 1.2/1.3, 300 mesh, gold) using a Vitrobot (Thermo Fisher) at 4 C and 100 % relative humidity. The grid was blotted for 4 s and plunged into ethane. Micrographs were collected on a FEI Titan Krios electron microscope operated at 300 kV with a Gatan K2 direct electron detector at nominal magnification of 29,000x. with a calibrated pixel size of 1 Å. Movies were collected using Leginon[165] at a dose rate of 7.29 electrons/Å^2/s with a total exposure of 8 s, for an accumulated dose of 60.18 electrons/Å^2. Intermediate frames were recorded every 0.2 s for a total of 40 frames per micrograph. A total of 1978 images were collected at a nominal defocus range of 0.8 – 2.0 µm. Tilted micrographs were collected similar to untilted micrographs with the following modifications: The grid was tilted 30 degrees. Movies were collected at a dose rate of 8.45 electrons/Å^2/s for an accumulated dose of 65.6 electrons/Å^2. Intermediate frames were recorded every 0.1 s for a total of 100 frames per micrograph. A total of 2283 images were collected at a nominal defocus range of 1.0 – 2.1 µm. Particle picking and motion correction was performed using Warp.[167] Untilted data included a total of 167k particles, titled data included 190k particles. Further data analysis, including 2D classification, 3D reconstruction and 3D refinement, was performed using cryoSPARC[166] and RELION 3.0.[168] 2D classification and ab initio 3D reconstruction was performed for the untilted and tilted dataset, as well as a combined dataset (including both untilted and tilted data). The untilted dataset yielded a total of 99k particles, the tilted dataset yielded 108k particles and the combined dataset yielded 311k particles after 2D classification. Ab initio 3D reconstruction and 3D refinement was performed for all three datasets.

3.3 Results

3.3.1 Generation and validation of a stable, membrane-bound complex of TF, FVIIa and XK1

Generation of a membrane-bound TF-FVIIa-XK1 included purification of all components and subsequent assembly. TF-ND were successfully purified (Figure S 3.1 A) and the ratio of TF:MSP was confirmed as 0.5, indicating that NDs contained one TF molecule for every two molecules of MSP (Figure S 3.1 B). Purified TF-ND were subsequently combined with equimolar

amounts of purified XK1 and FVIIa (Sekisui Diagnostics). A model of the TF-FVIIa-XK1 complex on a ND (Figure 3.1 A) shows how the trimolecular complex sits on the phospholipid bilayer which is surrounded by two copies of MSP. The composition of the complex was verified by gel electrophoresis followed by Coomassie staining and densitometry, confirming 1:1:1 stoichiometry for TF, FVIIa and XK1 (Figure 3.1 B).

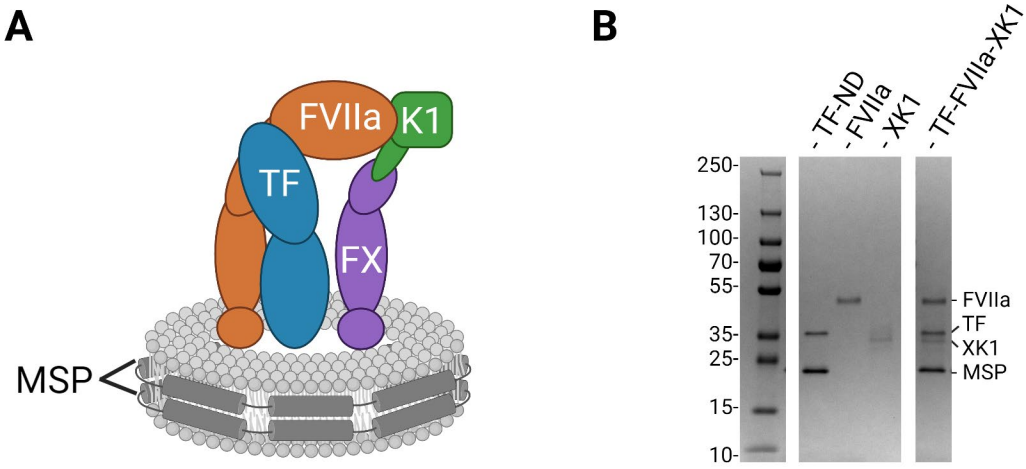

Figure 3.1 The membrane-bound TF-FVIIa-XK1 complex. (A) Model of TF-FVIIa-XK1 on a ND. ND is composed of a phospholipid bilayer surrounded by two copies of MSP. (B) Gel electrophoresis followed by Coomassie staining and densitometry was used to confirm 1:1:1 stoichiometry of the TF-FVIIa-XK1 complex. Known concentrations of all proteins were used as a control. Figure was created with BioRender.com.

Protein interactions within the TF-FVIIa-XK1 complex were analyzed using enzymatic assays. The goal of these experiments was to determine if XK1 interacts with TF the same way as wildtype FX. FX activation by TF-FVIIa was measured with and without XK1 comparing wildtype TF with TF exosite mutants K165A and K166A. In the presence of these TF mutants (relative to wildtype TF) FX activation by TF-FVIIa was reduced fivefold (Figure 3.2 A), and it similarly required a fivefold higher XK1 concentration to inhibit TF-FVIIa (Figure 3.2 C). In a low-PS environment, FX activation rates were even more reduced (Fig. 3.2 B), and even higher XK1 concentrations were needed to inhibit TF-FVIIa (Figure 3.2 D). These results support the idea that XK1 probes the TF exosite similarly to wildtype FX.

Enzymatic assays also revealed that XK1 binds the TF-FVIIa complex tightly. XK1 inhibits wildtype TF-FVIIa with an IC_{50} value of 43 pM (Figure 3.2 C). In comparison to this pM affinity for XK1, wildtype FX shows ~20 μM affinity in solution.[85] These results support the choice of XK1 as a FX mimetic to generate a stable trimolecular complex with TF-FVIIa that can be used for structural studies.

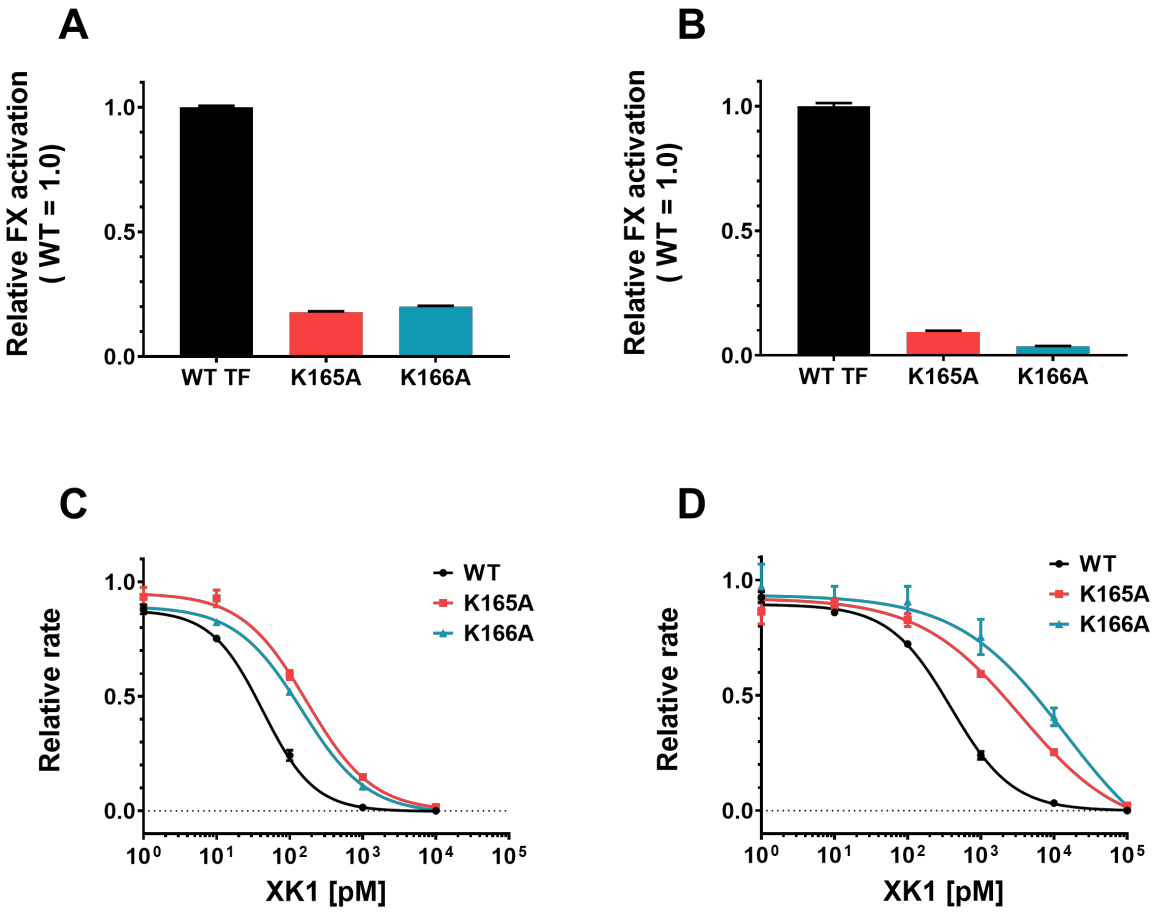

Figure 3.2 FX activation by TF-FVIIa and TF-FVIIa inhibition by XK1 in the presence of TF exosite mutants. (A-B) FX activation by TF-FVIIa. Enzymatic assays were performed with mTF-liposomes containing either 20% PS and 80% PC (A) or 5% PS and 95% PC (B). FX activation rates in the presence of TF mutants (K165A, K166A) were normalized to those measured in the presence of WT TF with the same phospholipid composition. (C-D) TF-FVIIa inhibition by XK1. Enzymatic assays were performed with mTF-liposomes containing either 20% PS and 80% PC (C) or 5% PS and 95% PC (D). FX activation rates for WT or mutant TF in the presence of different XK1 concentrations were normalized to activation rates in the absence of XK1. Data in all panels are mean ± standard error; $n \geq 3$.

3.3.2 Structure determination of TF-FVIIa-XK1

The structure of the TF-FVIIa-XK1 complex was determined via imaging using negative stain EM and cryo-EM. These experiments were performed in collaboration with the Cianfrocco lab (University of Michigan). Negative stain EM images (Figure S 3.2 A-B) and the resulting 2D class averages (Figure S 3.2 C) clearly show a ring-shaped ND with a protein complex sticking out of the disc. Negative stain EM experiments confirmed that TF-FVIIa-XK1 is a suitable sample for a more in-depth structural analysis.

The complex was further analyzed using cryo-EM. Cryo-EM images (Figure S 3.3 A) and the resulting 2D class averages (Figure S 3.3 C) from a standard cryo-EM data collection (EM grid not tilted) showed particles resembling TF-FVIIa-XK1. Upon further data analysis, the resulting 3D reconstruction revealed an EM map that seems to contain the protein complex but misses the ND (Figure S 4.1 A). The ND, which was clearly visible in negative stain EM images, could be "lost" in the cryo-EM data because the complex is too flexible. If the complex is dynamic and moves around on the ND, this could result in the ND being averaged out during EM data processing.[169]

Cryo-EM data analysis also revealed another problem with the protein complex. The complex seemed to adapt a preferred orientation on the grid surface during grid preparation.[170] Preferred orientation indicates that individual proteins sit on the grid in the same orientation by sticking to the air-water interface, resulting in a 3D reconstruction that is based on very few orientations of the complex. A non-uniform distribution of angular projection orientations of the individual particles (Supplementary Fig. 4.1 B) is a strong indicator for preferred orientation.[171]

Collection of a tilted dataset (with images taken at a tilt angle of 30 degrees) is commonly used to help with preferred orientation and obtain more particle orientations.[171] Cryo-EM images (Supplementary Fig. 3.3 B) and resulting 2D class averages (Supplementary Fig. 3.3 D) of the tilted dataset clearly showed the TF-FVIIa-XK1 complex. The two datasets (untilted and tilted) were also combined to yield one large dataset and 2D class averages show a distinct complex (Supplementary Fig. 3.3 D). The 3D reconstructions for both the tilted dataset (Supplementary Fig. 3.4 C) and the combined dataset (Supplementary Fig. 3.4 E) showed improved distribution of particle orientations (Supplementary Fig. 3.4 D and 3.4 F).

The best cryo-EM map to date is derived from the combined dataset (Fig. 3.3 A). Although data analysis reports a "4.3 Å" resolution for this map, the preferred orientation results in overfitting of the data, making the resolution estimate less accurate. We have not modeled TF-FVIIa-XK1 in the "4.3 Å" density. However, preliminary modeling of TF-FVIIa-XK1 into a lower resolution EM density map ("6 Å" resolution) was performed by our collaborators in the Tajkhorshid lab (University of Illinois Urbana-Champaign). The model indicates that the bulk of the FX light chain part of XK1 projects into the solvent, away from TF-FVIIa. The model supports the idea of potential interactions between the TF exosite region and the N-terminal portion of the FX light chain.

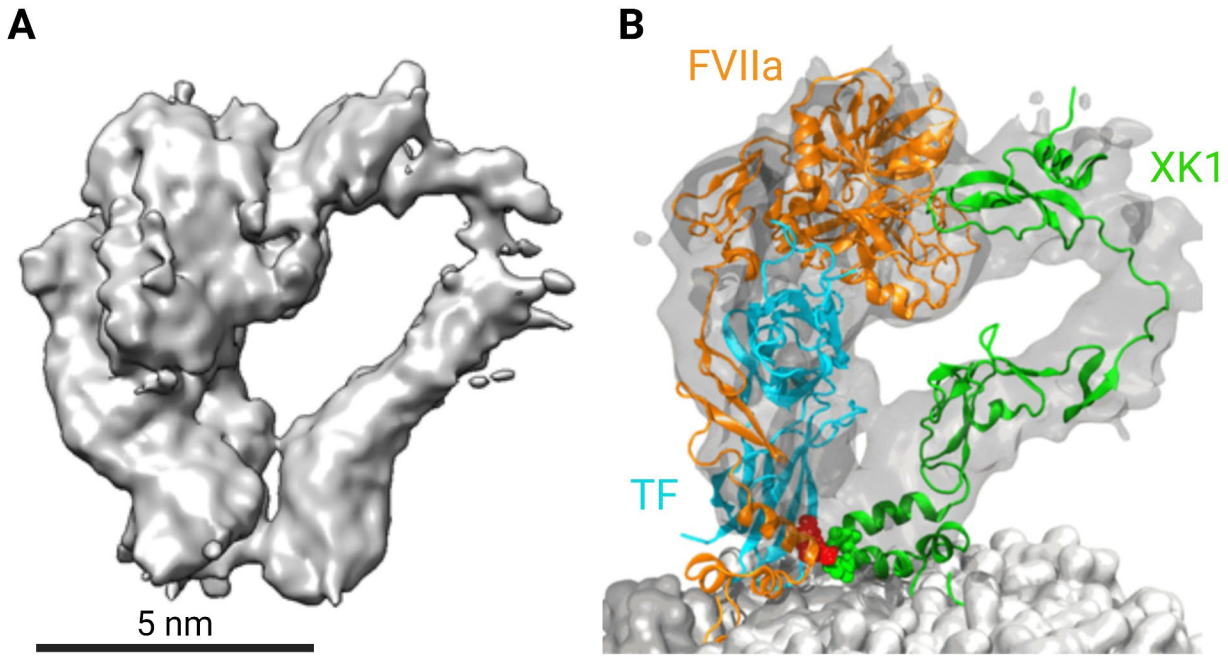

Figure 3.3 3D Model of TF-FVIIa-XK1. (A) EM density map ("4.3 Å" resolution) generated using cryo-EM data from the tilted and untilted dataset (also referred to as the combined dataset). (B) EM density map generated using an untilted dataset ("6 Å" resolution) with TF-FVIIa-XK1 complex modelled into the density (membrane added). Model indicates potential interactions between TF exosite (red) and FX GLA domain residues (green).

3.4 Discussion

The results of this study provide the first preliminary EM density map of membrane-bound TF-FVIIa in complex with the FX substrate mimetic, XK1. Our preliminary TF-FVIIa-XK1 model indicates possible interactions between the TF exosite and the FX GLA domain, suggesting that the TF exosite could act as an extended substrate recognition site.

The role of the TF exosite in substrate activation was clearly identified in several mutagenesis studies.[79-81] Mutating specific TF exosite residues, especially Lys165 and Lys166, decreases FX and FIX activation by up to 100-fold.[79,81,83,84] Due to the abundance of lysine residues, the TF exosite has a net positive charge, suggesting interactions with the negatively charged Gla residues at the N-terminus of FX. This hypothesis is supported by a previous study from our lab reporting that TF exosite mutants were equivalent to wildtype TF in supporting activation of GLA-domainless FX.[84] Additionally, deletion of the GLA domain of FVIIa decreases FX activation.[72] These findings led to our hypothesis that both the TF exosite and FVIIa Gla domain are involved in substrate activation, potentially by binding the Gla domain of FIX and FX. However, FIX and FX have a low affinity for TF-FVIIa[85] which impeded progress towards

generating a stable trimolecular complex and obtaining a structure of this complex. In this study, we generated a stable, membrane-bound complex of TF, FVIIa and the FX mimetic XK1 that enabled structural studies via negative stain and cryo-EM. The preliminary cryo-EM density map shows potential interactions of TF exosite and the FX GLA domain, which are in line with several previous studies suggesting direct protein-protein interactions between these two proteins.[72,84]

Although our preliminary map provides first insights into the TF-FVIIa-XK1 structure, adjustments to both sample preparation and data collection are needed to further optimize the density and visualize the "missing" ND. Changes performed to date (e.g., collection of tilted dataset) have shown some improvement of the EM map. Other approaches could include analyzing the complex in more detail using negative stain EM. Comparing ND containing just TF to ND containing TF-FVIIa or TF-FVIIa-XK1 will allow us to track the changes in the EM map after addition of each part of the trimolecular complex. This approach will ensure that every change in EM density can be attributed to a distinct protein.

Another option to improve the current EM density map and visualize the ND are adjustments to the sample preparation which might stabilize the proteins on the ND. This includes changing the composition of the ND. Using phospholipids with a higher phase transition temperature (e.g., fully saturated PC or PS with T_m = ~30-35°C) would minimize lipid fluidity during freezing of the protein sample. The ND could be assembled at 37-41°C (at above the transition temperature), but the lipid orientation could be preserved by cooling the sample to 4°C right before freezing. Limiting lipid fluidity after complex formation could stabilize its orientation on the membrane. Further adjustments in sample preparation could include changes to the protein complex, in particular TF. TF contains an unstructured linker region that tethers its extracellular domain to the transmembrane domain. Shortening the linker should limit freedom of motion for TF and result in a more stable complex.

Further insights into the interactions of TF-FVIIa with its substrates could be obtained by generating a complex of TF, FVIIa and a FIX mimetic. FIX is another important substrate of TF-FVIIa and previous studies showed that FIX and FX interact similarly with TF-FVIIa.[81] A FIX mimetic has not been described in the literature yet. However, we generated a construct that includes the FIX light chain in place of the FX light chain and performed initial purification trials. A structure of TF-FVIIa bound to this FIX mimetic, IXK1, could be obtained using cryo-EM. This would allow us to compare the structures of TF-FVIIa bound to both substrates and describe

potential differences between the trimolecular complexes.

This study has provided the first steps towards obtaining a membrane-bound structure of TF-FVIIa in complex with its substrate which will ultimately reveal new molecular details of TF-FVIIa substrate recognition.

3.5 Supplementary Information

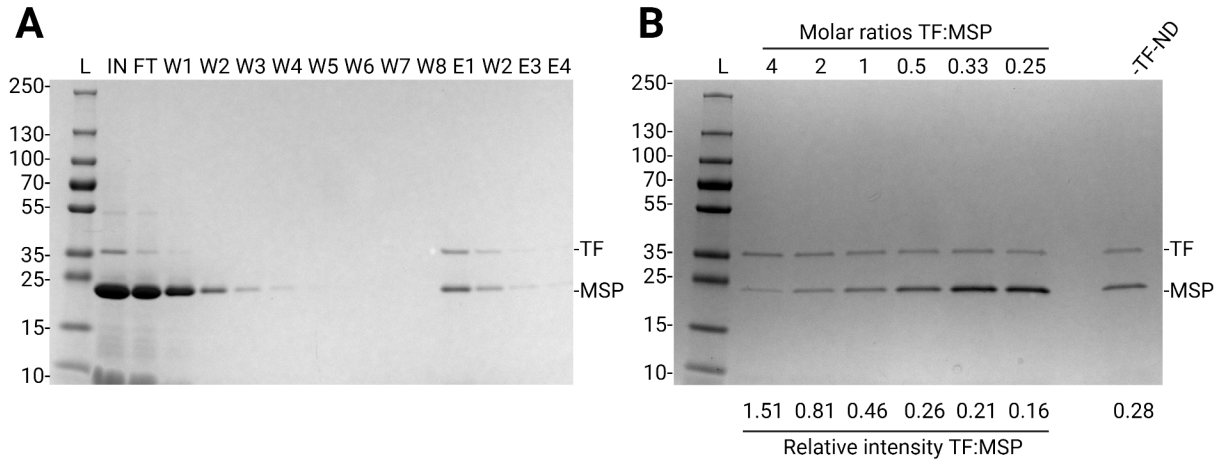

Figure S 3.1 Generation of TF-ND. (A) Purification of TF-ND via affinity chromatography. Gel electrophoresis followed by Coomassie staining showing samples of TF-ND purification steps. L=ladder, IN=input, FT=flow-through, W1-7=Wash 1-7, E1-4=Elution 1-4. (B) Densitometry analysis of TF-ND. Gel electrophoresis followed by Coomassie staining showing molar ratios of TF:MSP and their corresponding band intensities. The purified TF-ND show band intensities that correspond to a 0.5 ratio of TF:MSP (1 TF for every 2 MSP).

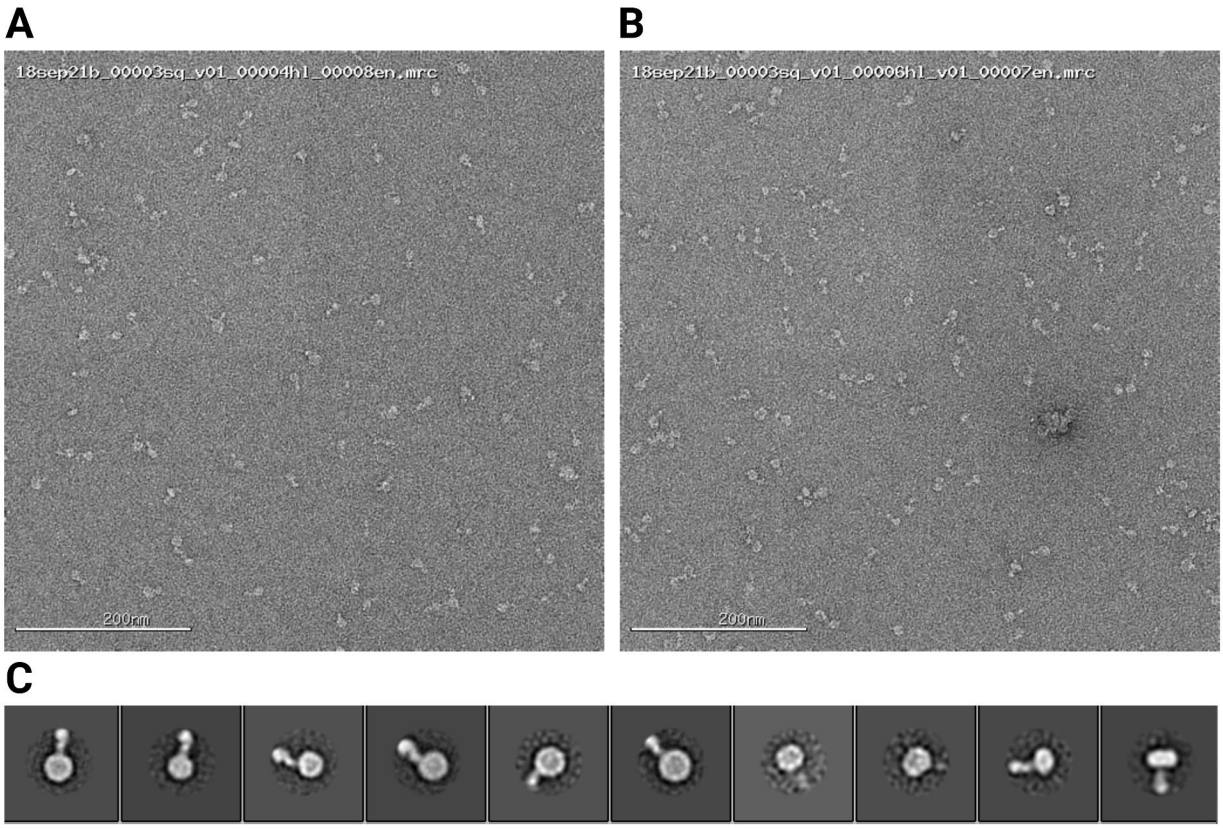

Figure S 3.2 Micrographs and select 2D class averages of the TF-FVIIa-XK1 complex by negative stain EM. (A-B) Micrographs of TF-FVIIa-XK1 sample. (C) Select 2D class averages.

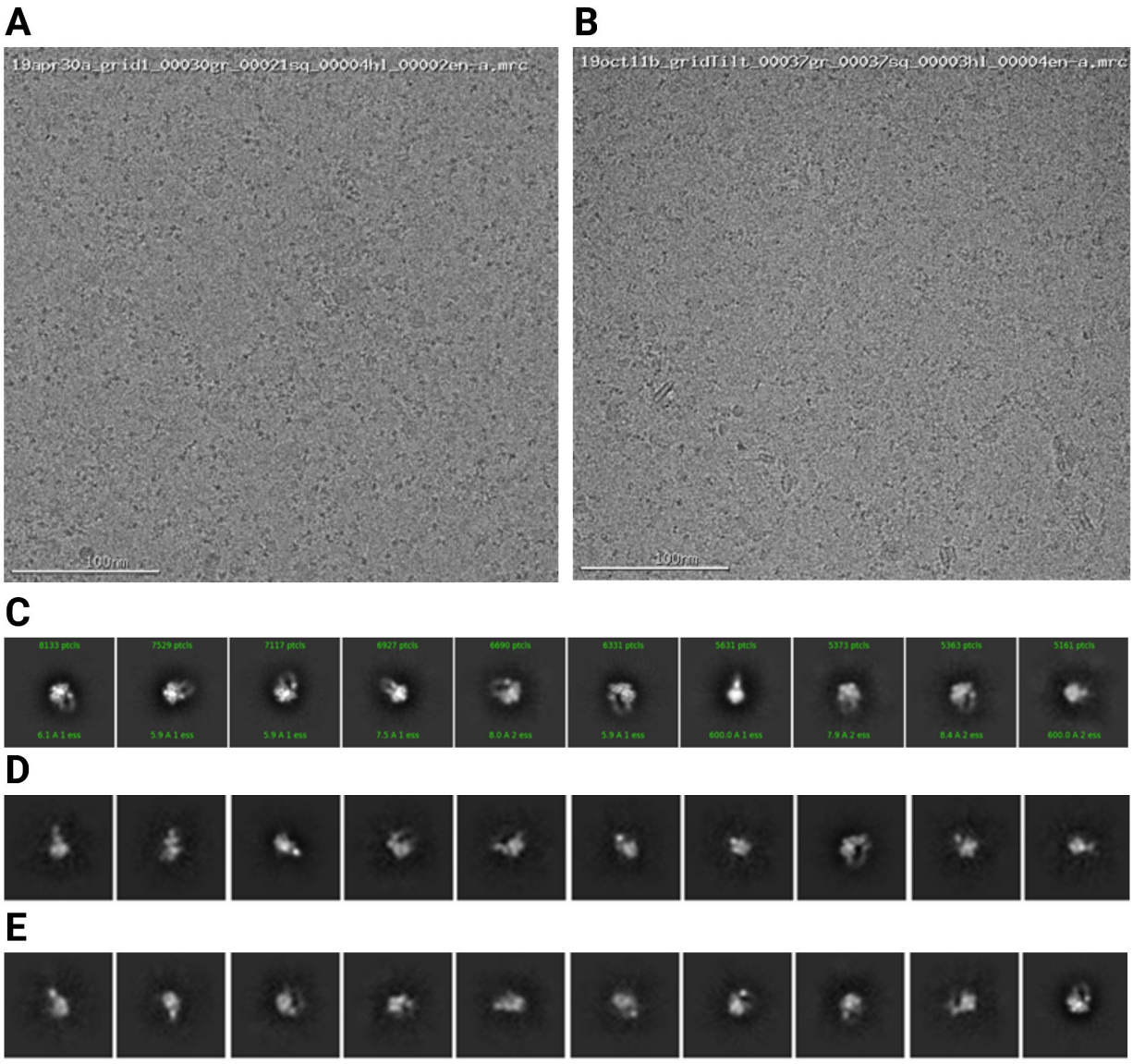

Figure S 3.3 Micrographs and select 2D class averages of the TF-FVIIa-XK1 complex by cryo-EM. (A) Micrographs of untilted sample. (B) Micrographs of tilted sample. (C) Select 2D class averages for untilted data. (D) Select 2D class averages for tilted data. (C) Select 2D class averages for combined (untilted and tilted) data.

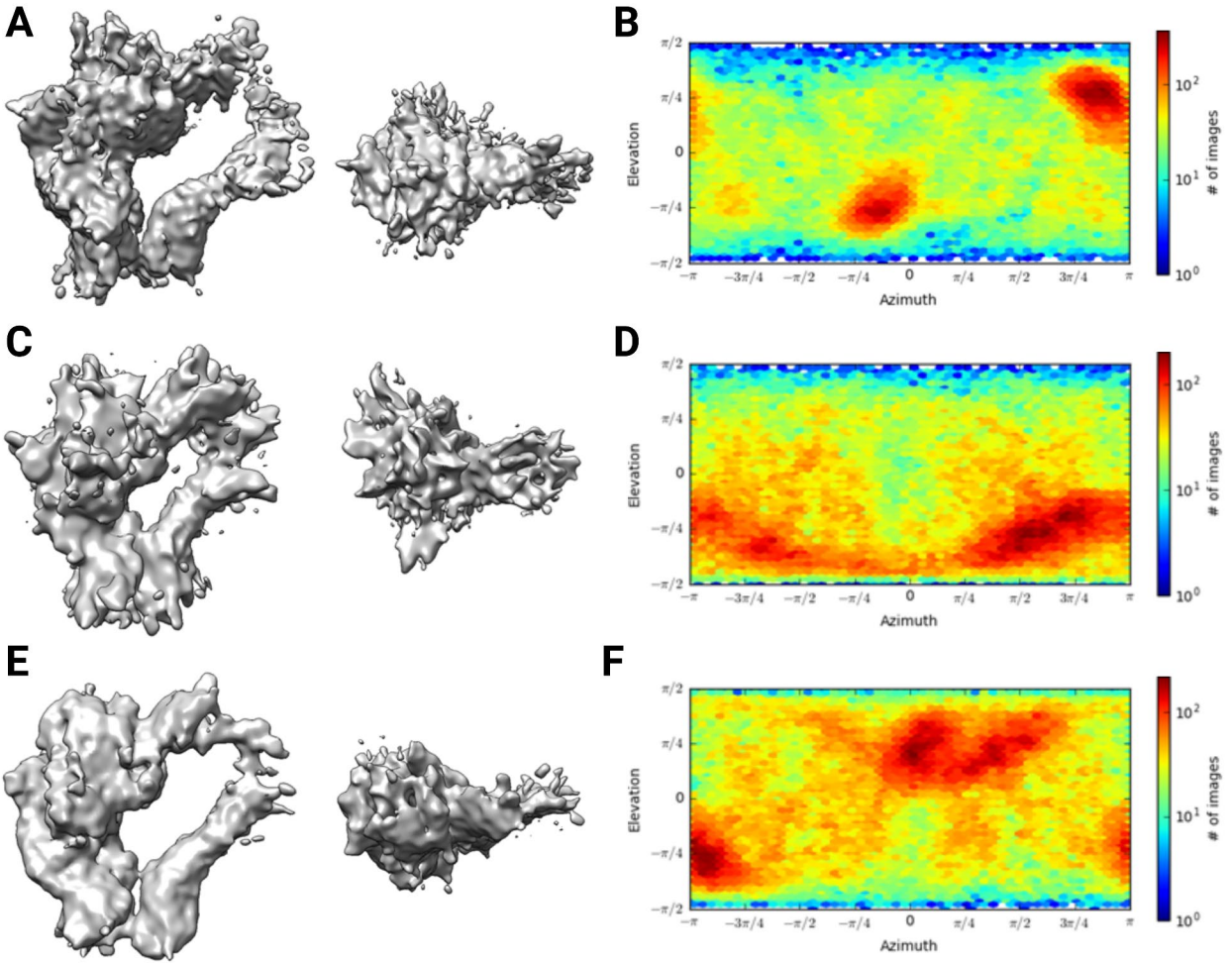

Figure S 3.4 3D reconstruction and distribution of angular projection orientations of the TF-FVIIa-XK1 complex. (A, C, E) Best 3D reconstruction after refinement is shown for (A) untitled data, (C) tilted data and (E) combined data. The side and top views of the 3D models are shown. (B, D, F) Distribution of angular projection orientations (plotted as azimuth against elevation angles) for particles included in the calculation of the final 3D map for (B) untitled data, (D) tilted data and (F) combined data.

Chapter 4 Nucleotides Inhibit Serine Proteases[c]

4.1 Introduction

Nucleotides serve important functions inside the cell as energy sources, enzyme cofactors or co-substrates, and building blocks of nucleic acids.[172] The most abundant nucleotide is adenosine triphosphate (ATP), with a surprisingly high cytosolic concentration of approximately 2 to 9 mM.[173] Recent studies have shown that these high intracellular ATP concentrations play important roles in enhancing the stability and solubility of many proteins.[174,175]

Most secreted proteins progress through the endoplasmic reticulum (ER) and Golgi. We wondered whether similarly high ATP concentrations in the lumen of these compartments could stabilize proteins as they transit through these compartments. In particular, serine proteases are typically synthesized and secreted as inactive precursors or zymogens,[176] which remain catalytically inactive until they reach their target location, where they are converted into active enzymes by limited proteolysis. Premature activation of a serine protease zymogen while still in the ER or Golgi could be dangerous, since indiscriminate proteolysis could cause ER stress and cellular damage. A pathological example of damage caused by premature protease activation before delivery to its final destination is hereditary pancreatitis, which results from premature activation of trypsinogen while it is still within the pancreas rather than in the small intestine.[177-179]

In this study, we tested the idea that ATP and certain other nucleotides can inhibit the activity of serine proteases. In the ER and Golgi lumen, nucleotides and their derivatives serve as the energy source for protein folding and degradation, and as co-substrates for post-translational

[c] This chapter was adapted from a research report under submission. MD experiments were performed by the Tajkhorshid lab (University of Illinois Urbana-Champaign). NMR experiments were performed by the Rienstra lab (University of Madison-Wisconsin) with help from the Komives lab (University of California San Diego). Current citation: Fabienne Birkle, Yan Wang, Hale S. Hasdemir, Karan Kapoor, Marco Tonelli, Ronnie O. Frederick, Riley B. Peacock, Elizabeth A. Komives, Chad M. Rienstra, Emad Tajkhorshid, and James H. Morrissey. Nucleotides inhibit serine proteases, 2022, under submission.

modifications of many proteins[180] including serine proteases. Although the absolute concentration of ATP or other nucleotides within the ER or Golgi does not appear to be known, it is well known that ATP, nucleotide sugars, and 3′-phosphoadenosine-5′-phosphosulfate (PAPS) are transported actively into the lumen of these compartments, and that their transporters can increase the luminal concentrations of nucleotides and nucleotide derivatives some 50- to 100-fold.[180,181] Furthermore, chaperone proteins such as BiP are themselves present in millimolar concentrations in the ER lumen.[182] As BiP is an ATP-utilizing protein, one would expect that ATP within the ER lumen must also be present at millimolar levels. We now report that millimolar concentrations of ATP and other nucleotides strongly inhibit the enzymatic activities of eleven serine proteases involved in processes as varied as blood clotting, fibrinolysis and food digestion.

4.2 Materials and Methods

4.2.1 Materials

Materials were sourced as follows: ribonucleotides, PAPS, bovine trypsin, N-methylsulfonyl-D-Phe-Gly-Arg-pNA (FVIIa substrate), N-succinyl-Ala-Ala-Pro-Phe-pNA (chymotrypsin substrate), sodium pyrophosphate and sodium tripolyphosphate, Sigma (St. Louis, MI); recombinant human FVIIa, American Diagnostica (now Sekisui Diagnostics, Lexington, MA); biotinylated D-Phe-Pro-Arg chloromethyl ketone, and human FXIa, FXa, FIXa, thrombin, and plasmin, Haematologic Technologies (Essex Junction, VT); human FXIIa and plasma kallikrein, Enzyme Research Laboratories (South Bend, IN); bovine chymotrypsin, Worthington Biochemical Corporation (Lakewood, NJ); human uPA, sc-tPA and tc-tPA, Molecular Innovations (Novi, MI); CH_3SO_2-D-CHG-Gly-Arg-pNA (FXIa substrate), Pentapharm (Parsippany, NJ); methoxycarbonyl-D-Nle-Gly-Arg-pNA (FXa and trypsin substrate), Pyr-Pro-Arg-pNA (FIXa substrate), D-Pro-Phe-Arg-pNA (FXIIa and plasma kallikrein substrate) and Sar-Pro-Arg-pNA (thrombin substrate), Bachem (Bubendorf, Switzerland); 1,5-dansyl-Glu-Gly-Arg chloromethyl ketone, Calbiochem (San Diego, CA); and phospholipids, Avanti Polar Lipids (Alabaster, AL).

4.2.2 Production and relipidation of recombinant TF

Recombinant human mTF (residues 3-244) with an N-terminal HPC4-epitope tag was expressed in *Escherichia coli* and purified as described.[161] mTF-liposomes were prepared by incorporating mTF into phospholipid vesicles containing 80% phosphatidylcholine (1-palmitoyl-

2-oleoyl-*sn*-glycero-3-phosphocholine) and 20% phosphatidylserine (1-palmitoyl-2-oleoyl-*sn*-glycero-3-phospho-L-serine), as described,[145] using 15 mM deoxycholate as the detergent. Relipidated mTF was typically employed to quantify FIX or FX activation by TF-FVIIa, as this reaction is highly membrane-dependent. Recombinant human sTF (residues 3-219) with a C-terminal 6×His-tag was expressed in *E. coli* and purified as described.[22] sTF was typically employed in the absence of membranes to quantify chromogenic substrate hydrolysis by TF-FVIIa, as this activity is membrane-independent.

4.2.3 Chromogenic substrate hydrolysis by serine proteases

Initial rates of chromogenic substrate hydrolysis were quantified in 96-well plates. Proteases were diluted in HBSA buffer (20 mM HEPES pH 7.4, 100 mM NaCl, 0.1% bovine serum albumin, 0.02% NaN_3), although for FVIIa or sTF-FVIIa, 5 mM $CaCl_2$ was included. Nucleotides at the desired concentration were then incubated with protease for 5 min at ambient temperature, after which the appropriate chromogenic substrate was added. Concentrations of protease and substrate varied as follows: 200 nM sTF plus 20 nM FVIIa (sTF-FVIIa) with 0.5 mM substrate; 5 nM FXa with 0.5 mM substrate; 1 nM FXIa with 1 mM substrate; 20 nM FXIIa with 1 mM substrate; 1 nM plasma kallikrein with 1 mM substrate; 10 nM thrombin with 1 mM substrate; 50 nM plasmin with 0.5 mM substrate; 30 nM uPA with 1 mM substrate; 100 nM sc-tPA with 0.5 mM substrate; 50 nM tc-tPA with 0.5 mM substrate; 10 nM trypsin with 0.5 mM substrate; and 10 nM chymotrypsin with 0.5 mM substrate. The rate of change in A_{405} was measured at ambient temperature using a Spectramax microplate reader (Molecular Devices, San Jose, CA). Initial rates of substrate hydrolysis in the presence of nucleotides were normalized to those with no nucleotides and plotted against the nucleotide concentrations on a logarithmic scale, from which IC_{50} values were determined by nonlinear regression.

4.2.4 Activation of FX and FIX by mTF-FVIIa

For most experiments, initial rates of FX activation by FVIIa bound to mTF were quantified using a continuous (one-stage) FX activation assay. mTF-liposomes (0.57 nM mTF, with 10 μM total phospholipid) were incubated with FVIIa (3 pM) in HBSA buffer plus 5 mM $CaCl_2$ in wells of a 96-well plate. Nucleotides or nucleotide derivatives were then incubated with mTF-FVIIa for 5 min at ambient temperature, after which reactions were initiated by adding 0.5 mM FXa

chromogenic substrate and 30 nM FX. The change in A_{405} was measured, from which initial rates of FX activation were derived as described.[183]

K_m and k_{cat} values for FIX and FX activation were measured in discontinuous (two-stage) assays in 96-well plates as described.[161] mTF-liposomes (for FIX activation: 10 nM mTF with 175 μM total phospholipid; for FX activation: 0.57 nM mTF with 10 μM total phospholipid) were incubated with FVIIa (for FIX activation: 1 nM; for FX activation: 3 pM) in HBSA plus 5 mM $CaCl_2$ at 37° C for 5 min, after which ADP (0-5 mM) was added and incubated for an additional 5 min. Reactions were then initiated by adding 0.1-2 μM FIX or 25-400 nM FX, after which timed, 10-μL aliquots were taken over 5 min and quenched on ice in microwells containing 80 μL stop buffer (for FIX activation: 1.25× concentrated HBSA with 12.5 mM EDTA and 28% (v/v) ethylene glycol; for FX activation: 1.25× concentrated HBSA with 12.5 mM EDTA). For the second stage, plates were warmed to ambient temperature and 10 μL of the appropriate chromogenic substrate solution (0.5 mM final) was added per well, after which the rate of change in A_{405} was measured and converted to FIXa or FXa concentrations by reference to a standard curve. To extract K_m and k_{cat} values, initial rates of FIX or FX activation were plotted versus FIX or FX concentration, to which the Michaelis-Menten equation was fitted by nonlinear regression.

K_i values for FIX and FX activation by mTF-FVIIa in the presence of ADP were determined graphically using Cornish-Bowden plots, in which the substrate concentrations (FIX or FX) were divided by activation rates to yield S/V, which was plotted against ADP concentrations (I).[184] Lines were then fitted to the data. For competitive inhibition, the lines will be parallel; for non-competitive inhibition, the lines intersect at $I = -K_i$ and $S/V = 0$; and for uncompetitive inhibition, the lines intersect at $I = -K_i$ and $S/V = K_m/V_{max}$.

4.2.5 SPR analyses

ATP binding affinities for FXa, thrombin and trypsin were determined by surface plasmon resonance (SPR) at ambient temperature using a Biacore T200 (Cytiva, Marlborough, MA). First, the active site of each serine protease was irreversibly inhibited using 1,5-dansyl-Glu-Gly-Arg chloromethyl ketone for FXa and trypsin, or biotinylated D-Phe-Pro-Arg chloromethyl ketone for thrombin. In each case, the protease was incubated with a tenfold molar excess of inhibitor for 20 min at ambient temperature, after which full inhibition was verified by chromogenic substrate hydrolysis as described above. Active-site inhibited proteases were bound to a Cytiva Series S

Sensorchip CM5 by standard amine coupling according to manufacturer's protocol, using 10 mM sodium acetate pH 4.5. Final coupling results were approximately 850 resonance units (RU) for FXa, 700 RU for thrombin and 500 RU for trypsin. Binding experiments were performed in running buffer (20 mM Hepes pH 7.4, 100 mM NaCl, 0.002% surfactant) in the presence of 0-100 mM ATP. In each case, the maximal steady-state RU values were recorded at each ATP concentration, and binding isotherms were generated by plotting maximal RU versus nucleotide concentration. The Hill equation was fitted to the binding data using nonlinear regression to determine the binding affinities (K_D) and Hill coefficients.

4.2.6 Flooding molecular dynamics (MD) simulations

The binding of ATP molecules to thrombin and trypsin was probed using flooding MD simulations, in which multiple ligand copies (ATP) were added to the simulation box to sample binding events of ATP to the protein, thereby increasing the efficiency of the search for putative binding sites.

For thrombin, the 1.9 Å-resolution, inhibitor-bound human thrombin structure (PDB code: 1PPB[185]) was employed, keeping the light and heavy chains in the system along with crystal water molecules, but removing the active-site inhibitor. Disulfide bonds in thrombin were added between C1-C122 (inter-chain) and between C42-C58, C168-C182 and C191-C220 (intra-heavy chain). For trypsin simulation we started from the structure of human trypsin (PDB ID: 1TRN). Five intra-chain disulfide bonds (C30-C160, C48-C64, C139-C206, C171-C185, and C196-C220) were then introduced to the trypsin structure. The protonation states of protein residues were determined by pK_a calculations using the Protonate-3D module in MOE (*Molecular Operating Environment)*, 2019.01 (Chemical Computing Group ULC, 1010 Sherbooke St. West, Suite #910, Montreal, QC, Canada, H3A 2R7, 2021). The systems were solvated in a water box and neutralized with 0.1 M NaCl. The final simulation systems consisted of ~100,000 and ~80,000 atoms, for thrombin and trypsin, respectively. ATP molecules at a 25 mM concentration (14 molecules in the thrombin system and 11 in the trypsin system) were added to the simulation box using the positions of randomly selected water molecules at least 20 Å from the protein surface. Water molecules clashing with added ATP molecules were removed. Respective number of Cl^- were also removed to maintain the charge neutrality of the system. Five replicas of such solvated, ATP-protease systems were created for production simulations.

The simulations were performed using NAMD[186,187] and CHARMM36m parameters for protein and ATP[188] and TIP3P for water[189] using 2-fs timesteps. The system was first energy-minimized for 1,000 steps using steepest descent algorithm followed by equilibration MD for 2 ns. In the equilibration phase, the protein backbone and side-chain heavy atoms were restrained with force constants of 10 and 5 kcal/mol/Å^2, respectively. The temperature was maintained at 303 K using Langevin thermostat[190] and the pressure was maintained at 1 bar using Nosé-hoover piston method.[191] The particle mesh Ewald (PME) method was used to calculate electrostatic interactions[192] without truncation within the periodic boundary conditions used for all the simulations. The non-bonded forces were calculated at 12-Å cutoff and 10-Å switching distances. Five independent simulation replicas for each protein (thrombin and trypsin) were performed to probe ATP-protein interactions. Each simulation replica was initiated with a randomized set of atomic velocities, and a different spatial distribution of ATP molecules around the protein. The production simulations were carried out for 2 μs for each replica, collecting 10 μs sampling of ATP interaction with thrombin or with trypsin.

4.2.7 MD clustering of ATP binding modes to identify putative ATP binding sites

First, total contact (C) between an ATP molecule and the protein was calculated as:

$$C = \sum_{i,j} \frac{1}{1 + \exp\left[5\ \text{Å}^{-1}\left(r_{ij} - 4\text{Å}\right)\right]}$$

In which the summation goes over all possible heavy atom pairs between thrombin and an ATP molecule with r_{ij} being the inter-atomic distance in a given frame of the MD trajectory. C can be defined for individual residues, domains, or the entire protein. Similar contact functions have been used to quantify molecular-level interactions in previous simulation studies.[193,194] Using C, "ATP-bound" frames were defined as frames with $C \geq 4$. In order to exclude transient interactions, only contiguous segments of the simulations where ATP remains bound to the protein for at least 10 ns were considered for further analysis.

For each "ATP-bound" frame, a vector composed of the C values of the individual protein residues was calculated. The data were scaled to unit variance and zero mean using the scikit-learn package.[195] Dimensionality of the full dataset was reduced with Uniform Manifold Approximation and Projection (UMAP) v.0.3.2[196] to 20 dimensions. During dimensionality reduction, UMAP keeps neighboring/similar data points in the high-dimensional space close to each other in the

reduced-dimensional space while preserving the global structure of the dataset. UMAP has been successfully used in previous studies to identify and cluster similar biological datasets in a lower-dimensional space.[197-199] Similarly, our goal here was to group "ATP-bound" frames in which ATPs are interacting with the same region of the protein to identify putative ATP interaction sites in clusters. To obtain well-separated clusters, UMAP parameters were set as follows: n_neighbors = 50, min_distance = 0.8, n_components = 20, random_state = 42, Euclidian distance metric. HDBSCAN (Hierarchical Density-Based Spatial Clustering of Applications with Noise)[200] was then carried out on the first five UMAP dimensions to classify the putative ATP interaction sites. HDBSCAN is a density-based clustering method for identifying clusters with varying shapes and sizes. Performing HDBSCAN on the first five UMAP dimensions prevented further splitting of the main clusters into additional subclusters. HDBSCAN parameters were set to: min_cluster_size = 700, cluster_selection_epsilon = 2. To better visualize the resulting clusters and the distribution of ATP interaction sites on the protein, the clusters of "ATP-bound" states were projected onto the first two UMAP dimensions. To determine the putative ATP interaction sites of trypsin, the same clustering workflow was used. Since trypsin is smaller in size than thrombin, a smaller *C* cutoff ($C \geq 2$) was used to select "ATP-bound" frames. For dimensionality reduction, UMAP parameters were set to n_neighbors = 30, min_distance = 0.25, n_components = 20, random_state = 42, Euclidian distance metric; for clustering, HDBSCAN parameters were: min_cluster_size = 600, cluster_selection_epsilon = 3. Electrostatic potentials were calculated using APBS (Adaptive Poisson-Boltzmann Solver) software,[201] and molecules were visualized in VMD.[202]

4.2.8 NMR Analyses of ATP Binding to Thrombin

NMR spectra were recorded on a $^{2}H,^{15}N$-labeled sample of the S195M mutant of thrombin bound to the TM456 fragment of thrombomodulin (natural abundance), expressed and purified as described.[203] The NMR sample was prepared with 25 mM phosphate buffer at pH 6.5, containing 0.025 % NaN_3, and 10% D_2O for a final protein concentration of 35 μM. A total volume of 100 μL of this solution was used in a 3 mm Shigemi tube. A 0.25 M stock solution of ATP dissolved in the same buffer was titrated into the sample of labeled thrombin in five steps to achieve ATP concentrations of 1 mM, 5 mM, 10 mM, 20 mM, and 40 mM (approximate ATP to protein concentration ratios of 30, 140, 290, 520 and 1,100, respectively).

All NMR experiments were performed on a Varian VNMRS spectrometer operating at 800 MHz (^{1}H) and equipped with a cryogenically cooled triple resonance probe with z-axis pulsed field gradients. The temperature of the sample was regulated to 298 K. Two dimensional ^{1}H,^{15}N HSQC-TROSY spectra[204] were recorded at the beginning and after each addition of ATP to the sample. Each spectrum was recorded with 1024 x 128 complex points in the direct ^{1}H and indirect ^{15}N dimensions, respectively. The frequency offsets and spectral widths were set to 4.77 ppm and 16.3 ppm for the ^{1}H dimension and 118.51 ppm and 37.5 ppm for the ^{15}N dimension. Each FID was accumulated with 192 transients and the recovery delay was set to 1.5 sec, resulting in a recording time of 22 hr for each 2D spectrum. The NMR spectra were processed using NMRPipe[205] and analyzed with NMRFAM-SPARKY[206]. Using the "Transfer and simulate assignments" extension (ta), we transferred the backbone amide chemical shift assignments from BMRB ID 50,678 deposition onto the thrombin HSQC-TROSY spectrum recorded before adding ATP. The titration spectra were analyzed using the "NMR Perturbation Plot" extension (np) in NMRFAM-SPARKY. The chemical shift perturbation (CSP) values for each assigned residue were calculated using the formula:

$$\sqrt{\left[\left(\Delta \mathrm{H}^2 + \left({}^{\Delta N}/_{5}\right)^2\right)/2\right]}$$

where ΔH and ΔN are the difference in ^{1}H and ^{15}N chemical shifts between the first and last points of the titration, respectively. To locate the ATP binding site, the calculated CSP values were displayed on the structure of thrombin (PDB ID: 1DX5[207]) using PyMOL.

4.3 Results

4.3.1 Nucleotides inhibit serine protease activity

We initially screened ATP as a potential inhibitor of eleven secreted human serine proteases involved in a variety of biological functions. Blood clotting proteases included FXa, FXIa, FXIIa, plasma kallikrein, thrombin, and sTF-FVIIa (the complex of FVIIa and its protein cofactor TF; in this case, using a truncated, soluble form of TF known as sTF). Digestive proteases included bovine trypsin and chymotrypsin. Fibrinolytic proteases included human plasmin, urinary-type plasminogen activator (uPA) and tissue-type plasminogen activator (tPA). The latter enzyme was tested in both the single-chain (sc-tPA) and two-chain (tc-tPA) forms, since uncleaved

sc-tPA, in what would normally be a zymogen, has nearly as much enzymatic activity as the two-chain form.[208] ATP inhibited the enzymatic activities (measured as cleavage of chromogenic substrates) of all eleven serine proteases (Figure 4.1 A-C), with IC_{50} values from 2 to 11 mM (Table S 4.1). ADP also inhibited these proteases (Figure 4.1 D-E), with very similar IC_{50} values that ranged from 2 to 9 mM (Table S 4.1). While AMP also inhibited these enzymes (Figure 4.1 G-I), it did so with higher IC_{50} values that ranged from 9 to 70 mM (Table S 1). The "zymogen" form of tPA (sc-tPA) exhibited similar IC_{50} values as did tc-tPA, with regard to inhibition by ATP, ADP or AMP.

We next compared ADP and ATP to the other major cellular ribonucleotide triphosphates (CTP, GTP, and UTP), as well as to the sulfate donor, PAPS, as inhibitors of chromogenic substrate hydrolysis by sTF-FVIIa. We found that 10 mM ADP, ATP, or CTP inhibited this enzyme >99%, while 10 mM GTP or UTP resulted in 82-86% inhibition and 10 mM PAPS resulted in 64% inhibition (Figure 4.1 J). These results show that ADP, ATP and CTP all strongly inhibit sTF-FVIIa, while GTP, UTP, and PAPS also inhibit sTF-FVIIa but required significantly higher concentrations (>10 mM) to achieve saturation.

Since the nature of the base in the nucleotide appears to be relatively unimportant, we examined whether the di- or triphosphate portion of nucleotides alone might be responsible for the observed protease inhibition. Accordingly, we tested sodium pyrophosphate (PP) or tripolyphosphate (PPP) at concentrations up to 10 mM. Neither PP nor PPP resulted in measurable inhibition of trypsin or thrombin (Figure S 4.1).

Much of the cytosolic ATP is bound to Mg^{2+}, while cytosolic ADP is largely Mg^{2+}-free.[209,210] Although the Mg^{2+} concentration in the ER lumen is not known with any certainty, it is known that the ER lumen contains millimolar concentrations of both Mg^{2+} and Ca^{2+},[210,211] either of which could associate to some extent with ADP or ATP. Accordingly, we examined whether low millimolar concentrations of these divalent metal ions affected the extent of inhibition by ADP or ATP in three cases: (1) chromogenic substrate hydrolysis by FVIIa; (2) chromogenic substrate hydrolysis by FXa; and (3) FX activation by mTF-FVIIa (the complex of FVIIa bound to relipidated mTF, or membrane-anchored TF). In all cases, there was no significant change in enzyme activity as a function of Ca^{2+} concentration, and a modest dependence on Mg^{2+} concentration (Figure S 4.2). These findings support the idea that both Mg-ATP and free ATP are

fully capable of inhibiting serine proteases, as are any complexes between ADP or ATP and Ca^{2+}, at reasonable concentrations of these divalent metal ions.

The luminal pH of the ER is reported to be 7.2 ± 0.2, while that of the Golgi is 6.4 ± 0.3.[212] We therefore examined whether the lower pH encountered in the Golgi lumen would influence the sensitivity of sTF-FVIIa to ATP inhibition (Figure S 4.3). When tested from pH 6.2 to 7.4, we found that 5 mM ATP was only slightly less effective in inhibiting chromogenic substrate hydrolysis by sTF-FVIIa at pH 6.2, 6.5 or 7.4, relative to assays conducted at pH 6.8 or 7.1. On the other hand, 10 mM ATP inhibited nearly 100% of the activity of this enzyme across the entire pH range. Secretory granules are typically even more acidic (luminal pH ~5),[212] but since serine proteases have essentially unmeasurable enzymatic activities at pH 5, we did not attempt to investigate nucleotide inhibition at this pH.

4.3.2 ADP is an uncompetitive inhibitor of TF-FVIIa protease activity

We performed more detailed kinetic studies of the protease activity of mTF-FVIIa, the membrane-bound enzyme complex that triggers blood clotting, to determine how ADP influences the ability of this enzyme to activate its major protein substrates, FX and FIX, by limited proteolysis. Initial rates of FX activation were diminished by increasing ADP concentration (Figure 4.2 A), resulting in an increase in K_m, and a decrease in both k_{cat} and k_{cat}/K_m (Table S 4.2). To further address the inhibition type, we utilized Cornish-Bowden plots,[184] in which S/V (the quotient of the substrate concentration (S) and activation rate (V)) is plotted against I, the inhibitor (ADP) concentration, using data collected over a range of substrate (FX) concentrations (Figure 4.2 B). The resulting plot was consistent with uncompetitive inhibition, with the family of lines intersecting at $I = -K_i$ and $S/V = K_m/V_{max}$, yielding a K_i of 2.5 mM for ADP inhibition of FX activation by mTF-FVIIa (Table S 2).

FIX activation by mTF-FVIIa was also inhibited by increasing ADP concentrations (Figure 4.2 C). For this substrate, we observed reductions in both k_{cat} and K_m, corresponding to a 1.6-fold decrease in k_{cat}/K_m for FIX activation by 5 mM ADP (Table S 4.2). Cornish-Bowden plots were also consistent with uncompetitive inhibition (Figure 4.2 D), yielding a K_i of 0.7 mM for ADP inhibition of FIX activation by mTF-FVIIa (Table S 4.2).

4.3.3 ATP binds cooperatively to FXa, trypsin and thrombin

We used SPR to quantify ATP binding to immobilized FXa, trypsin and thrombin, all of whose enzymatic activities had been blocked via covalent modification of their active sites (Figure 4.2 E-G). We observed sigmoidal binding isotherms with all three proteases, consistent with cooperative ligand binding. The Hill equation fit well to the data, resulting in K_D values ranging from 15.8 to 23.5 mM, and Hill coefficients from 1.48 to 1.76 (Table S 4.3). Interestingly, K_D values for FXa, trypsin and thrombin are 4- to 7-fold higher than IC_{50} values for these proteins (Table S 4.1). To measure the K_D in SPR experiments, the active site of each enzyme was covalently inhibited which might explain the discrepancy.

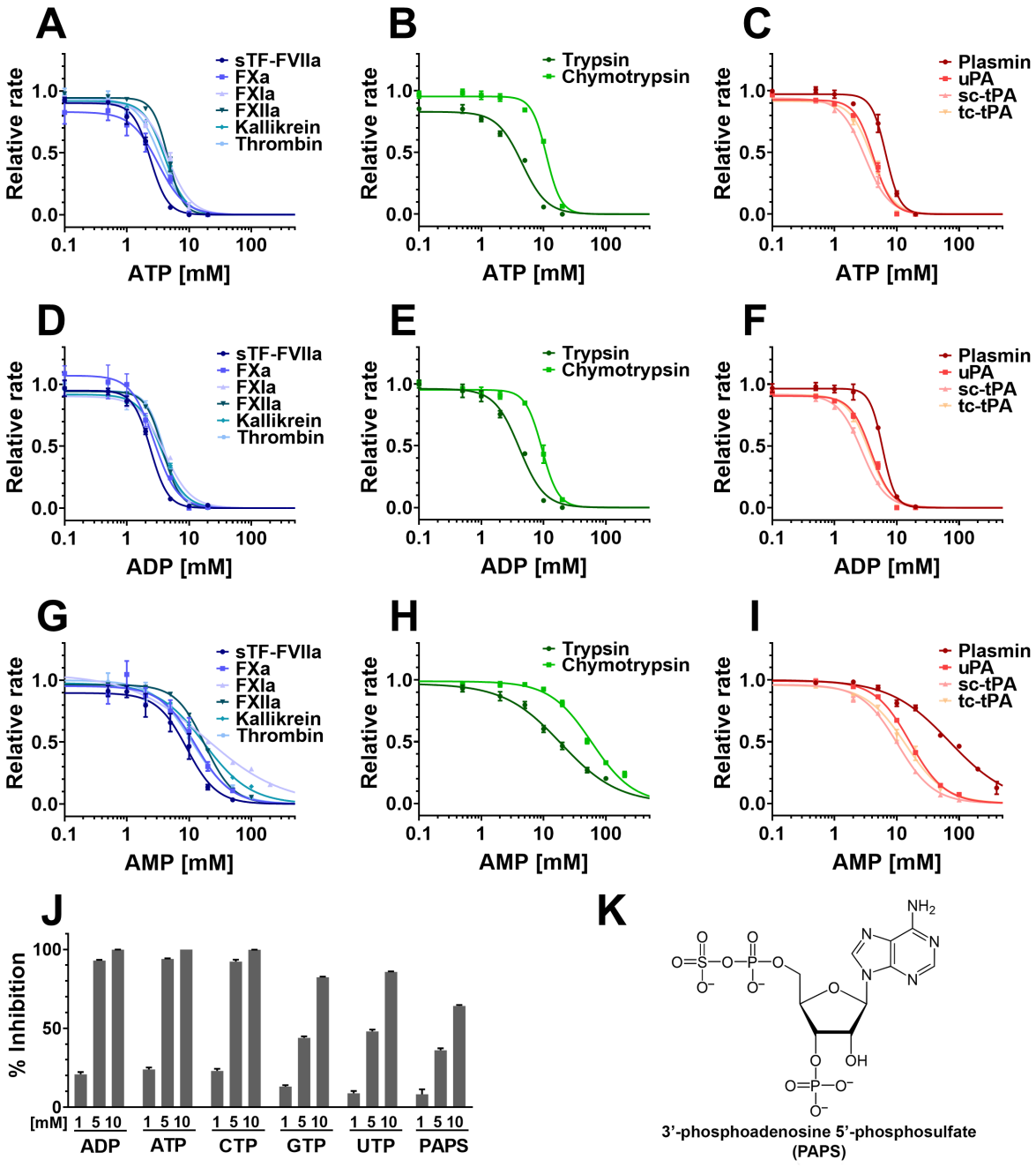

Figure 4.1 Nucleotides inhibit serine protease activity. (A-I) Enzymatic activities of serine proteases involved in blood clotting (blue), food digestion (green) or fibrinolysis (red) were quantified in the presence of increasing ATP, ADP or AMP concentrations, then normalized to rates without nucleotide. Protease inhibition by ATP for (A) clotting proteases (sTF-FVIIa, FXa, FXIa, FXIIa, plasma kallikrein, thrombin), (B) digestive proteases (trypsin, chymotrypsin) or (C) fibrinolytic proteases (plasmin, uPA, sc-tPA and tc-tPA). (D-F) Protease inhibition by ADP. (G-I) Protease inhibition by AMP. (J) Rates of chromogenic substrate hydrolysis by sTF-FVIIa were measured in the presence of 1, 5 or 10 mM ATP, CTP GTP, UTP, ADP or PAPS, and expressed as percent inhibition of the rate without nucleotides. (K) Structure of PAPS. Data in all panels are mean ± standard error; n ≥ 3.

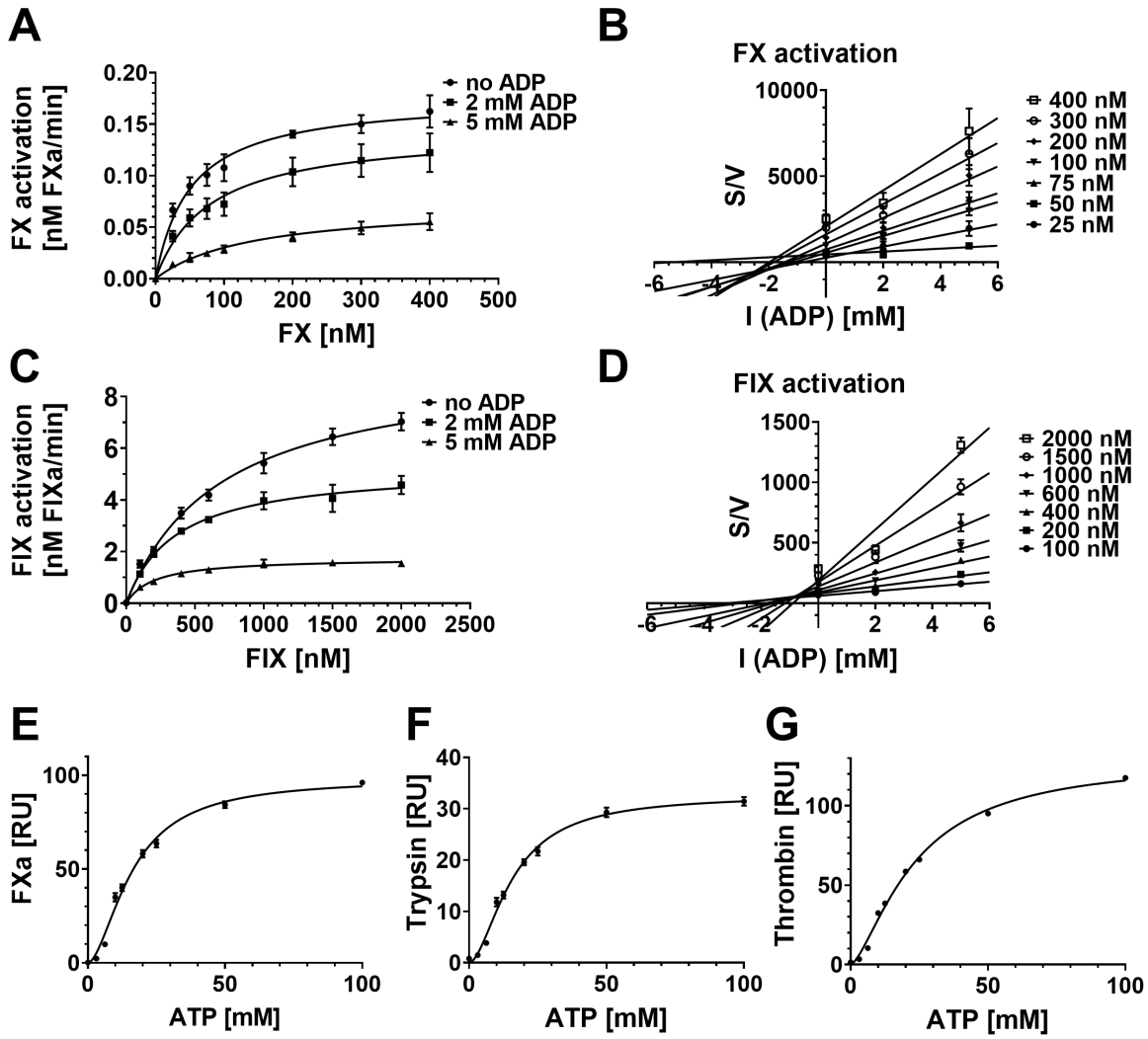

Figure 4.2 Nucleotides act as uncompetitive inhibitors and exhibit cooperative binding to serine proteases. (A-D) ADP inhibits FX and FIX activation by mTF-FVIIa, consistent with uncompetitive inhibition. Activation of varying concentrations of FX or FIX by mTF-FVIIa was measured in the presence of 0, 2 or 5 mM ADP. (A) Initial rates of FX activation by mTF-FVIIa, and (C) initial rates of FIX activation by mTF-FVIIa (in both panels, the Michaelis-Menten equation was fitted to the data). The data from panels A and C were replotted in panels B and D, respectively, as Cornish-Bowden plots, in which the y-axes are S/V, the quotient of the substrate concentration (S) (i.e., the FX or FIX concentration) divided by activation rate (V), to which lines were fitted. (E-G) Evidence of cooperative binding of ATP to FXa, trypsin and thrombin. ATP binding to serine proteases was detected using SPR. Active-site inactivated serine proteases were immobilized on a CM5 sensorchip, over which increasing ATP concentrations (up to 100 mM) were flowed and the maximal, steady-state RU values recorded for each ATP concentration. Plotted here as RU versus ATP, the Hill equation was fitted to the binding data, from which K_D values and Hill coefficients were determined. (E) ATP binding to FXa; (F) ATP binding to trypsin; and (G) ATP binding to thrombin. Data in all panels are mean ± standard error; n = 3.

4.3.4 Clustering and characterization of putative ATP binding sites of thrombin and trypsin

We employed all-atom MD simulations to probe ATP binding to thrombin and trypsin. Multiple flooding simulations were carried out for thrombin and trypsin at 25 mM ATP, allowing enhanced sampling of ATP binding events. To further characterize the putative ATP interaction sites captured during the MD simulations, clustering was performed using the degree of contact between ATP and individual amino acids of the protein in "ATP-bound" trajectory frames.

Four ATP-binding clusters were identified in thrombin (Figure 4.3 A) with the residue contact frequencies shown in Figure 4.3 B (numbered by homology to chymotrypsinogen[185]). These binding clusters represent the four major interaction sites for ATP in thrombin (Figure 4.3 C). Interaction site 1 corresponds to thrombin's anion-binding exosite 2 (ABE2) (Figure 4.3 C, inset 1), with residues R126, Q131, R165, F181, and R233 being the most important for ATP interaction. ABE2, which forms a positive electrostatic potential surface (Figure S 4.4 B), is also a known interaction epitope for heparin,[213] platelet glycoprotein Ibα,[214-217] and anionic fibrinogen γ′ chain.[218] Interaction site 2 (Figure 4.3 C, inset 2) corresponds to the Na^+ binding site of thrombin, well known as a modulator of thrombin's catalytic activity.[219,220] R221 and K224 in this site are important for Na^+ binding which consequently positions D189 to engage with the thrombin's substrate Arg side chain in the P1 site. [219] We might speculate that perturbation of Na^+ binding caused by ATP molecules might prevent proper engagement of D189 with the substrate and thus contribute to thrombin inhibition. Interaction site 3 (Figure 4.3 C, inset 3) and interaction site 4 (Figure 4.3 C, inset 4) correspond to the γ-loop and the 70-loop (i.e., anion-binding exosite 1 (ABE1)), respectively. R67, R75, K81, and K149 are the key basic residues from ABE1 that interact with bound ATP. ABE1 has an overall positive electrostatic potential (Figure S 4.4 A) and has been shown to interact with fibrinogen,[221-223] fibrin,[222,224] and thrombomodulin.[207,221,225-227] Binding of ATP to ABE1 may thus follow a similar inhibition mechanism to ABE2 by interfering with substrate binding. The average number of ATPs bound to thrombin throughout the trajectory of each simulated replica (Figure S 4.5) was calculated as 1.58 ± 0.51, which is in line with the Hill coefficient for ATP binding to thrombin estimated from SPR experiments (1.48 ± 0.08, Table S 4.3). As an example of potential cooperative binding, simultaneous binding of ATPs to interaction site 1 is shown in Figure 4.3 D-E.

We also simulated trypsin in the presence of experimental ATP concentrations and similarly performed clustering on "ATP-bound" frames of the trajectory. Three putative ATP

interaction sites were identified on trypsin, with residues R68, K112, R116 and K240 identified as the key basic residues interacting with bound ATPs (Figure S 4.6). The 60-loop and the 99-loop, corresponding to interaction site 1 (Figure S 4.6 C, inset 1), are important allosteric regulatory loops of trypsin-like serine proteases.[228] ATP binding to this site may interfere with allosteric communication between different regions of the protein.

4.3.5 NMR analyses of ATP binding to thrombin

We used solution NMR to investigate ATP binding to human thrombin by titrating natural-abundance ATP into a solution of $^{2}H,^{15}N$-labeled thrombin (using the catalytically inactive S195M mutant of thrombin, bound to natural-abundance TM456 fragment of thrombomodulin). In total, we measured six spectra with concentrations of 0, 1, 5, 10, 20 and 40 mM ATP. Two-dimensional $^{1}H,^{15}N$-HSQC-TROSY spectra, recorded before adding ATP and after each addition, show clear changes in the chemical shifts of thrombin backbone amides (Figure 4.4 A and Figure S 4.7), indicating that ATP binds thrombin. The large excess of ATP compared to thrombin that was used for the titration (>1,100:1 for the last titration point) implies that ATP binding to the protein is relatively weak, consistent with the mM binding affinities observed throughout this study. Nevertheless, the chemical shift changes are localized at four sections of the thrombin sequence, with residues A1B, R126, Q131, I176 and L234 showing the largest shifts (Figure 4.4 B). When displayed on the structure, these residues cluster in a single region of thrombin, indicating a prominent ATP binding site coincident with ABE2 (Figure 4.4 C). Notably, R126 and Q131 were also identified as among the most important ATP-interacting residues in the MD simulations of thrombin binding to ATP (Figure 4.3 C, inset 1, and Figure 4.3 E).

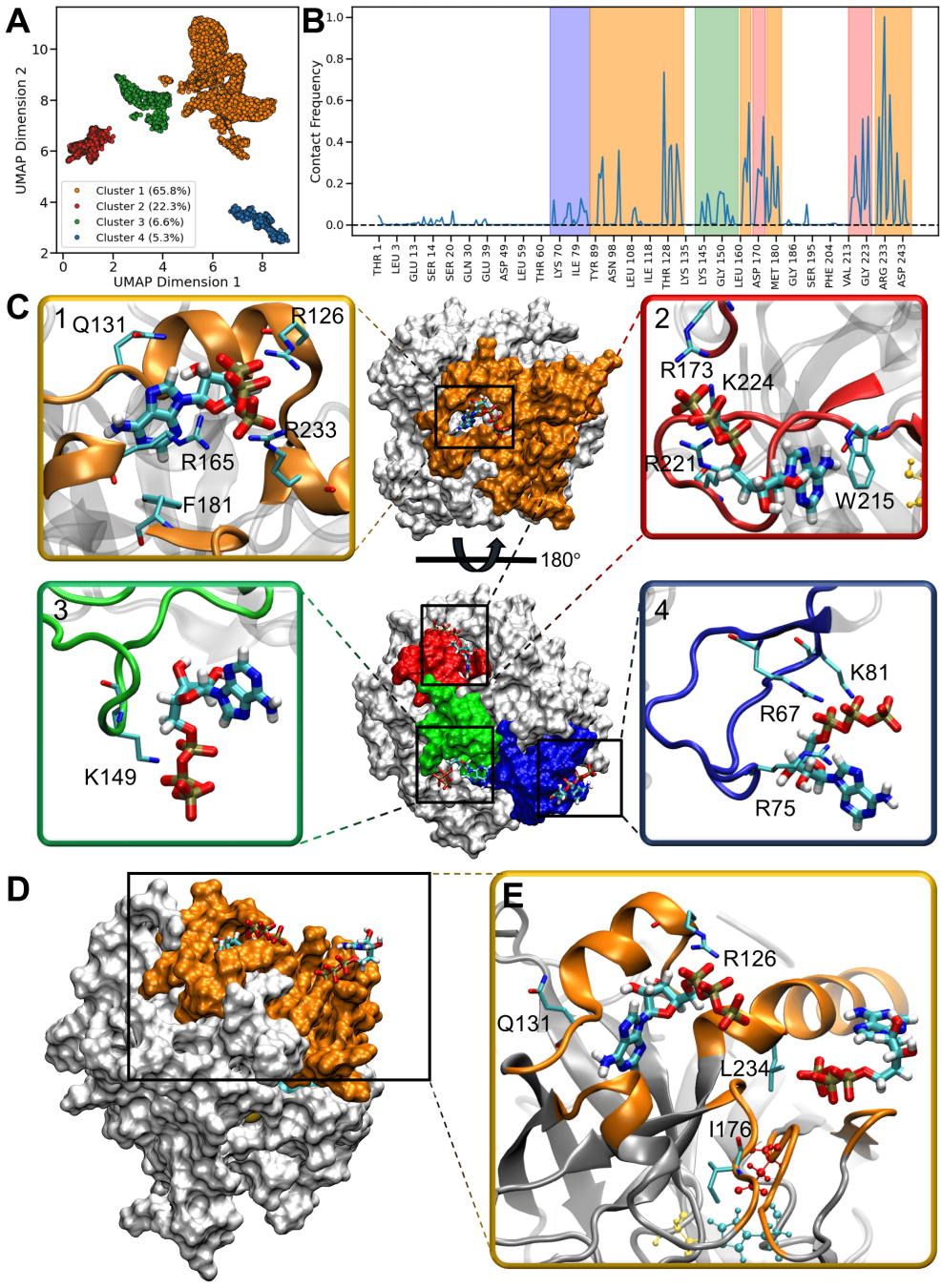

Figure 4.3 MD clustering analysis of ATP-bound thrombin and representative interaction sites. (A) ATP-bound frames are projected on UMAP dimension 1 and UMAP dimension 2, with clusters 1, 2, 3 and 4 colored in orange, red, green, and blue, respectively. The population of each cluster is denoted as percentage. (B) Contact frequencies of residues, calculated by normalizing the total contact of each residue from all "ATP-bound" frames with respect to the maximum total contact, using the color scheme in panel A to identify the cluster in which each residue is present. (C) Representative snapshot of ATP interaction sites, showing ATP molecules with the highest contact numbers, corresponding to the four identified clusters. Center panel shows the surface representation of thrombin in white, with four ATP interaction sites highlighted using the color scheme used from panels A/B. Insets 1-4 are closeup views of each interaction site, showing bound ATPs and numbering the important thrombin residues surrounding them. (D) An example of two ATP molecules simultaneously bound to interaction site 1, colored as in panel C. (E) Closeup view of D, showing details of the bound ATPs and interacting residues.

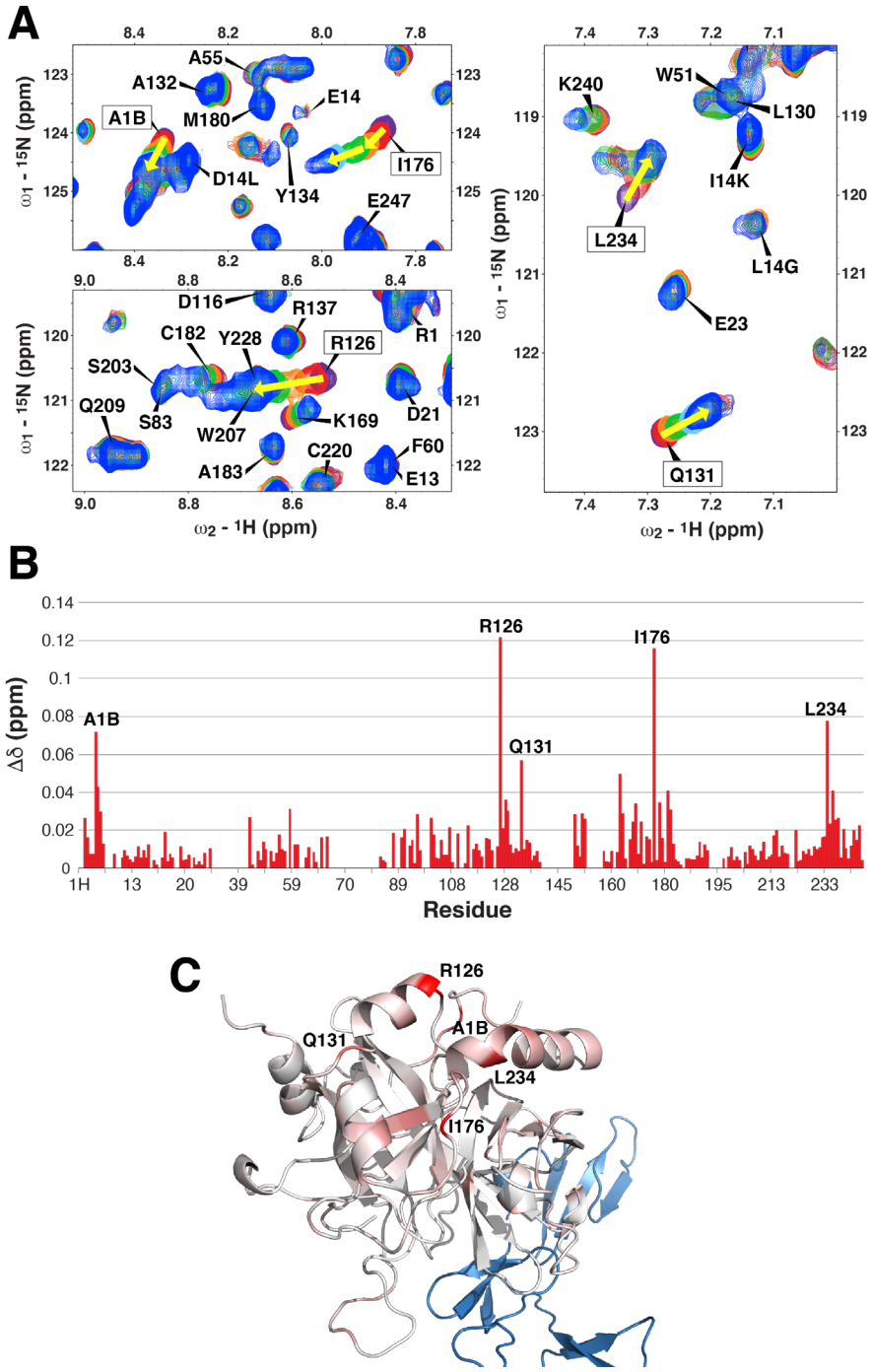

Figure 4.4 NMR analyses identify ATP interaction with ABE2 of thrombin. (A) Expansions from the full two-dimensional 1H,15N-HSQC-TROSY spectra of thrombin (from SI Appendix, Fig. S7), highlighting residues with largest chemical shift changes after adding ATP to the sample (in particular, residues A1B, R126, Q131, I176 and L234). (B) Chemical shift perturbation (CSP) plot showing the magnitude of chemical shift changes of thrombin backbone amides between the spectrum recorded with no ATP and the last point of the titration after adding 40 mM ATP to the sample. The five residues with the largest CSP values (A1B, R126, Q131, I176 and L23) are indicated. (C) Crystal structure of thrombin bound to TM456 (PDB ID: 1DX5), with TM456 colored light blue, and thrombin color-coded to highlight residues whose chemical shifts changed after ATP addition (white, no change; red, largest change). The five residues with the largest chemical shift changes (A1B, R126, Q131, I176 and L234) are clustered on the face of the thrombin away from TM456, coincident with thrombin's ABE2.

4.4 Discussion

From the results of this study on eleven serine proteases of disparate function, we propose a new role for ATP and other ribonucleotides known to be present in the ER and Golgi lumen: namely, to keep any prematurely activated serine proteases catalytically quiescent prior to secretion. Most secreted serine proteases are synthesized as inert zymogens, which should remain catalytically silent during their transit through the ER and Golgi. Any accidental conversion of such zymogens into active proteases while still inside the secretory machinery could be dangerous, as they could indiscriminately proteolyze multiple proteins, leading to ER stress and cellular damage. In addition, some cells such as hepatocytes secrete multiple serine protease zymogens, so premature activation of any one of these enzymes within the ER or Golgi could trigger a cascade of proteolytic activation events which may be catastrophic for the cell.

ADP, ATP and UTP were approximately equally effective inhibitors of serine protease activity, with IC_{50} values in the low mM range. GTP, CTP and PAPS also inhibited the proteases, albeit with slightly higher IC_{50} values. We therefore propose that it is the sum total of the nucleotide concentration in the lumen of the ER and Golgi that acts to keep these proteases quiescent if they are prematurely activated. And although the exact concentrations of nucleotides with the ER or Golgi lumen is not known, the IC_{50} values we found for ATP inhibition of all eleven serine protease are in line with the known cytosolic ATP concentrations of 2 to 9 mM.[173] Interestingly, we found evidence of cooperativity in binding of nucleotides to proteases. Cooperative binding allows steeper concentration-dependence curves, which could be beneficial in inhibiting these proteases in the presence of low mM nucleotide concentrations, while allowing them to achieve full enzymatic activity extracellularly, where nucleotide concentrations are only in the low μM range.[173]

Some serine proteases, such as sc-tPA, have nearly full enzymatic activity even in the uncleaved "zymogen" form. [208] An endogenous protease inhibitor in the ER and Golgi therefore makes sense to prevent such catalytically active zymogens from indiscriminately proteolyzing other proteins. Also, some clotting proteases undergo autoactivation as part of the triggering mechanism of blood clotting. For example, TF strongly promotes FVII autoactivation, [157] which could be a problem for cells that synthesize both TF and FVII. [229,230] Indeed, TF-FVIIa had the lowest IC_{50} value for ADP or ATP inhibition (2.4 ± 0.1 mM), compared to the other serine proteases tested.

We presented structural data obtained from MD simulations and solution NMR analyses of ATP association with thrombin and trypsin, thereby identifying putative binding sites that coincide with cationic regions of the proteins known to be involved in the regulation of their catalytic activity. The findings are consistent with relatively low-affinity binding and cooperative association of ATP with these proteases.

The role of nucleotides in keeping serine proteases in the ER and Golgi quiescent prior to secretion has potential relevance to human health. Hereditary pancreatitis results from certain mutations in the gene for cationic trypsinogen, which are thought to allow premature activation of trypsin while it is still in the pancreas.[177-179] One of these pancreatitis-associated mutations, R116C, [231] is of particular relevance to our results, since R116 was identified as a key ATP-interacting site in our MD simulations. Expressing recombinant trypsinogen carrying this mutation in cell culture was reported to severely reduce protein secretion with concomitant induction of the ER unfolded protein response. [232] That study concluded that the effects of the R116C mutation were unrelated to trypsinogen activation but instead were due to mutation-induced proenzyme misfolding and consequent ER stress. It is tempting, however, to speculate that an additional mechanism leading to ER stress associated with this trypsinogen mutation could be the loss of an ATP-binding site which then allows premature activation of the protease in the ER.

In conclusion, our study proposes a new role for nucleotides as inhibitors of serine proteases prior to secretion, in a novel cellular safety mechanism that prevents their premature activation in the ER and Golgi. It would be of interest to examine if nucleotides can similarly inhibit other secreted enzymes and proenzymes while they are transiting through the cellular secretory machinery.

4.5 Supplementary Information

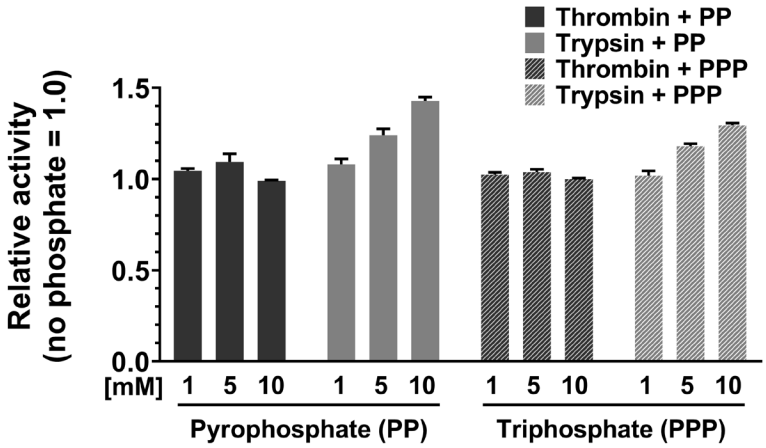

Figure S 4.1 Lack of inhibition of thrombin or trypsin by pyrophosphate or tripolyphosphate. Initial rates of chromogenic substrate hydrolysis by thrombin or trypsin were quantified in the presence of varying concentrations of sodium pyrophosphate (PP) or sodium tripolyphosphate (PPP), normalized to rates without phosphate and expressed as percent inhibition. Data are mean ± standard error; n = 3.

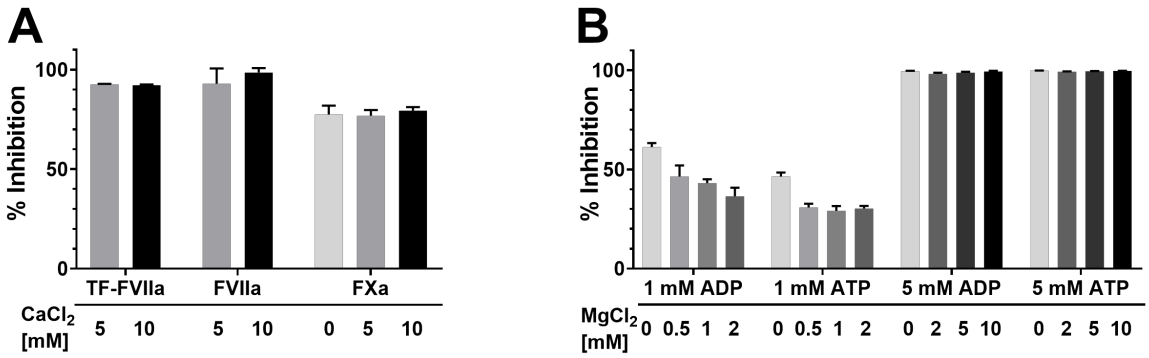

Figure S 4.2 Inhibition of the serine proteases, FVIIa and FXa, by ADP and ATP is largely independent of divalent metal ions. (A) Initial rates of FX activation by mTF-FVIIa (first two bars), or chromogenic substrate hydrolysis by FVIIa or FXa (remaining four bars), were measured in the presence of 5 mM ADP and the indicated $CaCl_2$ concentrations. Since FVIIa is a calcium-dependent enzyme, we routinely include 5 mM Ca^{2+} in its reactions. Note that raising the Ca^{2+} concentration from 5 to 10 mM had essentially no effect on inhibition of TF-FVIIa or FVIIa by ADP. Since cleavage of chromogenic substrates by FXa is calcium-independent, we typically omit Ca^{2+} from this reaction. Adding 5 or 10 mM Ca^{2+} had no discernable effect on the inhibition of FXa by ADP, relative to no calcium. (B) Initial rates of FX activation by mTF-FVIIa were measured in the presence of 0, 1 or 5 mM ADP or ATP, and varying concentrations of $MgCl_2$ (up to 10 mM), all in the presence of 5 mM $CaCl_2$. Mg^{2+} partially blunted the inhibition of mTF-FVIIa by 1 mM ADP or ATP, while Mg^{2+} had essentially no effect on inhibition of mTF-FVIIa by 5 mM ADP or ATP. For both panels, enzyme activities in the presence of nucleotides were normalized to those without nucleotides and expressed as percent inhibition. Data are mean ± standard error; n ≥ 3.

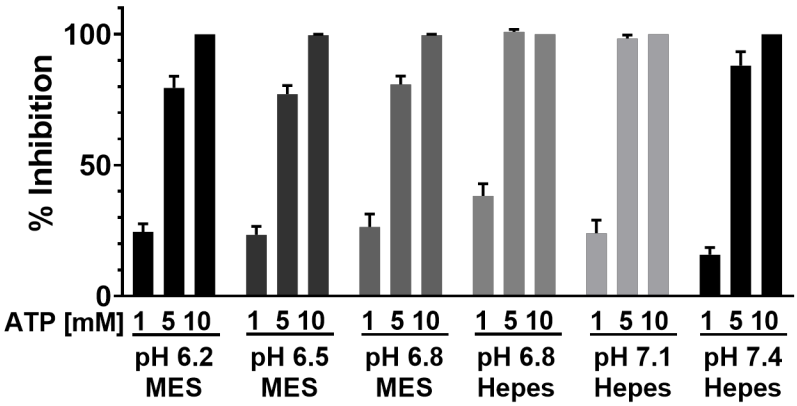

Figure S 4.3 ATP inhibits chromogenic substrate hydrolysis by sTF-FVIIa with similar effectiveness from pH 6.2 to 7.4. Chromogenic substrate hydrolysis by sTF-FVIIa was measured at varying pH values in a buffered solution containing 20 mM MES (pH 6.2 to 6.8) or Hepes (pH 6.8 to 7.4), 100 mM NaCl, 5 mM $CaCl_2$, 0.1% bovine serum albumin, 0.02% NaN_3, and 0, 1, 5 or 10 mM ATP. Enzyme concentrations were as follows: pH 6.2: 150 nM FVIIa, 1 µM sTF; pH 6.5: 100 nM FVIIa, 1 µM sTF; pH 6.8: 40 nM FVIIa, 400 nM sTF; pH 7.1: 30 nM FVIIa, 300 nM sTF; and pH 7.4: 20 nM FVIIa, 200 nM sTF. Enzyme activities in the presence of nucleotides were normalized to those without nucleotides and expressed as percent inhibition. Data are mean ± standard error; n = 3.

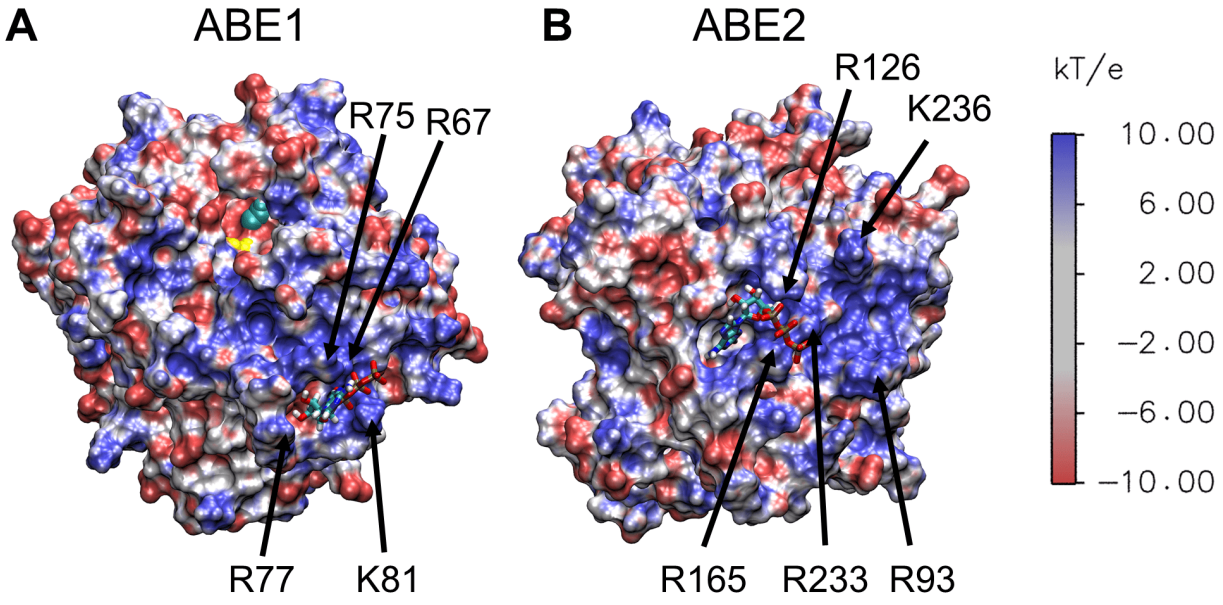

Figure S 4.4 Electrostatic potential maps of thrombin after binding of ATP to anion-binding exosites (ABE), ABE1 or ABE2. Positive and negative potential surfaces are shown in shades of blue and red, respectively (values in legend). (A) Electrostatic potential surface map of thrombin with ATP bound to ABE1 (from Figure 4.3 C, inset 4). Key basic residues of ABE1 are highlighted with arrows. H57 and S195 in the catalytic site of thrombin are visible in this view and shown in cyan and yellow, respectively. (B) Electrostatic potential map of thrombin with ATP bound to ABE2 (from Figure 4.3 C, inset 1). Key basic residues of ABE2 are highlighted with arrows.

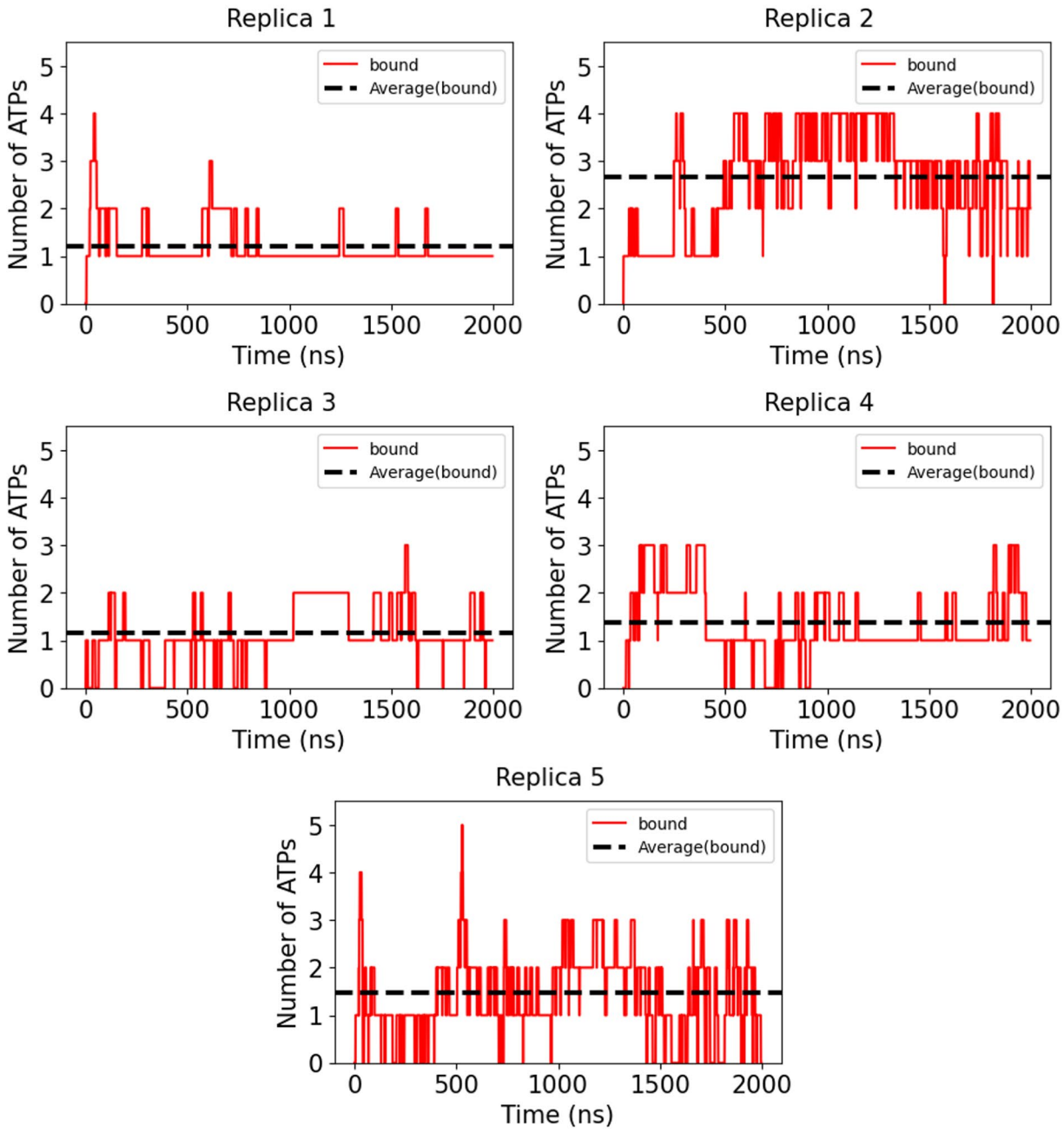

Figure S 4.5 Simultaneous binding of multiple ATP molecules to thrombin. The number of ATP molecules bound to thrombin during the 5 independent MD trajectories are shown in solid red lines, with the average number of ATP molecules bound to the protein in each simulation indicated using the horizontal, dashed black line. For reference, experimentally derived Hill coefficients are in the range of 1.48-1.76 (see results).

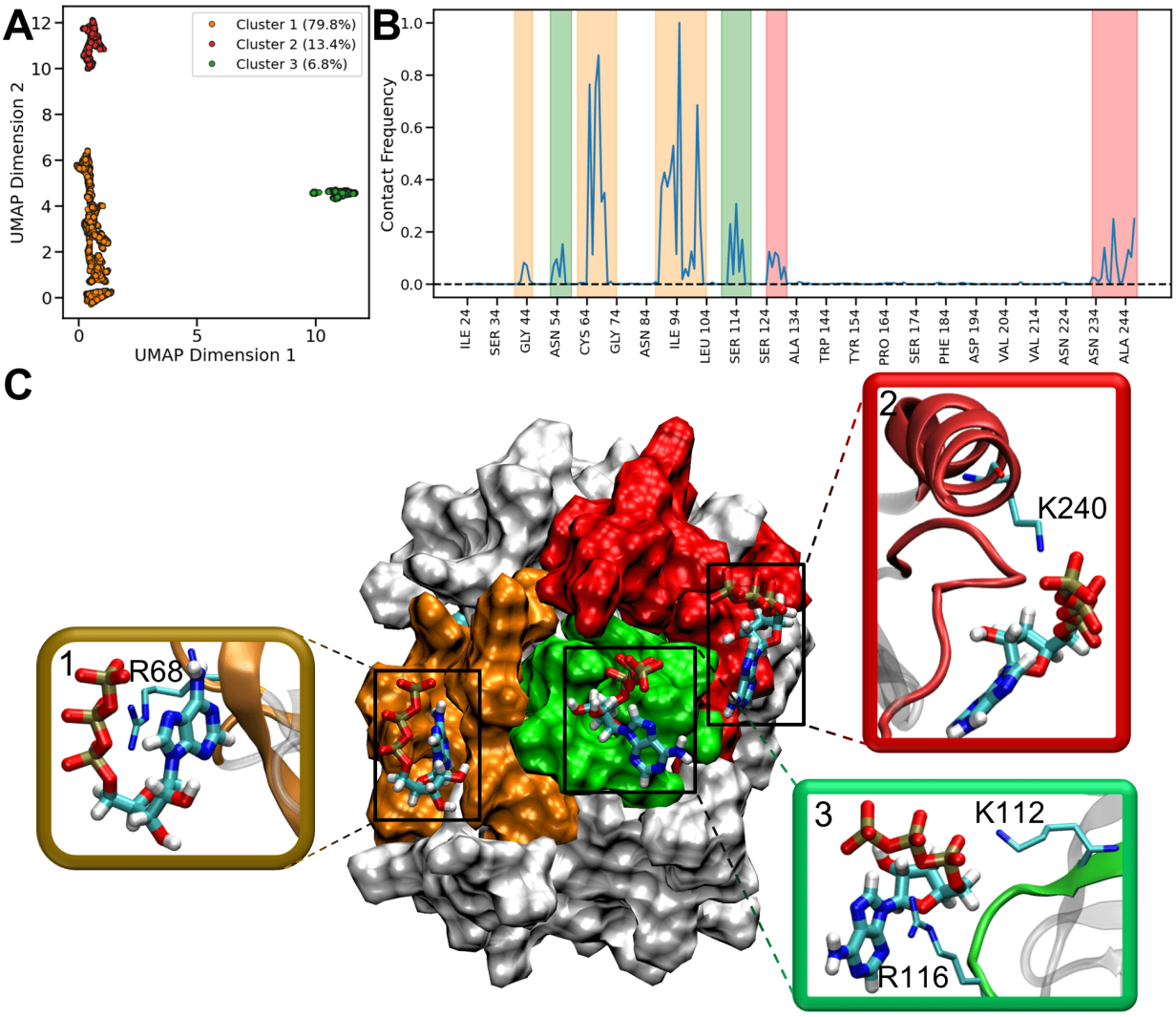

Figure S 4.6 MD clustering analysis of ATP-bound trypsin and representative interaction sites. (A) ATP-bound frames are projected on UMAP dimension 1 and UMAP dimension 2. Clusters 1, 2, and 3 are colored in orange, red, and green, respectively. The population size of clusters is denoted as percentages. (B) The contact frequency of residues was calculated by normalizing total contact of each residue in all ATP-bound frames with respect to the maximum total contact. The color scheme from panel A is used to denote the respective cluster in which each residue is present. (C) Representative snapshot for each ATP interaction site corresponding to the three identified clusters, showing the ATP molecule with the highest contact numbers. The center panel shows the surface representation of trypsin in white, with three ATP interaction sites colored as in panels A and B. Insets 1-3 show enlarged views of each interaction site. Bound ATP molecules and important residues surrounding them are drawn in licorice representation

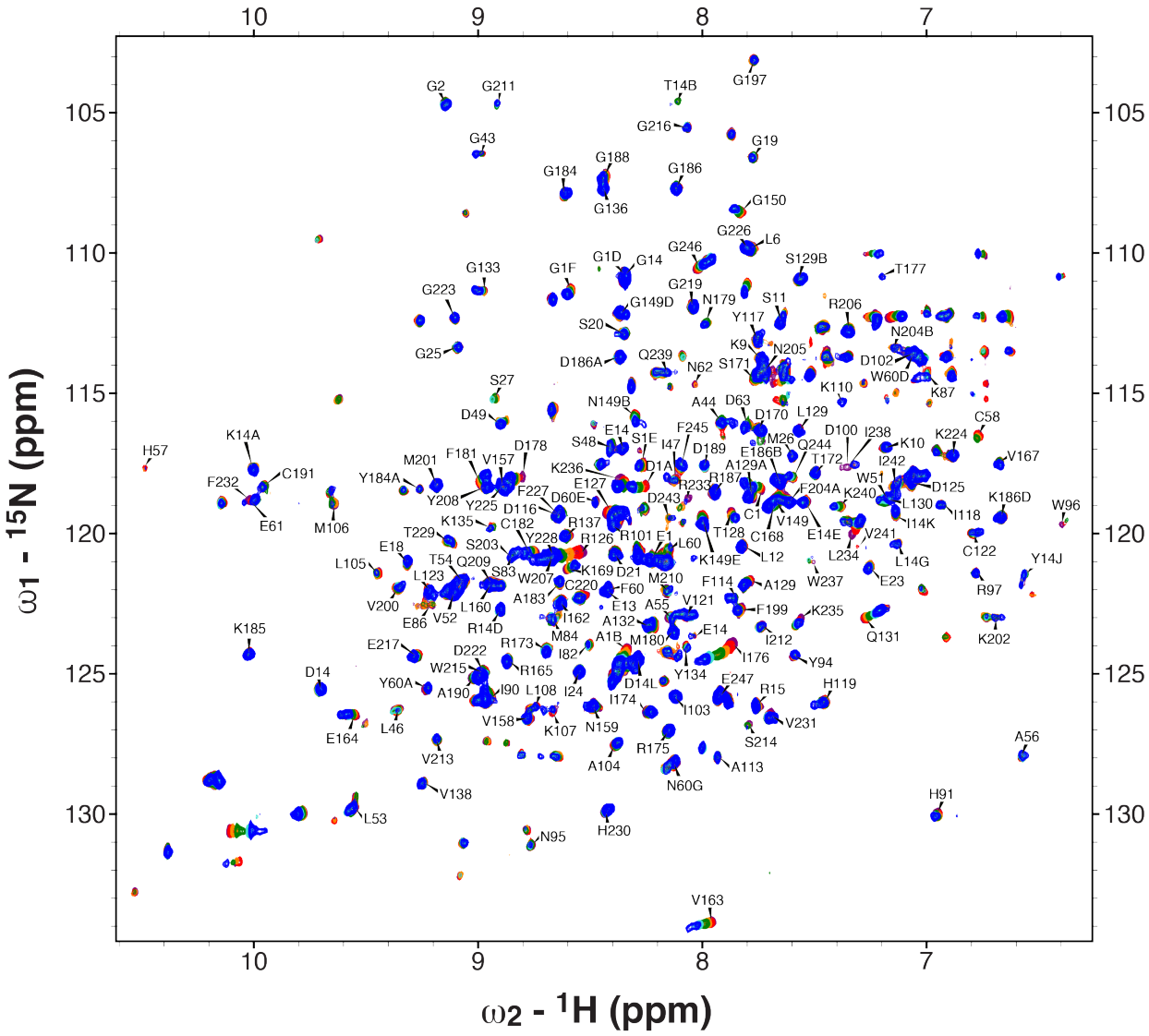

Figure S 4.7 Two-dimensional $^{1}H,^{15}N$-HSQC-TROSY spectra of $^{2}H,^{15}N$-labeled S195M thrombin bound to natural abundance TM456, recorded before and after each addition of ATP. In addition to the starting experiment recorded with no ATP (purple spectrum), five titration points were acquired with the concentration of ATP at each step being 1 mM (red), 5 mM (orange), 10 mM (green), 20 mM (cyan) and 40 mM (blue).

Table S 4.1 IC_{50} values for inhibition of serine proteases by ATP, ADP or AMP.

Enzyme role	Protease	IC_{50} [mM]* ATP	IC_{50} [mM]* ADP	IC_{50} [mM]* AMP
Blood clotting	sTF-FVIIa	2.4 ± 0.1	2.4 ± 0.1	9.2 ± 1.3
	FXa	3.2 ± 0.5	2.8 ± 0.3	12.7 ± 2.2
	FXIa	4.6 ± 0.3	4.0 ± 0.2	18.9 ± 2.3
	FXIIa	4.5 ± 0.2	3.8 ± 0.1	17.8 ± 0.3
	Plasma kallikrein	4.1 ± 0.2	3.7 ± 0.2	17.6 ± 1.0
	Thrombin	3.4 ± 0.3	4.0 ± 0.3	11.2 ± 1.2
Digestion	Trypsin	4.5 ± 0.3	4.1 ± 0.3	19.1 ± 2.2
	Chymotrypsin	11.1 ± 0.4	9.4 ± 0.4	59.3 ± 3.3
Fibrinolysis	Plasmin	6.7 ± 0.3	5.9 ± 0.2	70.2 ± 5.5
	uPA	4.2 ± 0.2	3.9 ± 0.2	16.3 ± 0.4
	sc-tPA	3.1 ± 0.1	2.8 ± 0.1	10.3 ± 0.5
	tc-tPA	4.0 ± 0.2	3.6 ± 0.2	13.8 ± 1.3

*IC_{50} values were derived from plots in Figure 4.1 A-I. Data are mean ± standard error; n ≥ 3.

Table S 4.2 Influence of ADP on kinetics of FX and FIX activation by mTF-FVIIa.

	ADP [mM]	FX activation	FIX activation
K_m [nM]*	0	51 ± 9	694 ± 90
	2	79 ± 23	362 ± 65
	5	140 ± 40	202 ± 34
k_{cat} [sec^{-1}]*	0	0.981 ± 0.052	0.156 ± 0.008
	2	0.801 ± 0.079	0.088 ± 0.005
	5	0.403 ± 0.048	0.029 ± 0.001
k_{cat}/K_m [$M^{-1}sec^{-1}$]	0	1.92×10^7	2.25×10^5
	2	1.01×10^7	2.43×10^5
	5	2.88×10^6	1.45×10^5
K_i [mM]**	-	2.5	0.7

*K_m and k_{cat} values are derived from plots in Figure 4.2 A and C.
**K_i values are derived graphically from plots in Figure 4.2 B and D.
Data are mean ± standard error; n = 3.

Table S 4.3 Binding constants for association of ATP with FXa, trypsin and thrombin.

	FXa	Trypsin	Thrombin
K_D [mM] *	16.3 ± 0.9	15.8 ± 0.8	23.5 ± 1.3
Hill coefficient [a]	1.74 ± 0.13	1.76 ± 0.13	1.48 ± 0.08

*K_D values and Hill coefficients are derived from plots in Figure 4.2 E-G.
Data are mean ± standard error; n = 3.

Chapter 5 Conclusion

This thesis investigates the regulation of serine proteases in blood clotting and beyond. Chapters 2 and 3 are focused on the physiological activator of blood clotting, the TF-FVIIa complex, and how this complex selects and interacts with its protein substrates. Chapter 4 is focused on secreted serine proteases more broadly and how ribonucleotides affect protease activity.

The TF-FVIIa complex plays a crucial role in hemostasis and many thrombotic diseases.[6,7,160] Although this complex has been studied extensively over the last few decades, it is still unknown how TF-FVIIa selects and interacts with its major protein substrates, FIX and FX. In chapter 2, we showed that a membrane-adjacent TF serine loop facilities TF-FVIIa substrate selectivity. Our results show that the precise length of the serine loop is essential for activation of FX but not FIX. Serine loop mutations decreased FX activation by almost 200-fold, with little to no effect on FIX activation. Previous studies have reported that some TF mutations, particularly mutations in the TF exosite, have a bigger effect on FX activation compared to FIX.[138,153] However, none of those studies reported such a strong influence on one substrate over another as we observed with the serine loop mutations. These findings open the door to investigate other TF-FVIIa protein substrates, including FVII[157] and PAR2,[158,159] and what role the TF serine loop plays in activation of these alternative substrates.

In chapter 3, we showed the generation and structural analysis of a membrane-bound complex of TF, FVIIa and the FX substrate mimetic XK1. Our current cryo-EM map includes densities for all three proteins and indicates potential interactions between the TF exosite and FX GLA domain. Although the TF-FVIIa crystal structure has been solved over 25 years ago,[44] this is the first reported structural model of TF-FVIIa bound to a substrate mimetic. Numerous studies over the last three decades have reported that TF exosite mutations decrease FX activation by up to 100-fold,[79-84] hypothesizing that the TF exosite could be an extended substrate recognition site that directly interacts with FX. Our cryo-EM model provides the first structural data to support

this hypothesis. Future studies will focus on obtaining a higher resolution structure of the TF-FVIIa-XK1 complex and structures of TF-FVIIa bound to other protein substrates.

In chapter 4, we went beyond blood clotting and showed that serine proteases involved in different cellular process are inhibited by low mM concentrations of ribonucleotides, including ADP and ATP. While ATP has been shown to stabilize and solubilize proteins at mM concentrations,[174,175] there are no reports of nucleotides acting as enzyme inhibitors. We hypothesize that serine protease inhibition might be a safety mechanism to prevent cellular damage caused by prematurely activated proteases while they transition through the ER and Golgi. These prematurely activated proteases can cause severe diseases[177-179] and any mechanism that would inhibit premature activation would be beneficial for cell homeostasis. Overall, our findings provide insights into novel functions of ribonucleotides and the regulation of serine proteases. Future studies will explore if nucleotides also inhibit other enzymes and if this mechanism indeed prevents cell damage.

Bibliography

1. Versteeg HH, Heemskerk JW, Levi M & Reitsma PH. New fundamentals in hemostasis. *Physiol Rev* **93:**327-358, 2013.
2. Davie EW & Ratnoff OD. Waterfall Sequence for Intrinsic Blood Clotting. *Science* **145:**1310-1312, 1964.
3. Macfarlane RG. An Enzyme Cascade in the Blood Clotting Mechanism, and Its Function as a Biochemical Amplifier. *Nature* **202:**498-499, 1964.
4. Smith SA, Travers RJ & Morrissey JH. How it all starts: Initiation of the clotting cascade. *Crit Rev Biochem Mol Biol* **50:**326-336, 2015. PMC4826570
5. Roth GA, Mensah GA, Johnson CO, Addolorato G, Ammirati E, Baddour LM, Barengo NC, Beaton AZ, Benjamin EJ, Benziger CP, Bonny A, Brauer M, Brodmann M, Cahill TJ, Carapetis J, Catapano AL, Chugh SS, Cooper LT, Coresh J, Criqui M, DeCleene N, Eagle KA, Emmons-Bell S, Feigin VL, Fernandez-Sola J, Fowkes G, Gakidou E, Grundy SM, He FJ, Howard G, Hu F, Inker L, Karthikeyan G, Kassebaum N, Koroshetz W, Lavie C, Lloyd-Jones D, Lu HS, Mirijello A, Temesgen AM, Mokdad A, Moran AE, Muntner P, Narula J, Neal B, Ntsekhe M, Moraes de Oliveira G, Otto C, Owolabi M, Pratt M, Rajagopalan S, Reitsma M, Ribeiro ALP, Rigotti N, Rodgers A, Sable C, Shakil S, Sliwa-Hahnle K, Stark B, Sundstrom J, Timpel P, Tleyjeh IM, Valgimigli M, Vos T, Whelton PK, Yacoub M, Zuhlke L, Murray C, Fuster V & Group G-N-JGBoCDW. Global Burden of Cardiovascular Diseases and Risk Factors, 1990-2019: Update From the GBD 2019 Study. *J Am Coll Cardiol* **76:**2982-3021, 2020. PMC7755038
6. Morrissey JH. Tissue factor: a key molecule in hemostatic and nonhemostatic systems. *Int J Hematol* **79:**103-108, 2004.
7. Gajsiewicz JM & Morrissey JH. Structure-Function Relationship of the Interaction between Tissue Factor and Factor VIIa. *Semin Thromb Hemost* **41:**682-690, 2015. PMC4862872
8. Drake TA, Morrissey JH & Edgington TS. Selective cellular expression of tissue factor in human tissues. Implications for disorders of hemostasis and thrombosis. *Am J Pathol* **134:**1087-1097, 1989. PMC1879887
9. Fleck RA, Rao LV, Rapaport SI & Varki N. Localization of human tissue factor antigen by immunostaining with monospecific, polyclonal anti-human tissue factor antibody. *Thromb Res* **59:**421-437, 1990.
10. Wilcox JN, Smith KM, Schwartz SM & Gordon D. Localization of tissue factor in the normal vessel wall and in the atherosclerotic plaque. *Proc Natl Acad Sci U S A* **86:**2839-2843, 1989. PMC287014
11. Toomey JR, Kratzer KE, Lasky NM, Stanton JJ & Broze GJ, Jr. Targeted disruption of the murine tissue factor gene results in embryonic lethality. *Blood* **88:**1583-1587, 1996.

12. Bugge TH, Xiao Q, Kombrinck KW, Flick MJ, Holmback K, Danton MJ, Colbert MC, Witte DP, Fujikawa K, Davie EW & Degen JL. Fatal embryonic bleeding events in mice lacking tissue factor, the cell-associated initiator of blood coagulation. *Proc Natl Acad Sci U S A* **93:**6258-6263, 1996. PMC39009
13. Carmeliet P, Mackman N, Moons L, Luther T, Gressens P, Van Vlaenderen I, Demunck H, Kasper M, Breier G, Evrard P, Muller M, Risau W, Edgington T & Collen D. Role of tissue factor in embryonic blood vessel development. *Nature* **383:**73-75, 1996.
14. Morrissey JH, Fakhrai H & Edgington TS. Molecular cloning of the cDNA for tissue factor, the cellular receptor for the initiation of the coagulation protease cascade. *Cell* **50:**129-135, 1987.
15. Spicer EK, Horton R, Bloem L, Bach R, Williams KR, Guha A, Kraus J, Lin TC, Nemerson Y & Konigsberg WH. Isolation of cDNA clones coding for human tissue factor: primary structure of the protein and cDNA. *Proc Natl Acad Sci U S A* **84:**5148-5152, 1987. PMC298811
16. Scarpati EM, Wen D, Broze GJ, Jr., Miletich JP, Flandermeyer RR, Siegel NR & Sadler JE. Human tissue factor: cDNA sequence and chromosome localization of the gene. *Biochemistry* **26:**5234-5238, 1987.
17. Fisher KL, Gorman CM, Vehar GA, O'Brien DP & Lawn RM. Cloning and expression of human tissue factor cDNA. *Thromb Res* **48:**89-99, 1987.
18. Harlos K, Martin DM, O'Brien DP, Jones EY, Stuart DI, Polikarpov I, Miller A, Tuddenham EG & Boys CW. Crystal structure of the extracellular region of human tissue factor. *Nature* **370:**662-666, 1994.
19. Muller YA, Ultsch MH, Kelley RF & de Vos AM. Structure of the extracellular domain of human tissue factor: location of the factor VIIa binding site. *Biochemistry* **33:**10864-10870, 1994.
20. Huang M, Syed R, Stura EA, Stone MJ, Stefanko RS, Ruf W, Edgington TS & Wilson IA. The mechanism of an inhibitory antibody on TF-initiated blood coagulation revealed by the crystal structures of human tissue factor, Fab 5G9 and TF.G9 complex. *J Mol Biol* **275:**873-894, 1998.
21. Paborsky LR, Caras IW, Fisher KL & Gorman CM. Lipid association, but not the transmembrane domain, is required for tissue factor activity. Substitution of the transmembrane domain with a phosphatidylinositol anchor. *J Biol Chem* **266:**21911-21916, 1991.
22. Waters EK & Morrissey JH. Restoring full biological activity to the isolated ectodomain of an integral membrane protein. *Biochemistry* **45:**3769-3774, 2006. PMC2525505
23. Ahamed J & Ruf W. Protease-activated receptor 2-dependent phosphorylation of the tissue factor cytoplasmic domain. *J Biol Chem* **279:**23038-23044, 2004.
24. Dorfleutner A & Ruf W. Regulation of tissue factor cytoplasmic domain phosphorylation by palmitoylation. *Blood* **102:**3998-4005, 2003.
25. Fadeel B & Xue D. The ins and outs of phospholipid asymmetry in the plasma membrane: roles in health and disease. *Crit Rev Biochem Mol Biol* **44:**264-277, 2009. PMC2787517
26. Lhermusier T, Chap H & Payrastre B. Platelet membrane phospholipid asymmetry: from the characterization of a scramblase activity to the identification of an essential protein mutated in Scott syndrome. *J Thromb Haemost* **9:**1883-1891, 2011.

27. Ke K, Yuan J & Morrissey JH. Tissue factor residues that putatively interact with membrane phospholipids. *PLoS One* **9:**e88675, 2014. PMC3916442
28. Ohkubo YZ, Morrissey JH & Tajkhorshid E. Dynamical view of membrane binding and complex formation of human factor VIIa and tissue factor. *J Thromb Haemost* **8:**1044-1053, 2010. PMC2890040
29. Muller MP, Wang Y, Morrissey JH & Tajkhorshid E. Lipid specificity of the membrane binding domain of coagulation factor X. *J Thromb Haemost*, 2017.
30. Chen VM, Ahamed J, Versteeg HH, Berndt MC, Ruf W & Hogg PJ. Evidence for activation of tissue factor by an allosteric disulfide bond. *Biochemistry* **45:**12020-12028, 2006.
31. Versteeg HH & Ruf W. Tissue factor coagulant function is enhanced by protein-disulfide isomerase independent of oxidoreductase activity. *J Biol Chem* **282:**25416-25424, 2007.
32. Ahamed J, Versteeg HH, Kerver M, Chen VM, Mueller BM, Hogg PJ & Ruf W. Disulfide isomerization switches tissue factor from coagulation to cell signaling. *Proc Natl Acad Sci U S A* **103:**13932-13937, 2006. PMC1599891
33. Bach RR & Monroe D. What is wrong with the allosteric disulfide bond hypothesis? *Arterioscler Thromb Vasc Biol* **29:**1997-1998, 2009.
34. Persson E. Protein disulfide isomerase has no stimulatory chaperone effect on factor X activation by factor VIIa-soluble tissue factor. *Thromb Res* **123:**171-176, 2008.
35. van den Hengel LG, Kocaturk B, Reitsma PH, Ruf W & Versteeg HH. Complete abolishment of coagulant activity in monomeric disulfide-deficient tissue factor. *Blood* **118:**3446-3448, 2011.
36. Bach RR. Tissue factor encryption. *Arterioscler Thromb Vasc Biol* **26:**456-461, 2006.
37. Del Conde I, Shrimpton CN, Thiagarajan P & Lopez JA. Tissue-factor-bearing microvesicles arise from lipid rafts and fuse with activated platelets to initiate coagulation. *Blood* **106:**1604-1611, 2005.
38. Mandal SK, Iakhiaev A, Pendurthi UR & Rao LV. Acute cholesterol depletion impairs functional expression of tissue factor in fibroblasts: modulation of tissue factor activity by membrane cholesterol. *Blood* **105:**153-160, 2005. PMC2835310
39. Morrissey JH, Macik BG, Neuenschwander PF & Comp PC. Quantitation of activated factor VII levels in plasma using a tissue factor mutant selectively deficient in promoting factor VII activation. *Blood* **81:**734-744, 1993.
40. Rosen ED, Chan JC, Idusogie E, Clotman F, Vlasuk G, Luther T, Jalbert LR, Albrecht S, Zhong L, Lissens A, Schoonjans L, Moons L, Collen D, Castellino FJ & Carmeliet P. Mice lacking factor VII develop normally but suffer fatal perinatal bleeding. *Nature* **390:**290-294, 1997.
41. Hagen FS, Gray CL, O'Hara P, Grant FJ, Saari GC, Woodbury RG, Hart CE, Insley M, Kisiel W, Kurachi K & et al. Characterization of a cDNA coding for human factor VII. *Proc Natl Acad Sci U S A* **83:**2412-2416, 1986. PMC323307
42. O'Hara PJ, Grant FJ, Haldeman BA, Gray CL, Insley MY, Hagen FS & Murray MJ. Nucleotide sequence of the gene coding for human factor VII, a vitamin K-dependent protein participating in blood coagulation. *Proc Natl Acad Sci U S A* **84:**5158-5162, 1987. PMC298813

43. Sabharwal AK, Birktoft JJ, Gorka J, Wildgoose P, Petersen LC & Bajaj SP. High affinity Ca(2+)-binding site in the serine protease domain of human factor VIIa and its role in tissue factor binding and development of catalytic activity. *J Biol Chem* **270:**15523-15530, 1995.
44. Banner DW, D'Arcy A, Chene C, Winkler FK, Guha A, Konigsberg WH, Nemerson Y & Kirchhofer D. The crystal structure of the complex of blood coagulation factor VIIa with soluble tissue factor. *Nature* **380:**41-46, 1996.
45. Schiodt J, Harrit N, Christensen U & Petersen LC. Two different Ca2+ ion binding sites in factor VIIa and in des(1-38) factor VIIa. *FEBS Lett* **306:**265-268, 1992.
46. Nemerson Y & Repke D. Tissue factor accelerates the activation of coagulation factor VII: the role of a bifunctional coagulation cofactor. *Thromb Res* **40:**351-358, 1985.
47. Neuenschwander PF, Fiore MM & Morrissey JH. Factor VII autoactivation proceeds via interaction of distinct protease-cofactor and zymogen-cofactor complexes. Implications of a two-dimensional enzyme kinetic mechanism. *J Biol Chem* **268:**21489-21492, 1993.
48. Masys DR, Bajaj SP & Rapaport SI. Activation of human factor VII by activated factors IX and X. *Blood* **60:**1143-1150, 1982.
49. Radcliffe R & Nemerson Y. Activation and control of factor VII by activated factor X and thrombin. Isolation and characterization of a single chain form of factor VII. *J Biol Chem* **250:**388-395, 1975.
50. Kisiel W, Fujikawa K & Davie EW. Activation of bovine factor VII (proconvertin) by factor XIIa (activated Hageman factor). *Biochemistry* **16:**4189-4194, 1977.
51. Tsujioka H, Suehiro A & Kakishita E. Activation of coagulation factor VII by tissue-type plasminogen activator. *Am J Hematol* **61:**34-39, 1999.
52. Harvey SB, Stone MD, Martinez MB & Nelsestuen GL. Mutagenesis of the gamma-carboxyglutamic acid domain of human factor VII to generate maximum enhancement of the membrane contact site. *J Biol Chem* **278:**8363-8369, 2003.
53. Nelsestuen GL. Enhancement of vitamin-K-dependent protein function by modification of the gamma-carboxyglutamic acid domain: studies of protein C and factor VII. *Trends Cardiovasc Med* **9:**162-167, 1999.
54. Bajaj SP, Schmidt AE, Agah S, Bajaj MS & Padmanabhan K. High resolution structures of p-aminobenzamidine- and benzamidine-VIIa/soluble tissue factor: unpredicted conformation of the 192-193 peptide bond and mapping of Ca2+, Mg2+, Na+, and Zn2+ sites in factor VIIa. *J Biol Chem* **281:**24873-24888, 2006.
55. Vadivel K, Agah S, Messer AS, Cascio D, Bajaj MS, Krishnaswamy S, Esmon CT, Padmanabhan K & Bajaj SP. Structural and functional studies of gamma-carboxyglutamic acid domains of factor VIIa and activated Protein C: role of magnesium at physiological calcium. *J Mol Biol* **425:**1961-1981, 2013. PMC4017951
56. Tavoosi N & Morrissey JH. Influence of membrane composition on the enhancement of factor VIIa/tissue factor activity by magnesium ions. *Thromb Haemost* **111:**770-772, 2014. PMC4862877
57. Gajsiewicz JM, Nuzzio KM, Rienstra CM & Morrissey JH. Tissue Factor Residues That Modulate Magnesium-Dependent Rate Enhancements of the Tissue Factor/Factor VIIa Complex. *Biochemistry* **54:**4665-4671, 2015. PMC4862878
58. Zhang E, St Charles R & Tulinsky A. Structure of extracellular tissue factor complexed with factor VIIa inhibited with a BPTI mutant. *J Mol Biol* **285:**2089-2104, 1999.

59. Komiyama Y, Pedersen AH & Kisiel W. Proteolytic activation of human factors IX and X by recombinant human factor VIIa: effects of calcium, phospholipids, and tissue factor. *Biochemistry* **29:**9418-9425, 1990.
60. Bom VJ & Bertina RM. The contributions of Ca2+, phospholipids and tissue-factor apoprotein to the activation of human blood-coagulation factor X by activated factor VII. *Biochem J* **265:**327-336, 1990. PMC1136891
61. Lawson JH, Butenas S & Mann KG. The evaluation of complex-dependent alterations in human factor VIIa. *J Biol Chem* **267:**4834-4843, 1992.
62. Neuenschwander PF, Branam DE & Morrissey JH. Importance of substrate composition, pH and other variables on tissue factor enhancement of factor VIIa activity. *Thromb Haemost* **70:**970-977, 1993.
63. Song H, Olsen OH, Persson E & Rand KD. Sites involved in intra- and interdomain allostery associated with the activation of factor VIIa pinpointed by hydrogen-deuterium exchange and electron transfer dissociation mass spectrometry. *J Biol Chem* **289:**35388-35396, 2014. PMC4271224
64. Rand KD, Jorgensen TJ, Olsen OH, Persson E, Jensen ON, Stennicke HR & Andersen MD. Allosteric activation of coagulation factor VIIa visualized by hydrogen exchange. *J Biol Chem* **281:**23018-23024, 2006.
65. Olsen OH, Rand KD, Ostergaard H & Persson E. A combined structural dynamics approach identifies a putative switch in factor VIIa employed by tissue factor to initiate blood coagulation. *Protein Sci* **16:**671-682, 2007. PMC2203332
66. Colina CM, Venkateswarlu D, Duke R, Perera L & Pedersen LG. What causes the enhancement of activity of factor VIIa by tissue factor? *J Thromb Haemost* **4:**2726-2729, 2006.
67. Soejima K, Yuguchi M, Mizuguchi J, Tomokiyo K, Nakashima T, Nakagaki T & Iwanaga S. The 99 and 170 loop-modified factor VIIa mutants show enhanced catalytic activity without tissue factor. *J Biol Chem* **277:**49027-49035, 2002.
68. McCallum CD, Hapak RC, Neuenschwander PF, Morrissey JH & Johnson AE. The location of the active site of blood coagulation factor VIIa above the membrane surface and its reorientation upon association with tissue factor. A fluorescence energy transfer study. *J Biol Chem* **271:**28168-28175, 1996.
69. Waters EK, Yegneswaran S & Morrissey JH. Raising the active site of factor VIIa above the membrane surface reduces its procoagulant activity but not factor VII autoactivation. *J Biol Chem* **281:**26062-26068, 2006.
70. McCallum CD, Su B, Neuenschwander PF, Morrissey JH & Johnson AE. Tissue factor positions and maintains the factor VIIa active site far above the membrane surface even in the absence of the factor VIIa Gla domain. A fluorescence resonance energy transfer study. *J Biol Chem* **272:**30160-30166, 1997.
71. Morrissey JH, Neuenschwander PF, Huang Q, McCallum CD, Su B & Johnson AE. Factor VIIa-tissue factor: functional importance of protein-membrane interactions. *Thromb Haemost* **78:**112-116, 1997.
72. Neuenschwander PF & Morrissey JH. Roles of the membrane-interactive regions of factor VIIa and tissue factor. The factor VIIa Gla domain is dispensable for binding to tissue factor but important for activation of factor X. *J Biol Chem* **269:**8007-8013, 1994.

73. Bevers EM & Williamson PL. Getting to the Outer Leaflet: Physiology of Phosphatidylserine Exposure at the Plasma Membrane. *Physiol Rev* **96:**605-645, 2016.
74. Zwaal RF, Comfurius P & Bevers EM. Lipid-protein interactions in blood coagulation. *Biochim Biophys Acta* **1376:**433-453, 1998.
75. Shaw AW, Pureza VS, Sligar SG & Morrissey JH. The local phospholipid environment modulates the activation of blood clotting. *J Biol Chem* **282:**6556-6563, 2007.
76. Kay JG, Koivusalo M, Ma X, Wohland T & Grinstein S. Phosphatidylserine dynamics in cellular membranes. *Mol Biol Cell* **23:**2198-2212, 2012. PMC3364182
77. Tavoosi N, Davis-Harrison RL, Pogorelov TV, Ohkubo YZ, Arcario MJ, Clay MC, Rienstra CM, Tajkhorshid E & Morrissey JH. Molecular determinants of phospholipid synergy in blood clotting. *J Biol Chem* **286:**23247-23253, 2011. PMC3123091
78. Neuenschwander PF, Bianco-Fisher E, Rezaie AR & Morrissey JH. Phosphatidylethanolamine augments factor VIIa-tissue factor activity: enhancement of sensitivity to phosphatidylserine. *Biochemistry* **34:**13988-13993, 1995.
79. Roy S, Hass PE, Bourell JH, Henzel WJ & Vehar GA. Lysine residues 165 and 166 are essential for the cofactor function of tissue factor. *J Biol Chem* **266:**22063-22066, 1991.
80. Ruf W, Miles DJ, Rehemtulla A & Edgington TS. Tissue factor residues 157-167 are required for efficient proteolytic activation of factor X and factor VII. *J Biol Chem* **267:**22206-22210, 1992.
81. Kirchhofer D, Lipari MT, Moran P, Eigenbrot C & Kelley RF. The tissue factor region that interacts with substrates factor IX and Factor X. *Biochemistry* **39:**7380-7387, 2000.
82. Kirchhofer D, Eigenbrot C, Lipari MT, Moran P, Peek M & Kelley RF. The tissue factor region that interacts with factor Xa in the activation of factor VII. *Biochemistry* **40:**675-682, 2001.
83. Ruf W, Miles DJ, Rehemtulla A & Edgington TS. Cofactor residues lysine 165 and 166 are critical for protein substrate recognition by the tissue factor-factor VIIa protease complex. *J Biol Chem* **267:**6375-6381, 1992.
84. Huang Q, Neuenschwander PF, Rezaie AR & Morrissey JH. Substrate recognition by tissue factor-factor VIIa. Evidence for interaction of residues Lys165 and Lys166 of tissue factor with the 4-carboxyglutamate-rich domain of factor X. *J Biol Chem* **271:**21752-21757, 1996.
85. Ruf W, Rehemtulla A, Morrissey JH & Edgington TS. Phospholipid-independent and -dependent interactions required for tissue factor receptor and cofactor function. *J Biol Chem* **266:**16256, 1991.
86. Kondo S & Kisiel W. Regulation of factor VIIa activity in plasma: evidence that antithrombin III is the sole plasma protease inhibitor of human factor VIIa. *Thromb Res* **46:**325-335, 1987.
87. Broze GJ, Jr. & Girard TJ. Tissue factor pathway inhibitor: structure-function. *Front Biosci (Landmark Ed)* **17:**262-280, 2012. PMC3692300
88. Rao LV, Rapaport SI & Hoang AD. Binding of factor VIIa to tissue factor permits rapid antithrombin III/heparin inhibition of factor VIIa. *Blood* **81:**2600-2607, 1993.
89. Lawson JH, Butenas S, Ribarik N & Mann KG. Complex-dependent inhibition of factor VIIa by antithrombin III and heparin. *J Biol Chem* **268:**767-770, 1993.
90. Smith SA & Morrissey JH. Rapid and efficient incorporation of tissue factor into liposomes. *J Thromb Haemost* **2:**1155-1162, 2004.

91. Girard TJ, Warren LA, Novotny WF, Likert KM, Brown SG, Miletich JP & Broze GJ, Jr. Functional significance of the Kunitz-type inhibitory domains of lipoprotein-associated coagulation inhibitor. *Nature* **338:**518-520, 1989.
92. Rao LV & Ruf W. Tissue factor residues Lys165 and Lys166 are essential for rapid formation of the quaternary complex of tissue factor.VIIa with Xa.tissue factor pathway inhibitor. *Biochemistry* **34:**10867-10871, 1995.
93. Girard TJ, MacPhail LA, Likert KM, Novotny WF, Miletich JP & Broze GJ, Jr. Inhibition of factor VIIa-tissue factor coagulation activity by a hybrid protein. *Science* **248:**1421-1424, 1990.
94. Kokoye Y, Ivanov I, Cheng Q, Matafonov A, Dickeson SK, Mason S, Sexton DJ, Renne T, McCrae K, Feener EP & Gailani D. A comparison of the effects of factor XII deficiency and prekallikrein deficiency on thrombus formation. *Thromb Res* **140:**118-124, 2016. PMC4821716
95. Lammle B, Wuillemin WA, Huber I, Krauskopf M, Zurcher C, Pflugshaupt R & Furlan M. Thromboembolism and bleeding tendency in congenital factor XII deficiency--a study on 74 subjects from 14 Swiss families. *Thromb Haemost* **65:**117-121, 1991.
96. Renne T, Pozgajova M, Gruner S, Schuh K, Pauer HU, Burfeind P, Gailani D & Nieswandt B. Defective thrombus formation in mice lacking coagulation factor XII. *J Exp Med* **202:**271-281, 2005. PMC2213000
97. Kleinschnitz C, Stoll G, Bendszus M, Schuh K, Pauer HU, Burfeind P, Renne C, Gailani D, Nieswandt B & Renne T. Targeting coagulation factor XII provides protection from pathological thrombosis in cerebral ischemia without interfering with hemostasis. *J Exp Med* **203:**513-518, 2006. PMC2118228
98. Matafonov A, Leung PY, Gailani AE, Grach SL, Puy C, Cheng Q, Sun MF, McCarty OJ, Tucker EI, Kataoka H, Renne T, Morrissey JH, Gruber A & Gailani D. Factor XII inhibition reduces thrombus formation in a primate thrombosis model. *Blood* **123:**1739-1746, 2014. PMC3954054
99. Reddigari SR, Shibayama Y, Brunnee T & Kaplan AP. Human Hageman factor (factor XII) and high molecular weight kininogen compete for the same binding site on human umbilical vein endothelial cells. *J Biol Chem* **268:**11982-11987, 1993.
100. Samuel M, Pixley RA, Villanueva MA, Colman RW & Villanueva GB. Human factor XII (Hageman factor) autoactivation by dextran sulfate. Circular dichroism, fluorescence, and ultraviolet difference spectroscopic studies. *J Biol Chem* **267:**19691-19697, 1992.
101. Rojkjaer R & Schousboe I. The surface-dependent autoactivation mechanism of factor XII. *Eur J Biochem* **243:**160-166, 1997.
102. Muller F & Renne T. Novel roles for factor XII-driven plasma contact activation system. *Curr Opin Hematol* **15:**516-521, 2008.
103. Cochrane CG, Revak SD & Wuepper KD. Activation of Hageman factor in solid and fluid phases. A critical role of kallikrein. *J Exp Med* **138:**1564-1583, 1973. PMC2139466
104. Tans G, Rosing J, Berrettini M, Lammle B & Griffin JH. Autoactivation of human plasma prekallikrein. *J Biol Chem* **262:**11308-11314, 1987.
105. Schmaier AH. Assembly, activation, and physiologic influence of the plasma kallikrein/kinin system. *Int Immunopharmacol* **8:**161-165, 2008. PMC2266068
106. Shariat-Madar Z, Mahdi F & Schmaier AH. Recombinant prolylcarboxypeptidase activates plasma prekallikrein. *Blood* **103:**4554-4561, 2004.

107. Thompson RE, Mandle R, Jr. & Kaplan AP. Association of factor XI and high molecular weight kininogen in human plasma. *J Clin Invest* **60:**1376-1380, 1977. PMC372495
108. Renne T, Gailani D, Meijers JC & Muller-Esterl W. Characterization of the H-kininogen-binding site on factor XI: a comparison of factor XI and plasma prekallikrein. *J Biol Chem* **277:**4892-4899, 2002.
109. Emsley J, McEwan PA & Gailani D. Structure and function of factor XI. *Blood* **115:**2569-2577, 2010. PMC4828079
110. Di Scipio RG, Kurachi K & Davie EW. Activation of human factor IX (Christmas factor). *J Clin Invest* **61:**1528-1538, 1978. PMC372679
111. Taran LD. Factor IX of the blood coagulation system: a review. *Biochemistry (Mosc)* **62:**685-693, 1997.
112. Orlova NA, Kovnir SV, Vorobiev, II, Gabibov AG & Vorobiev AI. Blood Clotting Factor VIII: From Evolution to Therapy. *Acta Naturae* **5:**19-39, 2013. PMC3695351
113. Tracy PB, Eide LL & Mann KG. Human prothrombinase complex assembly and function on isolated peripheral blood cell populations. *J Biol Chem* **260:**2119-2124, 1985.
114. Krishnaswamy S. Prothrombinase complex assembly. Contributions of protein-protein and protein-membrane interactions toward complex formation. *J Biol Chem* **265:**3708-3718, 1990.
115. Mann KG, Butenas S & Brummel K. The dynamics of thrombin formation. *Arterioscler Thromb Vasc Biol* **23:**17-25, 2003.
116. Davie EW, Fujikawa K & Kisiel W. The coagulation cascade: initiation, maintenance, and regulation. *Biochemistry* **30:**10363-10370, 1991.
117. Naito K & Fujikawa K. Activation of human blood coagulation factor XI independent of factor XII. Factor XI is activated by thrombin and factor XIa in the presence of negatively charged surfaces. *J Biol Chem* **266:**7353-7358, 1991.
118. Matafonov A, Sarilla S, Sun MF, Sheehan JP, Serebrov V, Verhamme IM & Gailani D. Activation of factor XI by products of prothrombin activation. *Blood* **118:**437-445, 2011. PMC3138693
119. Di Cera E. Thrombin. *Mol Aspects Med* **29:**203-254, 2008. PMC2491495
120. Herrick S, Blanc-Brude O, Gray A & Laurent G. Fibrinogen. *Int J Biochem Cell Biol* **31:**741-746, 1999.
121. Mosesson MW. Fibrinogen and fibrin structure and functions. *J Thromb Haemost* **3:**1894-1904, 2005.
122. Weisel JW & Litvinov RI. Fibrin Formation, Structure and Properties. *Subcell Biochem* **82:**405-456, 2017. PMC5536120
123. Chapin JC & Hajjar KA. Fibrinolysis and the control of blood coagulation. *Blood Rev* **29:**17-24, 2015. PMC4314363
124. Vassalli JD, Sappino AP & Belin D. The plasminogen activator/plasmin system. *J Clin Invest* **88:**1067-1072, 1991. PMC295552
125. Perona JJ & Craik CS. Structural basis of substrate specificity in the serine proteases. *Protein Sci* **4:**337-360, 1995. PMC2143081
126. Nemeth BC & Sahin-Toth M. Human cationic trypsinogen (PRSS1) variants and chronic pancreatitis. *Am J Physiol Gastrointest Liver Physiol* **306:**G466-473, 2014. PMC3949028
127. Raphael KL & Willingham FF. Hereditary pancreatitis: current perspectives. *Clin Exp Gastroenterol* **9:**197-207, 2016. PMC4968666

128. Whitcomb DC, Gorry MC, Preston RA, Furey W, Sossenheimer MJ, Ulrich CD, Martin SP, Gates LK, Jr., Amann ST, Toskes PP, Liddle R, McGrath K, Uomo G, Post JC & Ehrlich GD. Hereditary pancreatitis is caused by a mutation in the cationic trypsinogen gene. *Nat Genet* **14:**141-145, 1996.
129. Hedstrom L. Serine protease mechanism and specificity. *Chem Rev* **102:**4501-4524, 2002.
130. Di Cera E. Serine proteases. *IUBMB Life* **61:**510-515, 2009. PMC2675663
131. Page MJ, Macgillivray RT & Di Cera E. Determinants of specificity in coagulation proteases. *J Thromb Haemost* **3:**2401-2408, 2005.
132. Morrissey JH. Tissue factor: a key molecule in hemostatic and nonhemostatic systems. *Int J Hematol* **79:**103-108, 2004.
133. Mackman N. The role of tissue factor and factor VIIa in hemostasis. *Anesth Analg* **108:**1447-1452, 2009. 2838713
134. Wilcox JN, Smith KM, Schwartz SM & Gordon D. Localization of tissue factor in the normal vessel wall and in the atherosclerotic plaque. *Proc Natl Acad Sci U S A* **86:**2839-2843, 1989. 287014
135. Chiva-Blanch G, Laake K, Myhre P, Bratseth V, Arnesen H, Solheim S, Badimon L & Seljeflot I. Platelet-, monocyte-derived and tissue factor-carrying circulating microparticles are related to acute myocardial infarction severity. *PLoS One* **12:**e0172558, 2017. PMC5313202
136. Kappelmayer J, Berecki D, Misz M, Oláh L, Fekete I, Csiba L & Blaskó G. Monocytes express tissue factor in young patients with cerebral ischemia. *Cerebrovasc Dis* **8:**235-239, 1998.
137. Drake TA, Morrissey JH & Edgington TS. Selective cellular expression of tissue factor in human tissues. Implications for disorders of hemostasis and thrombosis. *Am J Pathol* **134:**1087-1097, 1989. PMC1879887
138. Kirchhofer D, Lipari MT, Moran P, Eigenbrot C & Kelley RF. The tissue factor region that interacts with substrates factor IX and factor X. *Biochemistry* **39:**7380-7387, 2000.
139. Roy S, Hass PE, Bourell JH, Henzel WJ & Vehar GA. Lysine residues 165 and 166 are essential for the cofactor function of tissue factor. *J Biol Chem* **266:**22063-22066, 1991.
140. Kirchhofer D, Eigenbrot C, Lipari MT, Moran P, Peek M & Kelley RF. The tissue factor region that interacts with factor Xa in the activation of factor VII. *Biochemistry* **40:**675-682, 2001.
141. Huang Q, Neuenschwander PF, Rezaie AR & Morrissey JH. Substrate recognition by tissue factor-factor VIIa. Evidence for interaction of residues Lys^{165} and Lys^{166} of tissue factor with the 4-carboxyglutamate-rich domain of factor X. *J Biol Chem* **271:**21752-21757, 1996.
142. Banner DW, D'Arcy A, Chène C, Winkler FK, Guha A, Konigsberg WH, Nemerson Y & Kirchhofer D. The crystal structure of the complex of blood coagulation factor VIIa with soluble tissue factor. *Nature* **380:**41-46, 1996.
143. Muller YA, Ultsch MH & de Vos AM. The crystal structure of the extracellular domain of human tissue factor refined to 1.7 Å resolution. *J Mol Biol* **256:**144-159, 1996.
144. Rezaie AR, Fiore MM, Neuenschwander PF, Esmon CT & Morrissey JH. Expression and purification of a soluble tissue factor fusion protein with an epitope for an unusual calcium-dependent antibody. *Protein Expr Purif* **3:**453-460, 1992.

145. Smith SA & Morrissey JH. Rapid and efficient incorporation of tissue factor into liposomes. *J Thromb Haemost* **2:**1155-1162, 2004.
146. Shaw AW, Pureza VS, Sligar SG & Morrissey JH. The local phospholipid environment modulates the activation of blood clotting. *J Biol Chem* **282:**6556-6563, 2007.
147. Ljungkvist M, Strandberg K, Berntorp E, Chaireti R, Holme PA, Larsen OH, Lassila R, Jouppila A, Szanto T & Zetterberg E. Evaluation of a standardized protocol for thrombin generation using the calibrated automated thrombogram: A Nordic study. *Haemophilia* **25:**334-342, 2019.
148. Hemker HC, Giesen P, AlDieri R, Regnault V, de Smed E, Wagenvoord R, Lecompte T & Beguin S. The calibrated automated thrombogram (CAT): a universal routine test for hyper- and hypocoagulability. *Pathophysiol Haemost Thromb* **32:**249-253, 2002.
149. Girard TJ, MacPhail LA, Likert KM, Novotny WF, Miletich JP & Broze GJ, Jr. Inhibition of factor VIIa-tissue factor coagulation activity by a hybrid protein. *Science* **248:**1421-1424, 1990.
150. Kim DJ & James HL. Expression of human factor X with normal biological activity in human embryonic kidney cells. *Biotechnol Lett* **16:**549-554, 1994.
151. Neuenschwander PF & Morrissey JH. Alteration of the substrate and inhibitor specificities of blood coagulation factor VIIa: importance of amino acid residue K192. *Biochemistry* **34:**8701-8707, 1995.
152. Baugh RJ, Dickinson CD, Ruf W & Krishnaswamy S. Exosite interactions determine the affinity of factor X for the extrinsic Xase complex. *J Biol Chem* **275:**28826-28833, 2000.
153. Dittmar S, Ruf W & Edgington TS. Influence of mutations in tissue factor on the fine specificity of macromolecular substrate activation. *Biochem J* **321:**787-793, 1997.
154. Morrissey JH, Neuenschwander PF, Huang Q, McCallum CD, Su B & Johnson AE. Factor VIIa-tissue factor: functional importance of protein-membrane interactions. *Thromb Haemost* **78:**112-116, 1997.
155. Bom VJ & Bertina RM. The contributions of Ca^{2+}, phospholipids and tissue-factor apoprotein to the activation of human blood-coagulation factor X by activated factor VII. *Biochem J* **265:**327-336, 1990.
156. Ohkubo YZ, Morrissey JH & Tajkhorshid E. Dynamical view of membrane binding and complex formation of human factor VIIa and tissue factor. *J Thromb Haemost* **8:**1044-1053, 2010. PMC2890040
157. Neuenschwander PF, Fiore MM & Morrissey JH. Factor VII autoactivation proceeds via interaction of distinct protease-cofactor and zymogen-cofactor complexes. Implications of a two-dimensional enzyme kinetic mechanism. *J Biol Chem* **268:**21489-21492, 1993.
158. Riewald M & Ruf W. Orchestration of coagulation protease signaling by tissue factor. *Trends Cardiovasc Med* **12:**149-154, 2002.
159. Camerer E, Huang W & Coughlin SR. Tissue factor- and factor X-dependent activation of protease-activated receptor 2 by factor VIIa. *Proc Natl Acad Sci U S A* **97:**5255-5260, 2000. 25815
160. Mackman N. The role of tissue factor and factor VIIa in hemostasis. *Anesth Analg* **108:**1447-1452, 2009. PMC2838713
161. Birkle F & Morrissey JH. A serine loop in tissue factor mediates substrate selectivity by the tissue factor-factor VIIa complex. *J Thromb Haemost* **19:**75-84, 2021. PMC7790960

162. Birkle F & Morrissey JH. A serine loop in tissue factor mediates substrate selectivity by the tissue factor-factor VIIa complex. *J Thromb Haemost* **19:**75-84, 2021. PMC7790960
163. Ritchie TK, Grinkova YV, Bayburt TH, Denisov IG, Zolnerciks JK, Atkins WM & Sligar SG. Chapter 11 - Reconstitution of membrane proteins in phospholipid bilayer nanodiscs. *Methods Enzymol* **464:**211-231, 2009.
164. Rezaie AR, Fiore MM, Neuenschwander PF, Esmon CT & Morrissey JH. Expression and purification of a soluble tissue factor fusion protein with an epitope for an unusual calcium-dependent antibody. *Protein Expr Purif* **3:**453-460, 1992.
165. Suloway C, Pulokas J, Fellmann D, Cheng A, Guerra F, Quispe J, Stagg S, Potter CS & Carragher B. Automated molecular microscopy: the new Leginon system. *J Struct Biol* **151:**41-60, 2005.
166. Punjani A, Rubinstein JL, Fleet DJ & Brubaker MA. cryoSPARC: algorithms for rapid unsupervised cryo-EM structure determination. *Nat Methods* **14:**290-296, 2017.
167. Tegunov D & Cramer P. Real-time cryo-electron microscopy data preprocessing with Warp. *Nat Methods* **16:**1146-1152, 2019. PMC6858868
168. Zivanov J, Nakane T, Forsberg BO, Kimanius D, Hagen WJ, Lindahl E & Scheres SH. New tools for automated high-resolution cryo-EM structure determination in RELION-3. *Elife* **7**, 2018. PMC6250425
169. Lyumkis D. Challenges and opportunities in cryo-EM single-particle analysis. *J Biol Chem* **294:**5181-5197, 2019. PMC6442032
170. Glaeser RM. How good can cryo-EM become? *Nature Methods* **13:**28-32, 2016.
171. Tan YZ, Baldwin PR, Davis JH, Williamson JR, Potter CS, Carragher B & Lyumkis D. Addressing preferred specimen orientation in single-particle cryo-EM through tilting. *Nat Methods* **14:**793-796, 2017. PMC5533649
172. Rudolph FB. The biochemistry and physiology of nucleotides. *J Nutr* **124:**124S-127S, 1994.
173. Traut TW. Physiological concentrations of purines and pyrimidines. *Mol Cell Biochem* **140:**1-22, 1994.
174. Patel A, Malinovska L, Saha S, Wang J, Alberti S, Krishnan Y & Hyman AA. ATP as a biological hydrotrope. *Science* **356:**753-756, 2017.
175. Sridharan S, Kurzawa N, Werner T, Gunthner I, Helm D, Huber W, Bantscheff M & Savitski MM. Proteome-wide solubility and thermal stability profiling reveals distinct regulatory roles for ATP. *Nat Commun* **10:**1155, 2019. PMC6411743
176. Neurath H & Dixon GH. Structure and activation of trypsinogen and chymotrypsinogen. *Fed Proc* **16:**791-801, 1957.
177. Nemeth BC & Sahin-Toth M. Human cationic trypsinogen (PRSS1) variants and chronic pancreatitis. *Am J Physiol Gastrointest Liver Physiol* **306:**G466-473, 2014. PMC3949028
178. Raphael KL & Willingham FF. Hereditary pancreatitis: current perspectives. *Clin Exp Gastroenterol* **9:**197-207, 2016. PMC4968666
179. Whitcomb DC, Gorry MC, Preston RA, Furey W, Sossenheimer MJ, Ulrich CD, Martin SP, Gates LK, Jr., Amann ST, Toskes PP, Liddle R, McGrath K, Uomo G, Post JC & Ehrlich GD. Hereditary pancreatitis is caused by a mutation in the cationic trypsinogen gene. *Nat Genet* **14:**141-145, 1996.

180. Hirschberg CB, Robbins PW & Abeijon C. Transporters of nucleotide sugars, ATP, and nucleotide sulfate in the endoplasmic reticulum and Golgi apparatus. *Annu Rev Biochem* **67:**49-69, 1998.
181. Hirschberg CB & Snider MD. Topography of glycosylation in the rough endoplasmic reticulum and Golgi apparatus. *Annu Rev Biochem* **56:**63-87, 1987.
182. Weitzmann A, Baldes C, Dudek J & Zimmermann R. The heat shock protein 70 molecular chaperone network in the pancreatic endoplasmic reticulum - a quantitative approach. *FEBS J* **274:**5175-5187, 2007.
183. Waters EK, Yegneswaran S & Morrissey JH. Raising the active site of factor VIIa above the membrane surface reduces its procoagulant activity but not factor VII autoactivation. *J Biol Chem* **281:**26062-26068, 2006.
184. Cornish-Bowden A. A simple graphical method for determining the inhibition constants of mixed, uncompetitive and non-competitive inhibitors. *Biochem J* **137:**143-144, 1974. PMC1166095
185. Bode W, Mayr I, Baumann U, Huber R, Stone SR & Hofsteenge J. The refined 1.9 Å crystal structure of human α-thrombin: interaction with D-Phe-Pro-Arg chloromethylketone and significance of the Tyr-Pro-Pro-Trp insertion segment. *EMBO J* **8:**3467-3475, 1989. PMC401503
186. Phillips JC, Braun R, Wang W, Gumbart J, Tajkhorshid E, Villa E, Chipot C, Skeel RD, Kale L & Schulten K. Scalable molecular dynamics with NAMD. *J Comput Chem* **26:**1781-1802, 2005. 2486339
187. Phillips JC, Hardy DJ, Maia JDC, Stone JE, Ribeiro JV, Bernardi RC, Buch R, Fiorin G, Hénin J, Jiang W, McGreevy R, Melo MCR, Radak BK, Skeel RD, Singharoy A, Wang Y, Roux B, Aksimentiev A, Luthey-Schulten Z, Kalé LV, Schulten K, Chipot C & Tajkhorshid E. Scalable molecular dynamics on CPU and GPU architectures with NAMD. *J Chem Phys* **153:**044130, 2020. PMC7395834
188. Huang J, Rauscher S, Nawrocki G, Ran T, Feig M, de Groot BL, Grubmüller H & MacKerell AD, Jr. CHARMM36m: an improved force field for folded and intrinsically disordered proteins. *Nat Methods* **14:**71-73, 2017. PMC5199616
189. Jorgensen WL, Chandrasekhar J, Madura JD, Impey RW & Klein ML. Comparison of simple potential functions for simulating liquid water. *J Chem Phys* **79:**926-935, 1983.
190. Ryckaert J-P, Ciccotti G & Berendsen HJC. Numerical integration of the cartesian equations of motion of a system with constraints: molecular dynamics of *n*-alkanes. *J Comput Phys* **23:**327-341, 1977.
191. Martyna GJ, Tobias DJ & Klein ML. Constant pressure molecular dynamics algorithms. *J Chem Phys* **101:**4177-4189, 1994.
192. Essmann U, Perera L, Berkowitz ML, Darden T, Lee H & Pedersen LG. A smooth particle mesh Ewald method. *J Chem Phys* **103:**8577-8593, 1995.
193. Vermaas JV & Tajkhorshid E. Differential Membrane Binding Mechanics of Synaptotagmin Isoforms Observed in Atomic Detail. *Biochemistry* **56:**281-293, 2017. PMC5557660
194. Lam K & Tajkhorshid E. Membrane interactions of Cy3 and Cy5 fluorophores and their effects on membrane-protein dynamics. *Biophys J* **119:**24-34, 2020. PMC7335937
195. Pedregosa F, Varoquaux G, Gramfort A, Michel V, Thirion B, Grisel O, Blondel M, Prettenhofer P, Weiss R, Dubourg V, Vanderplas J, Passos A, Cournapeau D, Brucher M,

Perrot M & Duchesnay É. Scikit-learn: Machine learning in python. *J Mach Learn Res* **12:**2825–2830, 2011.
196. McInnes L, Healy J & Melville J. UMAP: Uniform manifold approximation and projection for dimension reduction.arXiv:1802.03426, 2018.
197. Becht E, McInnes L, Healy J, Dutertre CA, Kwok IWH, Ng LG, Ginhoux F & Newell EW. Dimensionality reduction for visualizing single-cell data using UMAP. *Nat Biotechnol*, 2018.
198. Cao J, Spielmann M, Qiu X, Huang X, Ibrahim DM, Hill AJ, Zhang F, Mundlos S, Christiansen L, Steemers FJ, Trapnell C & Shendure J. The single-cell transcriptional landscape of mammalian organogenesis. *Nature* **566:**496-502, 2019. PMC6434952
199. Packer JS, Zhu Q, Huynh C, Sivaramakrishnan P, Preston E, Dueck H, Stefanik D, Tan K, Trapnell C, Kim J, Waterston RH & Murray JI. A lineage-resolved molecular atlas of C. elegans embryogenesis at single-cell resolution. *Science* **365**, 2019. PMC7428862
200. McInnes L, Healy J & Astels S. hdbscan: Hierarchical density based clustering. *J Open Source Softw* **2:**205, 2017.
201. Jurrus E, Engel D, Star K, Monson K, Brandi J, Felberg LE, Brookes DH, Wilson L, Chen J, Liles K, Chun M, Li P, Gohara DW, Dolinsky T, Konecny R, Koes DR, Nielsen JE, Head-Gordon T, Geng W, Krasny R, Wei GW, Holst MJ, McCammon JA & Baker NA. Improvements to the APBS biomolecular solvation software suite. *Protein Sci* **27:**112-128, 2018. PMC5734301
202. Humphrey W, Dalke A & Schulten K. VMD: visual molecular dynamics. *J Mol Graph* **14:**33-38, 27-38, 1996.
203. Peacock RB, McGrann T, Tonelli M & Komives EA. Serine protease dynamics revealed by NMR analysis of the thrombin-thrombomodulin complex. *Sci Rep* **11:**9354, 2021. PMC8087772
204. Pervushin K, Riek R, Wider G & Wüthrich K. Attenuated T2 relaxation by mutual cancellation of dipole-dipole coupling and chemical shift anisotropy indicates an avenue to NMR structures of very large biological macromolecules in solution. *Proc Natl Acad Sci U S A* **94:**12366-12371, 1997. PMC24947
205. Delaglio F, Grzesiek S, Vuister GW, Zhu G, Pfeifer J & Bax A. NMRPipe: a multidimensional spectral processing system based on UNIX pipes. *J Biomol NMR* **6:**277-293, 1995.
206. Lee W, Tonelli M & Markley JL. NMRFAM-SPARKY: enhanced software for biomolecular NMR spectroscopy. *Bioinformatics* **31:**1325-1327, 2015. PMC4393527
207. Fuentes-Prior P, Iwanaga Y, Huber R, Pagila R, Rumennik G, Seto M, Morser J, Light DR & Bode W. Structural basis for the anticoagulant activity of the thrombin-thrombomodulin complex. *Nature* **404:**518-525, 2000.
208. Madison EL, Kobe A, Gething MJ, Sambrook JF & Goldsmith EJ. Converting tissue plasminogen activator to a zymogen: a regulatory triad of Asp-His-Ser. *Science* **262:**419-421, 1993.
209. Clarke K, Kashiwaya Y, King MT, Gates D, Keon CA, Cross HR, Radda GK & Veech RL. The beta/alpha peak height ratio of ATP. A measure of free [Mg^{2+}] using ^{31}P NMR. *J Biol Chem* **271:**21142-21150, 1996.
210. Romani AM. Cellular magnesium homeostasis. *Arch Biochem Biophys* **512:**1-23, 2011. PMC3133480

211. Somlyo AV, McClellan G, Gonzalez-Serratos H & Somlyo AP. Electron probe X-ray microanalysis of post-tetanic Ca^{2+} and Mg^{2+} movements across the sarcoplasmic reticulum *in situ*. *J Biol Chem* **260:**6801-6807, 1985.
212. Wu MM, Llopis J, Adams S, McCaffery JM, Kulomaa MS, Machen TE, Moore HP & Tsien RY. Organelle pH studies using targeted avidin and fluorescein-biotin. *Chem Biol* **7:**197-209, 2000.
213. Carter WJ, Cama E & Huntington JA. Crystal structure of thrombin bound to heparin. *J Biol Chem* **280:**2745-2749, 2005.
214. De Cristofaro R, De Candia E, Rutella S & Weitz JI. The Asp^{272}-Glu^{282} region of platelet glycoprotein Ibα interacts with the heparin-binding site of α-thrombin and protects the enzyme from the heparin-catalyzed inhibition by antithrombin III. *J Biol Chem* **275:**3887-3895, 2000.
215. Ramakrishnan V, DeGuzman F, Bao M, Hall SW, Leung LL & Phillips DR. A thrombin receptor function for platelet glycoprotein Ib-IX unmasked by cleavage of glycoprotein V. *Proc Natl Acad Sci U S A* **98:**1823-1828, 2001. PMC29341
216. Celikel R, McClintock RA, Roberts JR, Mendolicchio GL, Ware J, Varughese KI & Ruggeri ZM. Modulation of α-thrombin function by distinct interactions with platelet glycoprotein Ibα. *Science* **301:**218-221, 2003.
217. Dumas JJ, Kumar R, Seehra J, Somers WS & Mosyak L. Crystal structure of the GpIbα-thrombin complex essential for platelet aggregation. *Science* **301:**222-226, 2003.
218. Pineda AO, Chen ZW, Marino F, Mathews FS, Mosesson MW & Di Cera E. Crystal structure of thrombin in complex with fibrinogen γ′ peptide. *Biophys Chem* **125:**556-559, 2007.
219. Di Cera E. A structural perspective on enzymes activated by monovalent cations. *J Biol Chem* **281:**1305-1308, 2006.
220. Di Cera E, Guinto ER, Vindigni A, Dang QD, Ayala YM, Wuyi M & Tulinsky A. The Na^+ binding site of thrombin. *J Biol Chem* **270:**22089-22092, 1995.
221. Tsiang M, Jain AK, Dunn KE, Rojas ME, Leung LL & Gibbs CS. Functional mapping of the surface residues of human thrombin. *J Biol Chem* **270:**16854-16863, 1995.
222. Ayala YM, Cantwell AM, Rose T, Bush LA, Arosio D & Di Cera E. Molecular mapping of thrombin-receptor interactions. *Proteins* **45:**107-116, 2001.
223. Pechik I, Madrazo J, Mosesson MW, Hernandez I, Gilliland GL & Medved L. Crystal structure of the complex between thrombin and the central "E" region of fibrin. *Proc Natl Acad Sci U S A* **101:**2718-2723, 2004. PMC365687
224. Pechik I, Yakovlev S, Mosesson MW, Gilliland GL & Medved L. Structural basis for sequential cleavage of fibrinopeptides upon fibrin assembly. *Biochemistry* **45:**3588-3597, 2006. PMC2531209
225. Hall SW, Nagashima M, Zhao L, Morser J & Leung LL. Thrombin interacts with thrombomodulin, protein C, and thrombin-activatable fibrinolysis inhibitor via specific and distinct domains. *J Biol Chem* **274:**25510-25516, 1999.
226. Pineda AO, Cantwell AM, Bush LA, Rose T & Di Cera E. The thrombin epitope recognizing thrombomodulin is a highly cooperative hot spot in exosite I. *J Biol Chem* **277:**32015-32019, 2002.

227. Xu H, Bush LA, Pineda AO, Caccia S & Di Cera E. Thrombomodulin changes the molecular surface of interaction and the rate of complex formation between thrombin and protein C. *J Biol Chem* **280:**7956-7961, 2005.
228. Goettig P, Brandstetter H & Magdolen V. Surface loops of trypsin-like serine proteases as determinants of function. *Biochimie* **166:**52-76, 2019.
229. Chapman HA, Jr., Allen CL, Stone OL & Fair DS. Human alveolar macrophages synthesize factor VII in vitro. Possible role in interstitial lung disease. *J Clin Invest* **75:**2030-2037, 1985. PMC425564
230. Wilcox JN, Noguchi S & Casanova J. Extrahepatic synthesis of factor VII in human atherosclerotic vessels. *Arterioscler Thromb Vasc Biol* **23:**136-141, 2003.
231. Teich N, Bauer N, Mössner J & Keim V. Mutational screening of patients with nonalcoholic chronic pancreatitis: identification of further trypsinogen variants. *Am J Gastroenterol* **97:**341-346, 2002.
232. Kereszturi E, Szmola R, Kukor Z, Simon P, Weiss FU, Lerch MM & Sahin-Tóth M. Hereditary pancreatitis caused by mutation-induced misfolding of human cationic trypsinogen: a novel disease mechanism. *Hum Mutat* **30:**575-582, 2009. PMC2663013